Origin of methane at ancient methane seeps inferred from organic geochemical signatures in seep carbonates

By

YUSUKE MIYAJIMA

Thesis submitted for the degree of doctor of science

Department of Geology and Mineralogy
Division of Earth and Planetary Sciences
Graduate School of Science
Kyoto University

1st December, 2017

Abstract

Knowing the origin of methane at submarine methane seeps (cold seeps) can provide valuable insights into the depth origin and migration process of the seep fluids as well as into the subsurface fluid circulation. The origin of methane at ancient seeps has been estimated indirectly based on geological backgrounds and carbon isotopic compositions of carbonates that formed via the anaerobic oxidation of methane (AOM). In this study, two approaches were attempted to estimate the origin of methane at ancient seeps: 1) carbon isotope analysis of lipid biomarkers for anaerobic methane-oxidizing archaea (ANME) and 2) analysis of the carbon isotopic and molecular compositions of residual gases within the methane-seep carbonates. A modern methane-seep carbonate rock obtained from the seafloor at a seep site offshore Joetsu, Niigata Prefecture, central Japan was examined to estimate the carbon isotope fractionation between methane and ANME biomarkers. For ancient seep carbonates, Miocene to Pleistocene methane-seep carbonate rocks collected at 11 sites in the Japan Sea region were examined.

The early-diagenetic, AOM-derived carbonate phases show various $\delta^{13}C$ values ranging between −64.7‰ and −4.7‰ (vs. VPDB). This result does not tell us which is plausible thermogenic (>−50‰) or biogenic (<−50‰) origin for the methane.

Pentamethylicosane (PMI) extracted from the modern methane-seep carbonate has a $\delta^{13}C$ value of −80‰, which shows an offset of 44‰ from the seep methane (−36‰) at this site. The ANME biomarkers PMI and crocetane were extracted from the ancient carbonates, with $\delta^{13}C$ values ranging between −137‰ and −93‰. The estimated offset of $\delta^{13}C$ (44‰) indicates that the methane at the ancient seep had $\delta^{13}C$ values mostly lower than −50‰ and are biogenic in origin, assuming that the $\delta^{13}C$ values of the ANME biomarkers are controlled by those of the source methane and isotopic fractionations during biosynthesis. The relationship of the $\delta^{13}C$ values between methane and ANME biomarkers was assessed by regression analysis based on data taken at modern seeps in other regions of the world. The obtained regression formulae were used to constrain the $\delta^{13}C$ values of methane at the ancient seeps with 95% prediction intervals, which provided the similar results as estimated from the $\delta^{13}C$ offset. It can be concluded that the methane contained in the seep fluids at the ancient seeps in the study area is mainly biogenic in origin and was produced in the shallow subsurface. Migration and seepage of thermogenic methane from the deep subsurface were probably minor before Pleistocene in the study area.

Methane and heavier hydrocarbons were extracted by acid digestion of powdered samples of the AOM-derived carbonate phases. The methane content tends to increase

with increasing age of the carbonate. The extracted methane has $\delta^{13}C$ values of −69.6‰ to −26.9‰ and methane to (ethane+propane) ratios of 2 to 518, and therefore both thermogenic and biogenic origins are possible. Methane was also released by heating and crushing of chipped samples of the Miocene seep carbonates at the Nakanomata 1 site. These methods produced a little amount of methane as compared with acid digestion and high amounts of carbon dioxide. The $\delta^{13}C$ values were measured for the methane and carbon dioxide liberated by the crushing. The methane shows $\delta^{13}C$ values from −55.1‰ to −49.9‰, while the carbon dioxide exhibits values ranging between −26.8‰ and −25.2‰. The obtained $\delta^{13}C$ values can be explained by methane oxidation. The results suggest a reasonable scenario of the origin of methane at Nakanomata 1 as follows: 1) biogenic methane was originally contained in the Miocene seep fluids; 2) isotopic fractionation during AOM enriched the methane in ^{13}C; and 3) the ^{13}C-enriched methane was trapped within the seep carbonate mainly as intracrystal inclusions. This scenario is also supported by a positive significant correlation of the $\delta^{13}C$ values between the methane and its host carbonate. The $\delta^{13}C$ values typically increase with increasing carbon number in thermogenic and biogenic hydrocarbons. In contrast, the $\delta^{13}C$ values of the methane, ethane, and propane liberated from the examined carbonates by acid digestion showed “reverse” isotopic trends. This “reverse” isotopic trends found

in the liberated hydrocarbons indicate that ethane and propane with unusually low $\delta^{13}C$ values (<−40‰) were mixed with normal thermogenic or biogenic gases. The unusually ^{13}C-depleted ethane and propane could have originated from secondary thermal cracking of ^{13}C-depleted organic compounds within the seep carbonates. They were extracted even from the samples of low maturity. The line of evidence indicates that the residual gases within the seep carbonates can contain incidental gases as well as original ones. The isotopic trend of the unusually ^{13}C-depleted ethane and propane was different between low and high maturities. This result suggests that the mixing ratio to the normal gases and the molecular ratio of the secondary-generated gases both depend on thermal maturity.

It is probable that the carbon isotopic compositions of the ANME biomarkers preserved within the methane-seep carbonates are less affected by thermal maturation, with respect to the petrographic textures and oxygen isotopic compositions of the carbonates. However, in some samples of high maturity, the ANME biomarkers were not preserved probably due to thermal break down. Residual gases within the seep carbonates could be affected seriously by incidental gases even in the samples of low maturity. Therefore, the residual gases should be examined using multiple extraction methods and with other signatures such as the isotopic compositions of the carbonates

and the biomarkers.

和文要旨

海底からのメタン湧水（冷湧水）中のメタンの起源を知ることは，流体の起源深度や湧出過程，地殻内の水循環などを理解するうえで重要である．地質時代の古メタン湧水で湧出していたメタンの起源は，メタンの嫌気的酸化によって形成された炭酸塩の炭素同位体比や地質学的な背景から間接的に推測されているのみで，それを推定する方法は確立されていない．本研究では，メタン酸化古細菌のバイオマーカーの炭素同位体比と，炭酸塩残留ガスの炭素同位体比や分子組成に着目することで，古メタン湧水のメタンの起源を推定することを試みた．そのために，新潟県上越沖海底で採取された現世のメタン湧水炭酸塩岩を用いて，メタンと古細菌のバイオマーカーとの間の炭素同位体分別を求めた．また，日本海側陸域 11 産地の中新統～更新統より採取した古メタン湧水炭酸塩岩試料を用いた．

試料中のメタン酸化起源の炭酸塩組織の炭素同位体比は−64.7‰～−4.7‰（vs. VPDB）と幅広い $\delta^{13}C$ 値を示した．この結果のみからは，メタンが熱分解起源（>−50‰）なのか微生物起源（<−50‰）なのか判別することはできない．現世のメタン湧水炭酸塩岩よりペンタメチルイコサンを抽出し，その $\delta^{13}C$ 値を測定

した結果，−80‰であった．この湧水中のメタンの $\delta^{13}C$ 値は先行研究によって−36‰と求められているので，バイオマーカーとメタンの $\delta^{13}C$ 値の差は 44‰と見積もられる．古メタン湧水炭酸塩岩のバイオマーカー分析を行った結果，嫌気的メタン酸化古細菌のバイオマーカーであるペンタメチルイコサンやクロセタンが抽出された．これらバイオマーカーの $\delta^{13}C$ 値を測定したところ，−137‰～−93‰であった．バイオマーカーの同位体比がメタンの同位体比と古細菌の同化・生合成に伴う同位体分別によって決まるとすれば，先述のバイオマーカーとメタンとの $\delta^{13}C$ 値の差（44‰）から，古メタン湧水のメタンの $\delta^{13}C$ 値は概ね−50‰より低く見積もられ，微生物起源であったと推定される．一方，世界各地の現世湧水のデータから，バイオマーカーの $\delta^{13}C$ 値とメタンの $\delta^{13}C$ 値の回帰分析を行い，メタンの $\delta^{13}C$ 値を 95%予測区間付きで制約するための回帰式を求めた．この式を用いて古メタン湧水のメタンの同位体比を推定した結果，バイオマーカーとメタンとの $\delta^{13}C$ 値の差から推定した結果と同様な結果を得た．以上の結果から，更新世以前の本研究地域では，主に地下浅部で生成した微生物メタンが湧出しており，地下深部からの熱分解メタンの湧出はまれであったと考えられる．

各試料中のメタン酸化起源の炭酸塩組織を粉末化して酸で溶解させたところ，メタンおよびエタン以上の炭化水素が抽出され，メタンの量は古い試料ほ

ど多い傾向を示した．抽出されたメタンは幅広い $\delta^{13}C$ 値（−69.6‰～−26.9‰）と低いメタン/（エタン+プロパン）比（2～518）を示し，熱分解起源と微生物起源のいずれの可能性も否定できない結果となった．中新世の 1 産地（中ノ俣 1）の炭酸塩小片を加熱・粉砕した結果，酸溶解の場合よりも少量のメタンと，高濃度の二酸化炭素が抽出された．粉砕により抽出したメタンと二酸化炭素の $\delta^{13}C$ 値はそれぞれ−55.1‰～−49.9‰，−26.8‰～−25.2‰であり，メタン酸化による同位体分別を受けた微生物メタンと二酸化炭素の値として解釈できる．中ノ俣 1 については，酸溶解によって抽出したメタンと炭酸塩の間で $\delta^{13}C$ 値に有意な正の相関が見られた．このことからも，メタン酸化による分別を受けた中新世当時の湧水中の微生物メタンが主に炭酸塩結晶内部に捕獲されたものが，試料中に残留していた可能性がある．一方，各産地で酸溶解によって抽出されたメタン，エタン，プロパンの $\delta^{13}C$ 値を比較した結果，炭素数とともに $\delta^{13}C$ 値が高くなる一般的な同位体比トレンドとは逆に，炭素数とともに $\delta^{13}C$ 値が低くなる傾向を示す場合が見られた．このことから，抽出されたガスは通常の熱分解ガスまたは微生物ガスに加えて，通常の熱分解ガスよりも低い異常な $\delta^{13}C$ 値（<−40‰）を示すエタンやプロパンを含むガスが混入したものであることがわかった．異常な $\delta^{13}C$ 値をもつエタンやプロパンは，炭酸塩岩中の $\delta^{13}C$ 値の低い有機物の二次的な熱分解によって生成したと考えられ，熟成度の比較

的低い試料からも抽出されている．以上から，メタン湧水炭酸塩岩中の残留ガスは，湧水中に含まれていたものだけでなく，炭酸塩岩の埋没過程で周囲から二次的に捕獲された熱分解ガスや微生物ガス，あるいは熱熟成の過程で炭酸塩内有機物の二次的な熱分解によって生成したガスが含まれていると考えられる．低熟成度の試料と高熟成度の試料では，異常な $\delta^{13}C$ 値のエタン，プロパンの同位体比トレンドが異なることから，炭酸塩内有機物から二次的に生成した熱分解ガスの混合比や分子組成は，熟成度によって変化することがあると考えられる．

メタン湧水炭酸塩岩中のメタン酸化古細菌のバイオマーカーの炭素同位体比は，炭酸塩の組織や酸素同位体比に比べて熱熟成の影響を受けにくいと考えられる．ただし，熟成度の高い試料では，バイオマーカーが熱分解によって保存されていない場合がある．炭酸塩残留ガスは，熟成度が低い場合でも二次的なガスの影響があるため，複数の抽出法を試すとともに，炭酸塩やバイオマーカーの同位体比などいくつかの指標を総合して結果を解釈する必要がある．

Acknowledgments

I am grateful to my supervisor Takao Ubukata (Kyoto University, Japan) for his precious help and understanding to my work, as well as critical comments on an early

draft of this thesis. I am also grateful to Takashi Hasegawa (Kanazawa University, Japan) for being my supervisor at Kanazawa, permitting the experiments in his laboratory, and providing invaluable comments and warm encouragement. I would thank Yumiko Watanabe (Kyoto University) for her considerate help in carbon and oxygen isotope analyses of carbonates and insightful comments. Hiroshige Matsuoka (Kyoto University) is thanked for his everyday encouragement and inspiring comments. I wish to express my sincere appreciation to Akira Ijiri (Japan Agency for Marine-Earth Science and Technology, JAMSTEC) for thoughtfully understanding my work, enabling the residual gas analyses at Kochi Institute for Core Sample Research, and providing many instructive comments that helped to improve my interpretation. I gratefully acknowledge Akiko S. Goto (Kanazawa University) for her innumerable support in laboratory, as well as constant incitement and discussions. Robert G. Jenkins (Kanazawa University) is acknowledged for his constructive discussions and suggestions and help in both laboratory and the field. He also provided me with carbonate samples collected from the Anazawa/Akanuda seep. Norimasa Shimobayashi (Kyoto University) kindly performed X-ray diffraction analyses. Saburo Sakai (JAMSTEC) generously measured carbon and oxygen isotopic compositions of the Takinoue and Anden carbonates. I am grateful to Ryo Matsumoto (Meiji University, Japan) for providing modern methane-

seep carbonate samples collected from the Umitaka Spur during the NT07-20 cruise and constructive comments, and also for conducting a field trip to my study sites with his colleagues at Meiji University. Akemi Imajo (JAMSTEC) courteously helped to perform residual gas analyses. Yukako Nabeshima, Yuki Fujimura, and Masafumi Murayama (Kochi University, Japan) are thanked for their permission and generous help to use their instrument for carbon and oxygen isotope analyses. Carbon isotopic analyses of total organic carbon were partly performed by Yuya Iwase (Kanazawa University). Soichiro Muta (Kanazawa University, now at Japan Oil, Gas and Metals National Corporation, JOGMEC) helped in lipid extraction and provided helpful information on biomarkers. Masaki Takaya (Kyoto University) graciously helped me in preparing thin sections of carbonate rocks. The Takinoue seep could not be found without great support in the field by Yoshio Tanigawa (Momijiyama, Yubari City, Japan). Field survey in the Yubari area was conducted under the permission of Sorachi District Forest Office (Iwamizawa City, Hokkaido, Japan). Yurihonjo Police and Fire stations (Akita Prefecture, Japan) saved my life in an emergency during the field work. Sampling at the Anden site was permitted by Akita Prefecture. I thank owners of guesthouses for their warm hospitality with providing nice meals. Takami Nobuhara (Shizuoka University, Japan) and Hakuichi Koike (Shinshushinmachi Fossil Museum,

Shiga Fossil Museum, Japan) are gratefully acknowledged for their discerning suggestions and kind help in the field. Staffs at Shiga Fossil Museum provided me an opportunity to give a public talk and encouraged my work at the Sorimachi and Anazawa/Akanuda sites. Kazutaka Amano (Joetsu University of Education, Japan) and Andrzej Kaim (Polish Academy of Sciences, Poland) are thanked for their help in the field work. Daichi Maeyama (Hokkaido University, Japan, now at Japan Petroleum Exploration Co., Ltd., JAPEX) and Noriyuki Suzuki (Hokkaido University, Japan) provided valuable information and discussions on residual gases within seep carbonates. Takashi Tsuji (JAPEX) provided information on vesicomyid fossils in Akita Prefecture. I would like to appreciate Crispin T. S. Little (University of Leeds, United Kingdom) for permitting to visit his laboratory and look through his collections and providing insightful suggestions to my work. I thank Jörn Peckmann (University of Hamburg, Germany), Jennifer Zwicker, and Daniel Smrzka (University of Vienna, Austria) for their kindness, interest in my work, and helpful comments. Hajime Naruse, Harutaka Sakai, Atsushi Yamaji, Katsushi Sato, Kei Sato, Junya Watanabe, Yuko Daket, and other members in the Department of Geology and Mineralogy, Kyoto University, Takahiro Kamiya, Takuya Sagawa, Kotaro Toyama, and other members in the Geology and Paleontology Group, Kanazawa University, and Kenta Yoshida (JAMSTEC) are

acknowledged for their valuable comments and continuous stimulation. I am sincerely grateful to Sakiko Miyakawa (Kanazawa University), Ikumi Kaifuku, and Hiroe Ito (Kyoto University) for their accommodating support in financial management. This study was financially supported by Grant-in-Aid (KAKENHI) from the Japan Society for the Promotion of Science (JSPS) for JSPS Research Fellow (No. 15J01158). Field trip to Tsushima Island was conducted under the financial support by Poland National Science Research Grant (No. 2014/15/B/ST10/0486) to Krzysztof Hryniewicz (Polish Academy of Sciences, Poland). Finally, I thank my family, friends, and partner for their daily support and understanding.

Contents

Preface

I. Origin of methane

Methane is the simplest organic molecule known as a potent greenhouse gas and the dominant component of natural gases. It is either generated from carbon dioxide or more complex organic molecules. The methane produced by archaeal methanogenesis is called biogenic (or microbial) methane. The pathways for biogenic methane production include hydrogenotrophic methanogenesis (carbonate reduction) and fermentative methanogenesis, both of which are performed by methanogenic archaea restricted to anaerobic environments such as shallow (<3 km) subsurface sediments (e.g., Inagaki et al., 2015). The methane produced by thermal decomposition of organic matter in the deep subsurface at >100°C is called thermogenic methane (e.g., Claypool and Kvenvolden, 1983). The methane produced by abiotic processes such as Fischer-Tropsch type reaction and Sabatier reaction (e.g., McCollom and Seewald, 2007) is called abiotic methane.

The origin of methane can be distinguished mainly by stable carbon and hydrogen isotopic compositions of methane and its molecular ratios to heavier hydrocarbons (Bernard et al., 1976; Whiticar, 1999; Kawagucci and Toki, 2010). The biogenic methane is characterized by $\delta^{13}C$ values ranging between −110‰ and −50‰ (vs.

VPDB) and methane to ethane+propane ($C_1/(C_2 + C_3)$) ratios higher than 1000. The thermogenic methane has been reported to have higher $\delta^{13}C$ values ranging between −50‰ and −20‰ and $C_1/(C_2 + C_3)$ ratios lower than 50. Methane of probably abiotic origins has been reported to show $\delta^{13}C$ values higher than −20‰ and be associated with heavier hydrocarbons, but the isotopic signatures and molecular compositions characterizing the abiotic methane remain to be constrained (e.g., Kawagucci and Toki, 2010; Suda et al., 2017).

II. Cold seeps as windows to the subsurface

Seepage of methane-rich geofluids from the seafloor is called methane seep or cold seep, after the fluid temperatures close to the ambient bottom water (e.g., Kulm et al., 1986). Since the first discoveries in the Gulf of Mexico (Paull et al., 1984; Kennicutt et al., 1985), cold seeps have been recognized on the seafloor at continental margins of the world by the unique biological communities, which resemble those at hydrothermal vents, and by venting of methane bubbles or oils (Sibuet and Olu, 1998; Campbell, 2006; Fig. P.1). Cold seeps are not only major sources for methane to the ocean and atmosphere (Boetius and Wenzhöfer, 2013) but also windows to the subsurface environments, because seep fluids contain methane and various elements derived from

biogeochemical processes and fluid-rock interactions in the crust (Hensen et al., 2004; Kawagucci and Toki, 2010).

Knowing the origin of methane discharging at cold seeps provides various insights into the depth origins and migration processes for the seep fluids and therefore into the subsurface fluid circulation. The origin of methane at cold seeps is either biogenic, thermogenic, or both (Fig. P.1). Seepage of biogenic methane from shallow subsurface is commonly driven by diffusion and fluid transport through subsurface faults (e.g., Himmler et al., 2015; Crémière et al., 2016a; Prouty et al., 2016; Pirre et al., 2017), while seepage of thermogenic methane and other hydrocarbons or oils from deep subsurface requires effective migration processes and thermal maturity of deep sediments (Milkov, 2005; Suess, 2014). As those of biogenic origins, methane seeps of thermogenic origins are known from both active and passive continental margins; they are known for example from mud volcanoes where deep-sourced fluids and muds are discharged such as on the Nankai Trough subduction zone (Toki et al., 2012; Pape et al., 2014) and on the Mediterranean Ridge (Pape et al., 2010a), a headless submarine canyon on the Cascadia accretionary prism where sediment compaction and deformation generate steep pore pressure gradients and drive focused fluid flow (Pohlman et al., 2005), hydrocarbon seeps sustained by subsurface salt diapirs in the

Gulf of Mexico (Roberts and Aharon, 1994; Sassen et al., 2004), and high-flux seepage sites sustained by deep-rooted faults in the Black Sea (Pape et al., 2010b), offshore Norway (Sauer et al., 2015), and the Japan Sea (Matsumoto et al., 2009).

III. Ancient cold seeps

Cold seeps in the geologic past are preserved in the sediments as peculiar authigenic carbonate rocks, which are commonly called seep carbonates or methane-derived authigenic carbonates (MDACs). The formation of the carbonate rocks at methane seeps is induced by an alkalinity increase during the sulfate-coupled anaerobic oxidation of methane (AOM) (e.g., Reeburgh, 1976; Ritger et al., 1987):

$$CH_4 + SO_4^{2-} \rightarrow HS^- + HCO_3^- + H_2O$$

The sulfate-coupled AOM is mediated by microbial consortia of anaerobic methane-oxidizing archaea (ANME) and sulfate-reducing bacteria, which thrive in anaerobic environments below or in a few cases above the sediment-water interface and within the carbonate rocks (Boetius et al., 2000; Michaelis et al., 2002; Teichert et al., 2005; Marlow et al., 2015). The cementation of the sediments and the microbial communities by the carbonates enables preservation of characteristic biomarkers (molecular fossils) derived from the lipids of the AOM-mediating microbes, as well as animal fossils

thriving in the cold-seep environments (Hinrichs et al., 1999; Peckmann et al., 1999; Campbell, 2006). Moreover, seep carbonates have been regarded as recorders of geochemistry of sediment, fluid, and gas in the past (e.g., Feng et al., 2009, 2014; Himmler et al., 2010; Crémière et al., 2016b).

Ever since the early 1990s, a number of carbonate deposits hosted within ancient marine sediments around the world have been identified as ancient methane-seep sites (Fig. P.1). The major criteria for identifying ancient seep carbonates include the association with peculiar animal fossils, petrographic features, ^{13}C-depleted isotopic compositions of the carbonate cements, and preservation of characteristic biomarkers. Animal fossils characteristic to Cenozoic seep environments include solemyid, thyasirid, lucinid, vesicomyid, and bathymodiolin bivalves, and *Provanna* gastropods (Amano and Kiel, 2007; Taylor and Glover, 2010; Kiel, 2013; Kiel and Amano, 2013; Amano and Little, 2014; Amano et al., 2015). Paleozoic and Mesozoic seeps were dominated either by extinct bivalves such as a modiomorphid *Caspiconcha* or brachiopods such as a dimerelloid *Peregrinella* (Campbell and Bottjer, 1995; Kiel and Little, 2006; Jenkins et al., 2013; Kiel et al., 2014). Although seep carbonates are mainly composed of microcrystalline carbonate crystals cementing the sediments as non-seep sedimentary concretions, they are known to show several petrographic

features such as stromatactoid cavities, banded and botryoidal cement, and microbial filaments (Peckmann et al. 2002, 2003; Bojanowski, 2007). The $\delta^{13}C$ values of the seep carbonates are commonly lower than −30‰, resulting from the oxidation of ^{13}C-depleted methane (Peckmann and Thiel, 2004; Campbell, 2006). Such highly negative $\delta^{13}C$ values of the carbonates allow us to distinguish seep carbonates from non-seep sedimentary concretions, whereas less negative values are in some cases indicative of ancient oil-seep carbonates (Peckmann et al., 2001, 2007; Kiel and Peckmann, 2007). Lipid biomarkers for ANME include diethers such as archaeol and hydroxyarchaeol and isoprenoid hydrocarbons such as pentamethylicosane (PMI) and crocetane, with extremely ^{13}C-depleted compound-specific isotopic signatures (Peckmann and Thiel, 2004; Blumenberg, 2010). These biomarkers can be preserved within ancient seep carbonates as old as the Carboniferous in age (Birgel et al., 2008), but their concentrations relative to other compounds could be altered by thermal maturation even in Cenozoic carbonates (Hryniewicz et al., 2016).

Despite the vast number of paleontological studies on ancient methane-seep carbonates around the world, few studies have attempted to estimate the origin of methane contained in the ancient seep fluids. The origin of methane at ancient seeps has been interpreted based on indirect evidences such as carbon isotopic signatures of the

carbonates (see Part 1) and geological settings. Agirrezabala et al. (2013) studied a Lower Cretaceous methane seep in the Basque-Cantabrian Basin, western Pyrenees, and claimed that it was sustained by thermogenic methane. They inferred that the thermogenic methane was sourced from sediments at ~900 m below the paleo-seafloor, which were heated by magmatic intrusions observed in a seismic profile. However, such geological features possibly related to past methane seepage are rarely observed in the field, particularly where sedimentary strata have been subjected to complex tectonic histories. There is an ongoing attempt to estimate the origin of seep fluids using trace-element geochemistry of the seep carbonates (Jakubowicz et al., 2015). Estimation of the origin of methane at ancient methane seeps, along with the origin of fluids, can provide valuable insights into biogeochemical processes and fluid circulation in subsurface environments in the geologic past. Knowing the fluid circulation and related fluid-flow pathways in the past would also help to understand tectonic histories of sedimentary basins such as fault activities.

IV. Objective of this study

The objective of this study is to estimate the origin of methane at ancient cold seeps distributed along the Japan Sea side of the Japanese archipelago. The present

study is based on organic geochemical signatures within the methane-seep carbonates, which could reflect carbon isotopic compositions of the source methane. Stable carbon isotopic compositions were measured in lipid biomarkers for ANME, as well as in the carbonates, and are used to constrain the carbon isotopic compositions of the source methane as shown in Part 1. For this purpose, carbon isotope fractionation or offset between methane and biomarkers was estimated by compiled data obtained from a modern seep carbonate and from literature. In addition, residual gases within the seep carbonates were examined to obtain more direct information on the isotopic compositions of methane contained in the seep fluids. In Part 2, the origin of the residual gases is discussed based on the molecular compositions and carbon isotopic compositions of hydrocarbons extracted from the seep carbonates. The isotopic compositions and thermal maturity of organic matter within the carbonates were also examined. The potential of the residual gas to preserve the original signatures of the methane and the risk of secondary processes affecting the residual gas are also discussed in this chapter. Such a multidisciplinary study of ancient methane seeps is rare and would shed new light on ancient seep carbonates as tools to know ancient subsurface environments.

The material for this study is Cenozoic methane-seep carbonates collected from the

area along the Japan Sea coast. The stratigraphy and developmental history of sedimentary basins in the study area have been revealed in detail, and therefore the estimated origin of methane at the ancient seeps can be verified from a geological perspective. In addition, the examined seep carbonates are from strata of different ages and thus could have experienced different thermal history. This is helpful to know possible effects of thermal alterations on the organic geochemical signatures mentioned above.

V. Geological setting and modern methane seeps of the Japan Sea

The Japan Sea is a back-arc basin that was formed in the Miocene (Burdigalian to Langhian). During the opening of the Japan Sea, several sedimentary basins were formed by rifting (e.g., Iijima and Tada, 1990; Jolivet and Tamaki, 1992; Takano, 2002). This early stage of formation of the Japan Sea was characterized by volcanic activity that produced rocks commonly referred to as the “Green Tuff”. These volcanic and pyroclastic rocks constitute the lower part of the sedimentary basins, and are overlain by a >5 km thick clastic marine sediments. The volcanic materials and organic-rich sediments in this region act as sources and reservoirs of oil and gas today (Kikuchi et al., 1991; Okui et al., 2008). The stress field in the Japan Sea region changed from

tensional to compressional during the late Miocene to Pliocene, causing reactivation of normal faults as reverse faults and uplift and transformation of the rift basins into anticlines (Jolivet and Tamaki, 1992; Sato, 1994; Okamura et al., 1995).

In the present-day Japan Sea, methane seeps originating from thermogenic methane, as well as biogenic methane, are known in several areas. Thermogenic gas and oil have been produced in this region by the thermal degradation of organic matter in the Miocene to Pliocene sediments at >1 km subsurface. Extensive gas hydrate fields have formed as a result of the gas migrating through permeable layers and along subsurface faults which were reactivated due to the compressional stress (Monzawa et al., 2006; Okui et al., 2008; Matsumoto et al., 2009).

References

Agirrezabala, L.M., Kiel, S., Blumenberg, M., Schäfer, N., Reitner, J., 2013. Outcrop analogues of pockmarks and associated methane-seep carbonates: a case study from the Lower Cretaceous (Albian) of the Basque-Cantabrian Basin, western Pyrenees. Palaeogeography, Palaeoclimatology, Palaeoecology 390, 94–115.

Amano, K., Kiel, S., 2007. Fossil vesicomyid bivalves from the North Pacific region. Veliger 49, 270–293.

Amano, K., Little, C.T.S., 2014. Miocene abyssochrysoid gastropod *Provanna* from Japanese seep and whale-fall sites. Acta Palaeontologica Polonica 59, 163–172.

Amano, K., Little, C.T.S., Campbell, K.A., Jenkins, R.G., Saether, K.P., 2015. Paleocene and Miocene *Thyasira* sensu stricto (Bivalvia: Thyasiridae) from chemosynthetic communities from Japan and New Zealand. Nautilus 129, 43–53.

Bernard, B.B., Brooks, J.M., Sackett, W.M., 1976. Natural gas seepage in the Gulf of Mexico. Earth and Planetary Science Letters 31, 48–54.

Birgel, D., Feng, D., Roberts, H.H., Peckmann, J., 2011. Changing redox conditions at cold seeps as revealed by authigenic carbonates from Alaminos Canyon, northern Gulf of Mexico. Chemical Geology 285, 82–96.

Birgel, D., Himmler, T., Freiwald, A., Peckmann, J., 2008. A new constraint on the antiquity of anaerobic oxidation of methane: Late Pennsylvanian seep limestones from southern Namibia. Geology 36, 543–546.

Blumenberg, M., 2010. Microbial chemofossils in specific marine hydrothermal and methane cold seep settings. In: Kiel, S. (Ed.), The Vent and Seep Biota, Topics in Geobiology 33. Springer, Heidelberg, pp. 73–106.

Boetius, A., Ravenschlag, K., Schubert, C.J., Rickert, D., Widdel, F., Gieseke, A., Amann, R., Jørgensen, B.B., Witte, U., Pfannkuche, O., 2000. A marine microbial

consortium apparently mediating anaerobic oxidation of methane. Nature 407, 623–626.

Boetius, A., Wenzhöfer, F., 2013. Seafloor oxygen consumption fueled by methane from cold seeps. Nature Geoscience 6, 725–734.

Bohrmann, G., Greinert, J., Suess, E., Torres, M., 1998. Authigenic carbonates from the Cascadia subduction zone and their relation to gas hydrate stability. Geology 26, 647–650.

Bojanowski, M.J., 2007. Oligocene cold-seep carbonates from the Carpathians and their inferred relation to gas hydrates. Facies 53, 347–360.

Bourry, C., Chazallon, B., Charlou, J.L., Donval, J.P., Ruffine, L., Henry, P., Geli, L., Çagatay, M.N., İnan, S., Moreau, M., 2009. Free gas and gas hydrates from the Sea of Marmara, Turkey: chemical and structural characterization. Chemical Geology 264, 197–206.

Brooks, J.M., Field, M.E., Kennicutt II, M.C., 1991. Observations of gas hydrates in marine sediments, offshore northern California. Marine Geology 96, 103–109.

Campbell, K.A., 2006. Hydrocarbon seep and hydrothermal vent paleoenvironments and paleontology: past developments and future research directions. Palaeogeography, Palaeoclimatology, Palaeoecology 232, 362–407.

Campbell, K.A., Bottjer, D.J., 1995. Brachiopods and chemosymbiotic bivalves in Phanerozoic hydrothermal vent and cold seep environments. Geology 23, 321–324.

Chien, C.W., Huang, C.Y., Lee, H.C., Yang, K.M., 2013. Patterns and sizes of authigenic carbonate formation in the Pliocene foreland in southwestern Taiwan: implications of an ancient methane seep. Terrestrial, Atmospheric and Oceanic Sciences 24, 971–984.

Claypool, G.E., Kvenvolden, K.A., 1983. Methane and other hydrocarbon gases in marine sediment. Annual Review of Earth and Planetary Sciences 11, 299–327.

Crémière, A., Lepland, A., Chand, S., Sahy, D., Condon, D.J., Noble, S.R., Martma, T., Thorsnes, T., Sauer, S., Brunstad, H., 2016a. Timescales of methane seepage on the Norwegian margin following collapse of the Scandinavian Ice Sheet. Nature Communications 7:11509.

Crémière, A., Lepland, A., Chand, S., Sahy, D., Kirsimäe, K., Bau, M., Whitehouse, M.J., Noble, S.R., Martma, T., Thorsnes, T., Brunstad, H., 2016b. Fluid source and methane-related diagenetic processes recorded in cold seep carbonates from the Alvheim channel, central North Sea. Chemical Geology 432, 16–33.

De Boever, E., Swennen, R., Dimitrov, L., 2006. Lower Eocene carbonate cemented chimneys (Varna, NE Bulgaria): formation mechanisms and the (a)biological

mediation of chimney growth? Sedimentary Geology 185, 159–173.

Feng, D., Birgel, D., Peckmann, J., Roberts, H.H., Joye, S.B., Sassen, R., Liu, X.-L., Hinrichs, K.-U., Chen, D., 2014. Time integrated variation of sources of fluids and seepage dynamics archived in authigenic carbonates from Gulf of Mexico gas hydrate seafloor observatory. Chemical Geology 385, 129–139.

Feng, D., Chen, D., Peckmann, J., 2009. Rare earth elements in seep carbonates as tracers of variable redox conditions at ancient hydrocarbon seeps. Terra Nova 21, 49–56.

Gill, F.L., Harding, I.C., Little, C.T.S., Todd, J.A., 2005. Palaeogene and Neogene cold seep communities in Barbados, Trinidad and Venezuela: an overview. Palaeogeography, Palaeoclimatology, Palaeoecology 227, 191–209.

Hachikubo, A., Sakagami, H., Minami, H., Nunokawa, Y., Shoji, H., Matveeva, T., Jin, Y.K., Obzhirov, A., 2009. Isotopic composition and crystallographic properties of gas hydrate in the Sea of Okhotsk. Journal of Geography 118, 207–221. (in Japanese with English abstract)

Hammer, Ø., Nakrem, H.A., Little, C.T.S., Hryniewicz, K., Sandy, M.R., Hurum, J.H., Druckenmiller, P., Knutsen, E.M., Høyberget, M., 2011. Hydrocarbon seeps from close to the Jurassic-Cretaceous boundary, Svalbard. Palaeogeography,

Palaeoclimatology, Palaeoecology 306, 15–26.

Hensen, C., Wallmann, K., Schmidt, M., Ranero, C.R., Suess, E., 2004. Fluid expulsion related to mud extrusion off Costa Rica—a window to the subducting slab. Geology 32, 201–204.

Himmler, T., Bach, W., Bohrmann, G., Peckmann, J., 2010. Rare earth elements in authigenic methane-seep carbonates as tracers for fluid composition during early diagenesis. Chemical Geology 277, 126–136.

Himmler, T., Birgel, D., Bayon, G., Pape, T., Ge, L., Bohrmann, G., Peckmann, J., 2015. Formation of seep carbonates along the Makran convergent margin, northern Arabian Sea and a molecular and isotopic approach to constrain the carbon isotopic composition of parent methane. Chemical Geology 415, 102–117.

Himmler, T., Freiwald, A., Stollhofen, H., Peckmann, J., 2008. Late Carboniferous hydrocarbon-seep carbonates from the glaciomarine Dwyka Group, southern Namibia. Palaeogeography, Palaeoclimatology, Palaeoecology 257, 185–197.

Hinrichs, K-U., Hayes, J.M., Sylva, S.P., Brewer, P.G., DeLong, E.F., 1999. Methane-consuming archaebacteria in marine sediments. Nature 398, 802–805.

Hovland, M., 2002. On the self-sealing nature of marine seeps. Continental Shelf Research 22, 2387–2394.

Hovland, M., Svensen, H., Forsberg, C.F., Johansen, H., Fichler, C., Fosså, J.H., Jonsson, R., Rueslåtten, H., 2005. Complex pockmarks with carbonate-ridges off mid Norway: products of sediment degassing. Marine Geology 218, 191–206.

Hryniewicz, K., Bitner, M.A., Durska, E., Hagström, J., Hjálmarsdóttir, H.R., Jenkins, R.G., Little, C.T.S., Miyajima, Y., Nakrem, H.A., Kaim, A., 2016. Paleocene methane seep and wood-fall marine environments from Spitsbergen, Svalbard. Palaeogeography, Palaeoclimatology, Palaeoecology 462, 41–56.

Hryniewicz, K., Hagström, J., Hammer, Ø., Kaim, A., Little, C.T.S., Nakrem, H.A., 2015. Late Jurassic–Early Cretaceous hydrocarbon seep boulders from Novaya Zemlya and their faunas. Palaeogeography, Palaeoclimatology, Palaeoecology 436, 231–244.

Iijima, A., Tada, R., 1990. Evolution of Tertiary sedimentary basins of Japan in reference to opening of the Japan Sea. Journal of the Faculty of Science, University of Tokyo, Section II 22, 121–171.

Inagaki, F., Hinrichs, K.-U., Kubo, Y., Bowles, M.W., Heuer, V.B., Hong, W.-L., Hoshino, T., Ijiri, A., Imachi, H., Ito, M., Kaneko, M., Lever, M.A., Lin, Y.-S., Methé, B.A., Morita, S., Morono, Y., Tanikawa, W., Bihan, M., Bowden, S.A., Elvert, M., Glombitza, C., Gross, D., Harrington, G.J., Hori, T., Li, K., Limmer, D.,

Liu, C.-H., Murayama, M., Ohkouchi, N., Ono, S., Park, Y.-S., Phillips, S.C., Prieto-Mollar, X., Purkey, M., Riedinger, N., Sanada, Y., Sauvage, J., Snyder, G., Susilawati, R., Takano, Y., Tasumi, E., Terada, T., Tomaru, H., Trembath-Reichert, E., Wang, D.T., Yamada, Y., 2015. Exploring deep microbial life in coal-bearing sediment down to ~2.5 km below the ocean floor. Science 349, 420–424.

Jakubowicz, M., Dopieralska, J., Belka, Z., 2015. Tracing the composition and origin of fluids at an ancient hydrocarbon seep (Hollard Mound, Middle Devonian, Morocco): a Nd, REE and stable isotope study. Geochimica et Cosmochimica Acta 156, 50–74.

Jenkins, R.G., Kaim, A., Little, C.T.S., Iba, Y., Tanabe, K., Campbell, K.A., 2013. Worldwide distribution of the modiomorphid bivalve genus *Caspiconcha* in late Mesozoic hydrocarbon seeps. Acta Palaeontologica Polonica 58, 357–382.

Jolivet, L., Tamaki, K., 1992. Neogene kinematics in the Japan Sea region and volcanic activity of the northeast Japan arc. In: Tamaki, K., Suyehiro, K., Allan, J., et al. (Eds.), Proceedings of the Ocean Drilling Program, Scientific Results, Vol. 127/128 (Part 2). Ocean Drilling Program, College Station, TX, pp. 1311–1331.

Judd, A., Hovland, M., 2007. Seabed Fluid Flow. Cambridge University Press, New York, 475 pp.

Kaim, A., Skupien, P., Jenkins, R.G., 2013. A new Lower Cretaceous hydrocarbon seep locality from the Czech Carpathians and its fauna. Palaeogeography, Palaeoclimatology, Palaeoecology 390, 42–51.

Kawagucci, S., Toki, T., 2010. Origin of methane in subseafloor geofluid systems. Chikyukagaku (Geochemistry) 44, 137–154. (in Japanese with English abstract)

Kennicutt II, M.C., Brooks, J.M., Bidigare, R.R., Fay, R.R., Wade, T.L., McDonald, J., 1985. Vent-type taxa in a hydrocarbon seep region on the Louisiana slope. Nature 317, 351–353.

Kiel, S., 2013. Lucinid bivalves from ancient methane seeps. Journal of Molluscan Studies 79, 346–363.

Kiel, S., Amano, K., 2013. The earliest Bathymodiolin mussels: an evaluation of Eocene and Oligocene taxa from deep-sea methane seep deposits in western Washington State, USA. Journal of Paleontology 87, 589–602.

Kiel, S., Birgel, D., Campbell, K.A., Crampton, J.S., Schiøler, P., Peckmann, J., 2013. Cretaceous methane-seep deposits from New Zealand and their fauna. Palaeogeography, Palaeoclimatology, Palaeoecology 390, 17–34.

Kiel, S., Glodny, J., Birgel, D., Bulot, L.G., Campbell, K.A., Gaillard, C., Graziano, R., Kaim, A., Lazăr, L., Sandy, M.R., Peckmann, J., 2014. The paleoecology, habitats,

and stratigraphic range of the enigmatic Cretaceous brachiopod *Peregrinella*. PLoS ONE 9(10), e109260.

Kiel, S., Krystyn, L., Demirtaş, F., Koşun, E., Peckmann, J., 2017. Late Triassic mollusk-dominated hydrocarbon-seep deposits from Turkey. Geology 45, 751–754.

Kiel, S., Little, C.T.S., 2006. Cold-seep mollusks are older than the general marine mollusk fauna. Science 313, 1429–1431.

Kiel, S., Peckmann, J., 2007. Chemosymbiotic bivalves and stable carbon isotopes indicate hydrocarbon seepage at four unusual Cenozoic fossil localities. Lethaia 40, 345–357.

Kiel, S., Peckmann, J., 2008. Paleoecology and evolutionary significance of an Early Cretaceous *Peregrinella*-dominated hydrocarbon-seep deposit on the Crimean Peninsula. Palaios 23, 751–759.

Kikuchi, Y., Tono, S., Funayama, M., 1991. Petroleum resources in the Japanese island-arc setting. Episodes 14, 236–241.

Kulm, L.D., Suess, E., Moore, J.C., Carson, B., Lewis, B.T., Ritger, S.D., Kadko, D.C., Thornburg, T.M., Embley, R.W., Rugh, W.D., Massoth, G.J., Langseth, M.G., Cochrane, G.R., Scamman, R.L., 1986. Oregon subduction zone: venting, fauna, and carbonates. Science 231, 561–566.

Lein, A., Vogt, P., Crane, K., Egorov, A., Ivanov, M., 1999. Chemical and isotopic evidence for the nature of the fluid in CH_4-containing sediments of the Håkon Mosby Mud Volcano. Geo-Marine Letters 19, 76–83.

Little, C.T.S., Birgel, D., Boyce, A.J., Crame, J.A., Francis, J.E., Kiel, S., Peckmann, J., Pirrie, D., Rollinson, G.K., Witts, J.D., 2015. Late Cretaceous (Maastrichtian) shallow water hydrocarbon seeps from Snow Hill and Seymour Islands, James Ross Basin, Antarctica. Palaeogeography, Palaeoclimatology, Palaeoecology 418, 213–228.

Lorenson, T.D., Collet, T.S., 2000. Gas content and composition of gas hydrate from sediments of the southeastern North American continental margin. In: Paull, C.K., Matsumoto, R., Wallace, P.J., Dillon, W.P. (Eds.), Proceedings of the Ocean Drilling Program, Scientific Results vol. 164, Ocean Drilling Program, College Station, TX, pp. 37–46.

Majima, R., Kase, T., Kawagata, S., Aguilar, Y.M., Hagino, K., Maeda, M., 2007. Fossil cold-seep assemblages from Leyte Island, Philippines. Journal of Geography 116, 643–652. (in Japanese with English abstract)

Marlow, J., Peckmann, J., Orphan, V., 2015. Autoendoliths: a distinct type of rock-hosted microbial life. Geobiology 13, 303–307.

Matos, S.A., Warren, L.V., Fürsich, F.T., Alessandretti, L., Assine, M.L., Riccomini, C., Simões, M.G., 2017. Paleoecology and paleoenvironments of Permian bivalves of the Serra Alta Formation, Brazil: ordinary suspension feeders or Late Paleozoic Gondowana seep organisms? Journal of South American Earth Sciences 77, 21–41.

Matsumoto, R., Okuda, Y., Hiruta, A., Tomaru, H., Takeuchi, E., Sanno, R., Suzuki, M., Tsuchinaga, K., Ishida, Y., Ishizaki, O., Takeuchi, R., Komatsubara, J., Freire, A.F., Machiyama, H., Aoyama, C., Joshima, M., Hiromatsu, M., Snyder, G., Numanami, H., Satoh, M., Matoba, Y., Nakagawa, H., Kakuwa, Y., Ogihara, S., Yanagawa, K., Sunamura, M., Goto, T., Lu, H., Kobayashi, T., 2009. Formation and collapse of gas hydrate deposits in high methane flux area of the Joetsu basin, eastern margin of Japan Sea. Journal of Geography 118, 43–71. (in Japanese with English abstract)

McCollom, T.M., Seewald, J.S., 2007. Abiotic synthesis of organic compounds in deep-sea hydrothermal environments. Chemical Reviews 107, 382–401.

Michaelis, W., Seifert, R., Nauhaus, K., Treude, T., Thiel, V., Blumenberg, M., Knittel, K., Gieseke, A., Peterknecht, K., Pape, T., Boetius, A., Amann, R., Jørgensen, B.B., Widdel, F., Peckmann, J., Pimenov, N.V., Gulin, M.B., 2002. Microbial reefs in the Black Sea fueled by anaerobic oxidation of methane. Science 297, 1013–1015.

Milkov, A.V., 2005. Molecular and stable isotope compositions of natural gas hydrates:

a revised global dataset and basic interpretations in the context of geological settings. Organic Geochemistry 36, 681–702.

Monzawa, N., Kaneko, M., Osawa, M., 2006. A review of petroleum system in the deep water area of the Toyama Trough to the Sado Island in the Japan Sea, based on the results of the METI Sado Nansei Oki drilling. Journal of the Japanese Association for Petroleum Technology 71, 618–627. (in Japanese with English abstract)

Natalicchio, M., Peckmann, J., Birgel, D., Kiel, S., 2015. Seep deposits from northern Istria, Croatia: a first glimpse into the Eocene seep fauna of the Tethys region. Geological Magazine 152, 444–459.

Okamura, Y., Watanabe, M., Morijiri, R., Satoh, M., 1995. Rifting and basin inversion in the eastern margin of the Japan Sea. Island Arc 4, 166–181.

Okui, A., Kaneko, M., Nakanishi, S., Monzawa, N., Yamamoto, H., 2008. An integrated approach to understanding the petroleum system of a frontier deep-water area, offshore Japan. Petroleum Geoscience 14, 223–233.

O'Reilly, S.S., Hryniewicz, K., Little, C.T.S., Monteys, X., Szpak, M.T., Murphy, B.T., Jordan, S.F., Allen, C.C.R., Kelleher, B.P., 2014. Shallow water methane-derived authigenic carbonates mounds at the Codling Fault Zone, western Irish Sea. Marine Geology 357, 139–150.

Panieri, G., Bünz, S., Fornari, D.J., Escartin, J., Serov, P., Jansson, P., Torres, M.E., Johnson, J.E., Hong, W.L., Sauer, S., Garcia, R., Gracias, N., 2017. An integrated view of the methane system in the pockmarks at Vestnesa Ridge, 79°N. Marine Geology 390, 282–300.

Pape, T., Bahr, A., Rethemeyer, J., Kessler, J.D., Sahling, H., Hinrichs, K.-U., Klapp, S.A., Reeburgh, W.S., Bohrmann, G., 2010b. Molecular and isotopic partitioning of low-molecular-weight hydrocarbons during migration and gas hydrate precipitation in deposits of a high-flux seepage site. Chemical Geology 269, 350–363.

Pape, T., Geprägs, P., Hammerschmidt, S., Wintersteller, P., Wei, J., Fleischmann, T., Bohrmann, G., Kopf, A.J., 2014. Hydrocarbon seepage and its sources at mud volcanoes of the Kumano forearc basin, Nankai Trough subduction zone. Geochemistry, Geophysics, Geosystems 15, 2180–2194.

Pape, T., Kasten, S., Zabel, M., Bahr, A., Abegg, F., Hohnberg, H-J., Bohrmann, G., 2010a. Gas hydrates in shallow deposits of the Amsterdam mud volcano, Anaximander Mountains, Northeastern Mediterranean Sea. Geo-Marine Letters 30, 187–206.

Paull, C.K., Hecker, B., Commeau, R., Freeman-Lynde, R.P., Neumann, C., Corso, W.P., Golubic, S., Hook, J.E., Sikes, E., Curray, J., 1984. Biological communities at the

Florida Escarpment resemble hydrothermal vent taxa. Science 226, 965–967.

Paull, C.K., Martens, C.S., Chanton, J.P., Neumann, A.C., Coston, J., Jull, A.J.T., Toolin, L.J., 1989. Old carbon in living organisms and young $CaCO_3$ cements from abyssal brine seeps. Nature 342, 166–168.

Peckmann, J., Campbell, K.A., Walliser, O.H., Reitner, J., 2007. A Late Devonian hydrocarbon-seep deposit dominated by dimerelloid brachiopods, Morocco. Palaios 22, 114–122.

Peckmann, J., Gischler, E., Oschmann, W., Reitner, J., 2001. An Early Carboniferous seep community and hydrocarbon-derived carbonates from the Harz Mountains, Germany. Geology 29, 271–274.

Peckmann, J., Goedert, J.L., Heinrichs, T., Hoefs, J., Reitner, J., 2003. The late Eocene 'Whiskey Creek' methane-seep deposit (western Washington State) Part II: petrology, stable isotopes, and biogeochemistry. Facies 48, 241–254.

Peckmann, J., Goedert, J.L., Thiel, V., Michaelis, W., Reitner, J., 2002. A comprehensive approach to the study of methane-seep deposits from the Lincoln Creek Formation, western Washington State, USA. Sedimentology 49, 855–873.

Peckmann, J., Kiel, S., Sandy, M.R., Taylor, D.G., Goedert, J.L., 2011. Mass occurrences of the brachiopod *Halorella* in Late Triassic methane-seep deposits,

eastern Oregon. Journal of Geology 119, 207–220.

Peckmann, J., Sandy, M.R., Taylor, D.G., Gier, S., Bach, W., 2013. An Early Jurassic brachiopod-dominated seep deposit enclosed by serpentinite, eastern Oregon, USA. Palaeogeography, Palaeoclimatology, Palaeoecology 390, 4–16.

Peckmann, J., Thiel, V., 2004. Carbon cycling at ancient methane-seeps. Chemical Geology 205, 443–467.

Peckmann, J., Thiel, V., Michaelis, W., Clari, P., Gaillard, C., Martire, L., Reitner, J., 1999. Cold seep deposits of Beauvoisin (Oxfordian; southeastern France) and Marmorito (Miocene; northern Italy): microbially induced authigenic carbonates. International Journal of Earth Sciences 88, 60–75.

Pierre, C., Demange, J., Blanc-Valleron, M.-M., Dupré, S., 2017. Authigenic carbonate mounds from active methane seeps on the southern Aquitaine Shelf (Bay of Biscay, France): evidence for anaerobic oxidation of biogenic methane and submarine groundwater discharge during formation. Continental Shelf Research 133, 13–25.

Pohlman, J.W., Canuel, E.A., Ross Chapman, N., Spence, G.D., Whiticar, M.J., Coffin, R.B., 2005. The origin of thermogenic gas hydrates on the northern Cascadia Margin as inferred from isotopic ($^{13}C/^{12}C$ and D/H) and molecular composition of hydrate and vent gas. Organic Geochemistry 36, 703–716.

Prouty, N.G., Sahy, D., Ruppel, C.D., Roark, E.B., Condon, D., Brooke, S., Ross, S.W., Demopoulos, A.W.J., 2016. Insights into methane dynamics from analysis of authigenic and chemosynthetic mussels at newly-discovered Atlantic Margin seeps. Earth and Planetary Science Letters 449, 332–344.

Reeburgh, W.S., 1976. Methane consumption in Cariaco Trench waters and sediments. Earth and Planetary Science Letters 28, 337–344.

Ritger, S., Carson, B., Suess, E., 1987. Methane-derived authigenic carbonates formed by subduction-induced pore-water expulsion along the Oregon/Washington margin. Geological Society of America Bulletin 98, 147–156.

Roberts, H.H., Aharon, P., 1994. Hydrocarbon-derived carbonate buildups of the northern Gulf of Mexico continental slope: a review of submersible investigations. Geo-Marine Letters 14, 135–148.

Römer, M., Torres, M., Kasten, S., Kuhn, G., Graham, A.G.C., Mau, S., Little, C.T.S., Linse, K., Pape, T., Geprägs, P., Fischer, D., Wintersteller, P., Marcon, Y., Rethemeyer, J., Bohrmann, G., shipboard scientific party ANT-XXIX/4, 2014. First evidence of widespread active methane seepage in the Southern Ocean, off the sub-Antarctic island of South Georgia. Earth and Planetary Science Letters 403, 166–177.

Sassen, R., Roberts, H.H., Carney, R., Milkov, A.V., DeFreitas, D.A., Lanoil, B., Zhang, C., 2004. Free hydrocarbon gas, gas hydrate, and authigenic minerals in chemosynthetic communities of the northern Gulf of Mexico continental slope: relation to microbial processes. Chemical Geology 205, 195–217.

Sato, H., 1994. The relationship between late Cenozoic tectonic events and stress field and basin development in northeast Japan. Journal of Geophysical Research 99(B11), 22261–22274.

Sauer, S., Knies, J., Lepland, A., Chand, S., Eichinger, F., Schubert, C.J., 2015. Hydrocarbon sources of cold seeps off the Vesterålen coast, northern Norway. Chemical Geology 417, 371–382.

Schmidt, M., Botz, R., Winn, K., Stoffers, P., Thiessen, O., Herzig, P., 2002. Seeping hydrocarbons and related carbonate mineralisations in sediments south of Lihir Island (New Ireland fore arc basin, Papua New Guinea). Chemical Geology 186, 249–264.

Sibuet, M., Olu, K., 1998. Biogeography, biodiversity and fluid dependence of deep-sea cold-seep communities at active and passive margins. Deep-Sea Research II 45, 517–567.

Smrzka, D., Zwicker, J., Kolonic, S., Birgel, D., Little, C.T.S., Marzouk, A.M., Chellai,

E.H., Wagner, T., Peckmann, J., 2017. Methane seepage in a Cretaceous greenhouse world recorded by an unusual carbonate deposit from the Tarfaya Basin, Morocco. Depositional Record 3, 4–37.

Stadnitskaia, A., Ivanov, M.K., Blinova, V., Kreulen, R., van Weering, T.C.E., 2006. Molecular and carbon isotopic variability of hydrocarbon gases from mud volcanoes in the Gulf of Cadiz, NE Atlantic. Marine and Petroleum Geology 23, 281–296.

Stadnitskaia, A., Muyzer, G., Abbas, B., Coolen, M.J.L., Hopmans, E.C., Baas, M., van Weering, T.C.E., Ivanov, M.K., Poludetkina, E., Sinninghe Damsté, J.S., 2005. Biomarker and 16S rDNA evidence for anaerobic oxidation of methane and related carbonate precipitation in deep-sea mud volcanoes of the Sorokin Trough, Black Sea. Marine Geology 217, 67–96.

Suda, K., Gilbert, A., Yamada, K., Yoshida, N., Ueno, Y., 2017. Compound- and position-specific carbon isotopic signatures of abiogenic hydrocarbons from on-land serpentinite-hosted Hakuba Happo hot spring in Japan. Geochimica et Cosmochimica Acta 206, 201–215.

Suess, E., 2014. Marine cold seeps and their manifestations: geological control, biogeochemical criteria and environmental conditions. International Journal of Earth Sciences 103, 1889–1916.

Suess, E., Torres, M.E., Bohrmann, G., Collier, R.W., Greinert, J., Linke, P., Rehder, G., Trehu, A., Wallmann, K., Winckler, G., Zuleger, E., 1999. Gas hydrate destabilization: enhanced dewatering, benthic material turnover and large methane plumes at the Cascadia convergent margin. Earth and Planetary Science Letters 170, 1–15.

Takano, O., 2002. Changes in depositional systems and sequences in response to basin evolution in a rifted and inverted basin: an example from the Neogene Niigata-Shin'etsu basin, Northern Fossa Magna, central Japan. Sedimentary Geology 152, 79–97.

Taylor, J.D., Glover, E.A., 2010. Chemosymbiotic bivalves. In: Kiel, S. (Ed.), The Vent and Seep Biota. Topics in Geobiology. Springer, Heidelberg, pp. 107–135.

Teichert, B.M.A., Bohrmann, G., Suess, E., 2005. Chemoherms on Hydrate Ridge—Unique microbially-mediated carbonate build-ups growing into the water column. Palaeogeography, Palaeoclimatology, Palaeoecology 227, 67–85.

Toki, T., Uehara, Y., Kinjo, K., Ijiri, A., Tsunogai, U., Tomaru, H., Ashi, J., 2012. Methane production and accumulation in the Nankai accretionary prism: results from IODP Expeditions 315 and 316. Geochemical Journal 46, 89–106.

Tong, H.P., Chen, D.F., 2012. First discovery and characterizations of late Cretaceous

seep carbonates from Xigaze in Tibet, China. Chinese Science Bulletin 57, 4363–4372.

Whiticar, M.J., 1999. Carbon and hydrogen isotope systematics of bacterial formation and oxidation of methane. Chemical Geology 161, 291–314.

Wiedicke, M., Sahling, H., Delisle, G., Faber, E., Neben, S., Beiersdorf, H., Marchig, V., Weiss, W., von Mirbach, N., Afiat, A., 2002. Characteristics of an active vent in the fore-arc basin of the Sunda Arc, Indonesia. Marine Geology 184, 121–141.

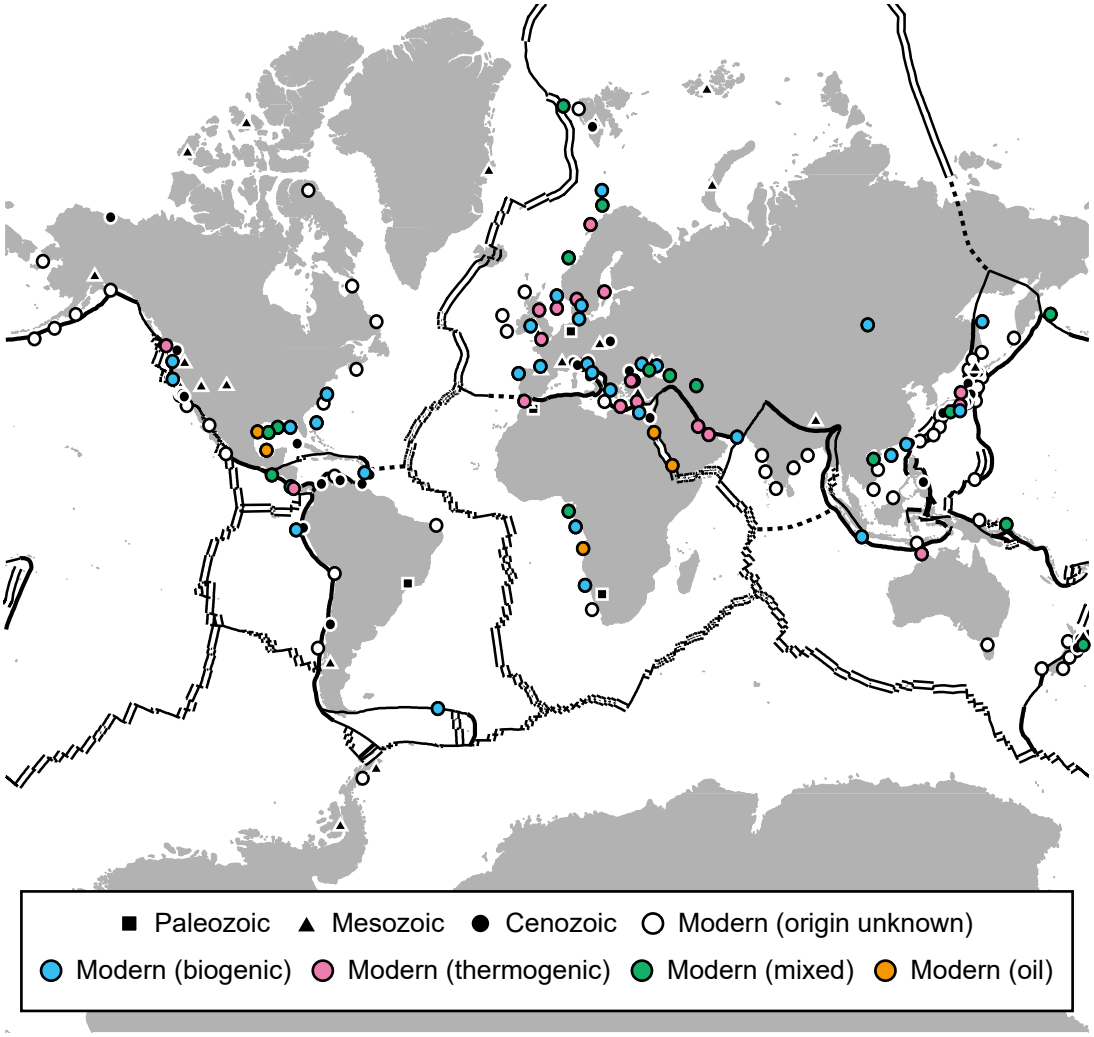

Fig. P.1. Worldwide distribution of modern and ancient cold seeps. The origin of methane at some modern seeps is indicated by colors. "Mixed" indicates a mixed origin between biogenic and thermogenic methane. Note the dense report of both modern and ancient seep sites around the Japanese Islands with respect to other regions in the world. The distribution and origin of modern seeps are from Paull et al. (1989), Brooks et al. (1991), Bohrmann et al. (1998), Lein et al. (1999), Suess et al. (1999), Lorenson and Collett (2000), Hovland (2002), Michaelis et al. (2002), Schmidt et al. (2002), Wiedicke et al. (2002), Sassen et al. (2004), Hovland et al. (2005), Milkov (2005), Pohlman et al. (2005), Stadnitskaia et al. (2005, 2006), Campbell (2006), Judd and Hovland (2007), Bourry et al. (2009), Hachikubo et al. (2009), Matsumoto et al. (2009), Pape et al. (2010a, b), Birgel et al. (2011), Toki et al. (2012), O'Reilly et al. (2014), Römer et al. (2014), Himmler et al. (2015), Crémière et al. (2016a, b), Prouty et al. (2016), Panieri et al. (2017), and Pirre et al. (2017). The distribution of ancient seeps is from Gill et al. (2005), Campbell (2006), De Boever et al. (2006), Bojanowski (2007), Majima et al. (2007), Kiel and Peckmann (2007, 2008), Himmler et al. (2008), Hammer et al. (2011), Peckmann et al. (2011, 2013), Tong and Chen (2012), Agirrezabala et al. (2013), Chien et al. (2013), Kaim et al. (2013), Kiel et al. (2013, 2014, 2017), Hryniewicz et al. (2015, 2016), Little et al. (2015), Natalicchio et al. (2015), Matos et al. (2017), and Smrzka et al. (2017).

Part 1. Constraining the origin of methane at ancient methane seeps based on carbon isotopic compositions of lipid biomarkers

1.1. Introduction

The origin of methane at ancient methane seeps has been roughly inferred from the carbon isotopic compositions of methane-seep carbonates. The seep carbonates are precipitated from bicarbonate ions produced by the anaerobic oxidation of methane (AOM, see Preface III). The stable carbon isotopic compositions of the seep carbonates therefore reflect those of the oxidized methane. The selective uptake of ^{13}C-depleted methane during the AOM should result in bicarbonate more enriched in ^{12}C than the parent methane, with isotope fractionation factors (α) of 1.002 to 1.039 (Whiticar and Faber, 1986; Alperin et al., 1988; Martens et al., 1999; Reeburgh, 2007; Holler et al., 2009). However, it is well known that the carbon isotopic compositions of bicarbonate in the AOM zone and the seep carbonates are often more ^{13}C-enriched than the parent methane, as a result of the mixing with bicarbonate from other sources. The other sources of bicarbonate include the inorganic carbon dissolved in seawater ($\delta^{13}C$ = ~0‰) and the sulfate reduction of sedimentary organic matter ($\delta^{13}C$ values typically range from −25‰ to −20‰) (e.g., Ritger et al., 1987; Suess and Whiticar, 1989; Formolo et al., 2004; Crémière et al., 2012). The mixing ratio, or relative contribution of each

bicarbonate source to the carbon isotopic compositions of the carbonates, can vary depending on environmental factors such as the organic content in sediments, input of heavier hydrocarbons than methane, and probably fluid flow rate (Formolo et al., 2004; Joye et al., 2004; Peckmann et al., 2009; Crémière et al., 2016). The mixing ratio also varies among carbonates at a certain seep site and even within a single carbonate crystal (Bojanowski et al., 2015). The mixing with bicarbonate from other sources makes it difficult to estimate the carbon isotopic compositions of methane contained in the ancient seep fluids based on the $\delta^{13}C$ values of the carbonates alone.

In this chapter of the thesis, the origin of methane at ancient seeps is estimated using carbon isotopic compositions of lipid biomarkers of the anaerobic methane-oxidizing archaea (ANME). The stable carbon isotopic composition of an organism is dictated primarily by the isotopic composition of the carbon source and kinetic isotope effects that depend on the process by which the carbon is assimilated (Pancost and Sinninghe Damsté, 2003). The carbon isotopic composition of lipids is further controlled by isotope effects during biosynthesis. The isotopic composition of carbon source can thus be estimated based on that of lipids, if the net isotope effects during biosynthesis are known. Lipids of ANME from methane-seep environments often show extremely low $\delta^{13}C$ values, ranging from −140‰ to −55‰ (mostly <−60‰) (Niemann

et al., 2005; Londry et al., 2008; Niemann and Elvert, 2008; Haas et al., 2010). This has been thought to be the result of methane-derived carbon uptake by the archaea, although carbon assimilation pathways of ANME remain not fully understood (Blumenberg et al., 2005; Nauhaus et al., 2007; Wegener et al., 2008). Most lipid biomarkers of ANME are present also in methanogenic archaea, but they can be distinguished from those of methanogens by their $\delta^{13}C$ values lower than −60‰, indicating methane consumption (Londry et al., 2008; but see Summons et al., 1998; Alperin and Hoehler, 2009). Although the isotope fractionation factor between methane and archaeal lipids has not yet been verified by culture experiments, carbon isotope offset ($\Delta\delta^{13}C_{methane-lipid}$) can be calculated based on $\delta^{13}C$ values of methane and biomarkers obtained from modern methane seeps (Niemann and Elvert, 2008). The $\Delta\delta^{13}C_{methane-lipid}$ values can be useful to estimate $\delta^{13}C$ values of source methane contained in the seep fluids (Niemann and Elvert, 2008; Birgel et al., 2011; Himmler et al., 2015). However, the $\Delta\delta^{13}C_{methane-lipid}$ values have not yet been applied to estimate the origin of methane at ancient seeps. Large variations have been reported for the $\Delta\delta^{13}C_{methane-lipid}$ values, which could be partly attributed to the fact that the $\delta^{13}C$ values of methane and biomarkers are not measurements from the same samples (Niemann and Elvert, 2008) and possibly to regional variation. The $\Delta\delta^{13}C_{methane-lipid}$ values proper to be applied to ancient seeps

thus remain unclear. This study tried to calculate the carbon isotope offset between methane and the ANME biomarkers at the same modern methane-seep site in the Japan Sea, which is applicable to ancient seeps along the Japan Sea coast. In addition, a single regression analysis was performed to formulate regression lines that are more generally applicable to predict the carbon isotopic composition of methane based on that of the ANME biomarkers, using literature data as well as the data in the Japan Sea.

1.2. Material

1.2.1. Modern methane-seep carbonates and literature data

Modern methane-seep carbonates for biomarker analysis were collected from the seafloor at the Umitaka Spur central seep site, offshore Joetsu City, Niigata Prefecture (Fig. 1.1 and Appendix). The $\delta^{13}C$ value of methane seeping at this site is known through previous works (Hachikubo et al., 2015). In addition, 19 modern methane-seep sites where both the carbon isotopic compositions of methane and ANME biomarkers are known were compiled based on literature, as listed in Table 1.1. Data in which methane and biomarkers had been examined at separate sites in the same region were excluded.

1.2.2. Ancient seep carbonates

Carbonate rock samples were collected at 11 sites along the Japan Sea coast ranging from the lower Miocene to Middle Pleistocene (Figs. 1.1 and 1.2). The study sites include: Fukusaki, Kanoura, and Tanohama sites, the Burdigalian Taishu Group; Takinoue site, the Langhian part of the Takinoue Formation; Anazawa/Akanuda and Sorimachi sites, the Serravallian part of the Bessho Formation; Kuroiwa site, the Tortonian part of the Ogaya Formation; Nakanomata 1 and 2 sites, the Tortonian or Messinian part of the Nodani Formation; Matsunoyama site, the Zanclean Tamugigawa Formation; and Anden site, the Middle Pleistocene Wakimoto Formation. These sites have been identified as ancient methane-seep sites, based on paleontological, petrographic, and geochemical characters of the carbonates (see Appendix). The study sites are underlain by over 1-km-thick sediments (Fig. 1.2).

1.3. Analytical methods

1.3.1. Calculation of carbon isotope offset and regression analysis

This study focused on isoprenoid hydrocarbons, i.e., PMI (2,6,10,15,19-pentamethylicosane) and crocetane (2,6,11,15-tetramethylhexadecane), because these compounds are the most common biomarkers for ANME at methane-seep environments

(e.g., Peckmann and Thiel, 2004; Blumenberg, 2010) and they are known to have higher potential for preservation in ancient samples compared with ether biomarkers such as archaeol (Blumenberg, 2010). The $\delta^{13}C$ value of PMI preserved within the Umitaka Spur seep carbonate was analyzed as described in section 1.3.3, and used to calculate the carbon isotope offset ($\Delta\delta^{13}C_{methane - PMI}$ value) at the Umitaka Spur as follows:

$$\Delta\delta^{13}C_{methane - PMI} = \delta^{13}C_{methane} - \delta^{13}C_{PMI}.$$

This isotope offset was applied to estimate the carbon isotopic composition of methane based on that of the ANME biomarkers at the ancient seeps along the Japan Sea coast, assuming that the isotope offset was similar in the past in this area. The $\Delta\delta^{13}C_{methane - PMI}$ and $\Delta\delta^{13}C_{methane - crocetane}$ values were calculated also based on the literature data (Table 1.1).

Combining the data from the Umitaka Spur and the literature (Table 1.1), a single regression analysis was performed using Microsoft Excel 2016, in which isotopic compositions (mean values were used) of methane are dependent and those of the lipid biomarkers (PMI or crocetane) are independent variables. Regression lines were calculated by a least-squares method to predict $\delta^{13}C$ values of methane based on those of the biomarkers with 95% prediction intervals. The 95% prediction interval of $\delta^{13}C$ values was calculated as the product of standard error of prediction and critical value of

t statistic with $\alpha = 0.025$ with $n-2$ degrees of freedom, where n is sample size.

1.3.2. Petrographic and stable carbon and oxygen isotopic analyses of carbonates

To identify early-diagenetic carbonate phases (described below), petrographic examination and stable carbon and oxygen isotope analysis of the carbonate samples were performed prior to biomarker analyses. The carbon and oxygen isotopes were used also to assess diagenetic alterations of the carbonates and the origin of methane estimated using biomarkers. Cut slabs of the carbonate rocks were polished using carborundum abrasives and were scanned. Thin sections (48 × 28 mm or 76 × 52 mm, ~30 μm thick) were then prepared and were examined using a polarizing microscope under plane- and cross-polarized light.

Powdered samples were collected from selected slabs using a hand-held rotary micromill. X-ray diffraction (XRD) analysis was then carried out on the powders using a diffractometer with CuKα radiation (Rigaku SmartLab) at the Department of Geology and Mineralogy, Kyoto University (DGMKU), Japan, to determine the mineralogy of the carbonates. Scans were run at 40 kV and 40 mA over a scanning range of 5 to 70° 2θ, at a rate of 10°/min and with a step size of 0.04° 2θ. The magnesium concentration of the calcite phases was inferred from the positions of the (104) peaks, in accordance

with Griffin (1971). Calcite containing <5 mol% $MgCO_3$ is referred to as low-Mg calcite, and calcite containing 5–20 mol% $MgCO_3$ is referred to as high-Mg calcite (Burton and Walter, 1987).

Powdered samples for carbon and oxygen isotope analyses were collected from the counterparts of the thin sections or other cut slabs using a hand-held micromill and a high-precision micromill (Izumo-Web Geomill 326) equipped with a computer-controlled microdrill. Some samples were prepared by crushing and grinding cut chips. Samples were taken from early-diagenetic carbonate phases recognized during thin section observation. Samples from the Fukusaki, Kanoura, Tanohama, and Umitaka Spur sites were analyzed by a Thermo Scientific GasBench II/Delta V Advantage isotope ratio mass spectrometer (IRMS) at the Laboratory of Evolution of Earth Environment, Kanazawa University (LEEKU), Kanazawa, Japan. The powders (~300–500 μg) were reacted with orthophosphoric acid in a glass vial under vacuum at 70°C in an online GasBench II system. The produced CO_2 was analyzed in a continuous-flow Delta V Advantage IRMS. Samples from the Takinoue and Anden sites were analyzed by an Isoprime MultiPrep/IsoPrime IRMS at the Japan Agency for Marine-Earth Science and Technology (JAMSTEC), Yokosuka, Japan. The samples (~30–95 μg) were reacted with orthophosphoric acid in a glass vial under vacuum at 90°C for 1000 s in an

online MultiPrep system. The produced CO_2 was analyzed in a dual-inlet IsoPrime IRMS. Samples from the remaining study sites were analyzed using the same instrument (MultiPrep/IsoPrime100) at the DGMKU (reported in Miyajima et al., 2016). All isotope values are reported as a per-mil difference between the sample and a Vienna Pee Dee Belemnite (VPDB) standard in delta notation ($[\delta = R_{sample}/R_{standard} - 1] \times 1000$, where R is the ratio of minor to major isotopes). The values measured by GasBench II/Delta V Advantage and by MultiPrep/IsoPrime were both calibrated with the international standard NBS19. The standard deviations of replicate analyses of NBS19 and working standards LSVEC and JLs-1 by GasBench II/Delta V Advantage were better than 0.18‰ and 0.13‰ for $\delta^{13}C$ and $\delta^{18}O$, respectively. The standard deviations of replicate analyses of a working standard of JAMSTEC (JAMSTEC-WS), which is composed of calcite, by MultiPrep/IsoPrime were better than 0.22‰ and 0.23‰ for $\delta^{13}C$ and $\delta^{18}O$, respectively. In this chapter, $\delta^{13}C$ and $\delta^{18}O$ data from late-diagenetic phases that could have not originated from the AOM are not presented, such as calcite veins with high $\delta^{13}C$ and low $\delta^{18}O$ values.

1.3.3. Biomarker analyses

Lipid biomarker analyses were performed on samples containing the early-

diagenetic phases. After removal of weathered surfaces, small pieces of rock were washed in distilled water and then in methanol (MeOH) and dichloromethane (DCM) using an ultrasonic bath for 10 min. The washed pieces were crushed into fine chips using an iron hammer, and then powdered using a tungsten mortar and pestle. Lipids were extracted from ~20 g of powdered sample by ultrasonication with DCM:MeOH (7:3, v:v) for 15 min, and separated after centrifugation for 20 or 30 min. Lipids were extracted from the residual powders in the same way two more times and were combined. Lipid extraction from the Fukusaki, Tanohama, and Kanoura samples (~10 g powders) was performed by a Thermo Scientific Accelerated Solvent Extractor System (Dionex ASE 350) at the LEEKU, using DCM as a solvent. For another ~10 g powder of a sample from Tanohama, hexane-washed distilled water was added to the powder and 1N HCl was slowly poured to dissolve the carbonate. After the carbonate was dissolved, lipids were separated by adding hexane:DCM (9:1, v:v) and centrifuging for 10 min (three cycles). The separated solvents were washed with hexane-washed distilled water and were combined. After removing elemental sulfur, the aliphatic hydrocarbon fractions of the extracted lipids were obtained through a silica gel column with *n*-hexane. The aromatic, ketone, and polar fractions separated with DCM and MeOH were not examined in this study. Finally, the hydrocarbon fractions were diluted with 200 μL

of *n*-hexane after drying. Individual compounds were detected using a gas chromatograph-mass spectrometer (SHIMADZU GCMS-QP2010) equipped with a HP-5MS capillary column (30 m × 0.25 mm × 0.25 μm; Agilent Technologies) at the LEEKU. The column oven temperature was increased from 50°C to 120°C at 30°C/min, then from 120°C to 310°C at 3.0°C/min, and kept at 310°C for 15 min. The splitless system inlet was kept at 310°C. Compounds were identified based on comparison of retention times and mass spectra with published data (e.g., Elvert et al. 1999 for PMI; Ogihara et al. 2003 for crocetane and phytane). Since crocetane is co-eluting with phytane, its presence was identified based on mass spectrum.

Stable carbon isotope compositions of the biomarkers were measured with a gas chromatograph-isotope ratio mass spectrometer (GC-IRMS: Thermo Scientific Delta V Advantage interfaced with a Thermo Scientific Trace GC Ultra through a GC Isolink) at the LEEKU. Each compound was combusted at 1030°C to make CO_2 gas. The configuration of the gas chromatograph was generally similar to that of the GC-MS, except that a DB-5MS capillary column (60 m × 0.25 mm × 0.10 μm; Agilent Technologies) was used. During sample measurement, a standard *n*-alkane mixture (C_{17}, C_{18}, C_{20}, C_{24}, C_{28}, and C_{32} with $\delta^{13}C$ values of −32.45‰ to −26.88‰ vs. VPDB) was measured one or two times per day for calibration. Because the biomarkers of methane-

oxidizing archaea show strongly ^{13}C-depleted carbon isotope compositions, a linear extrapolation of the calibration line from the standard measurements was used to calculate the isotope compositions of the samples. Carbon isotope compositions are given in δ notation ($\delta^{13}C$‰ vs. VPDB) after calibration.

1.4. Results

1.4.1. Carbon isotope offset and regression analysis between methane and ANME biomarkers

A lipid biomarker PMI was extracted from the modern seep carbonate at the Umitaka Spur, with a $\delta^{13}C$ value of −80‰. The $\delta^{13}C$ value of seep methane at the Umitaka Spur central seep was measured as −36.0‰ in average (n = 6; Hachikubo et al., 2015). The carbon isotope offset ($\Delta\delta^{13}C_{methane - PMI}$ value) between the methane and PMI at this site can thus be calculated as 44‰. Another biomarker crocetane was also detected from the Umitaka Spur carbonate, but its low concentration prevented determination of the carbon isotopic composition. Therefore, the carbon isotope offset between the methane and crocetane at this site could not be calculated.

Compilation of the literature data shows that the $\Delta\delta^{13}C_{methane - PMI}$ values range between 8‰ and 68‰ (average 40‰, n = 22 including Umitaka Spur), and the

$\Delta\delta^{13}C_{methane - crocetane}$ values range between 4‰ and 60‰ (average 36‰, n = 16) (Fig. 1.3A and Table 1.1). Despite the large variation, the $\Delta\delta^{13}C$ values are mostly within 30‰–60‰ in average.

The regression lines for the $\delta^{13}C$ values of methane and biomarkers (Table 1.1) were obtained as (Fig. 1.3B):

$$\delta^{13}C_{methane} = 0.35 \times \delta^{13}C_{PMI} - 26.48 \ (r^2 = 0.44),$$

$$\delta^{13}C_{methane} = 0.23 \times \delta^{13}C_{crocetane} - 39.59 \ (r^2 = 0.45).$$

The data for PMI and crocetane yielded a similar coefficient of determination (r^2).

1.4.2. Petrography and carbon and oxygen isotopic compositions of carbonates

The matrix of the studied carbonate rocks is composed mostly of microcrystalline calcite (micrite) or aragonite, which encloses detrital grains and animal fossils. Millimeter- to centimeter-scale void spaces within the microcrystalline matrix are rimmed with acicular to fibrous calcite or aragonite cements at the Nakanomata 1 seep (Fig. 1.4A). At the Takinoue seep, the void spaces are filled with pinkish micritic cements, instead of acicular cements (see Appendix). The above-mentioned carbonate phases that cement the matrix and void spaces are known as early-diagenetic phases in methane-seep carbonates, which originated from the AOM (e.g., Campbell et al., 2002;

Kiel et al., 2014). Carbonates at the Fukusaki, Tanohama, Kanoura, Anazawa/Akanuda, and Kuroiwa seeps are affected by recrystallization in which void spaces are filled with sparry calcite that shows ghost structures after acicular rim cements (Fig. 1.4B). The matrix of the Fukusaki, Tanohama, and Kanoura carbonates are almost completely recrystallized to larger mosaics of sparry calcite (see Appendix).

Stable carbon and oxygen isotopic compositions of the early-diagenetic carbonate phases, both original and recrystallized ones, from the study sites are shown in Fig. 1.5 and Table 1.2. The carbon isotopic composition of the carbonates shows a wide variation, with $\delta^{13}C$ values ranging from −64.7‰ to −4.7‰ (described in detail in Appendix). Nevertheless, except for the Nakanomata 2 and Umitaka Spur seeps, the mean $\delta^{13}C$ values of the carbonates at the study sites lie between −40‰ and −30‰: −38.7‰ at Fukusaki (n = 2); −33.2‰ at Tanohama (n = 16); −33.3‰ at Kanoura (n = 6); −40.5‰ at Takinoue (n = 19); −36.9‰ at Anazawa/Akanuda (n = 7); −29.7‰ at Sorimachi (n = 26); −30.4‰ at Kuroiwa (n = 7); −32.9‰ at Nakanomata 1 (n = 23); −37.3‰ at Matsunoyama (n = 26); and −31.6‰ at Anden (n = 14). Carbonates from the Nakanomata 2 and Umitaka Spur seeps are generally ^{13}C-enriched compared with other sites, with $\delta^{13}C$ values of −20.6‰ (n = 7) and −16.3‰ (n = 5) in average, respectively.

The oxygen isotopic composition of the recrystallized carbonates at the Fukusaki,

Tanohama, Kanoura seeps is highly depleted in ^{18}O, with $\delta^{18}O$ values as low as −14.5‰. The $\delta^{18}O$ values of the carbonates at the Anazawa/Akanuda and Kuroiwa seeps, which are less affected by recrystallization, are also negative, but not lower than −10‰. Carbonates at the Takinoue and Sorimachi seeps show both negative and positive $\delta^{18}O$ values around 0‰. Carbonates younger than the late Miocene (Nakanomata 1 and 2, Matsunoyama, Anden, and Umitaka Spur) show consistently positive $\delta^{18}O$ values as high as +5.4‰, except for one sample from Nakanomata 1.

1.4.3. Carbon isotopic compositions of ANME biomarkers

The hydrocarbon fractions extracted from the carbonates are shown in Fig. 1.6. The hydrocarbon fractions from Takinoue, Anazawa/Akanuda, Sorimachi, and Kuroiwa contain unresolved complex mixture (UCM), characterized by elevated baseline with abundant small peaks. It should be noted that the compound-specific carbon isotopic compositions shown below are somewhat affected by the overlapping UCM that is composed of ^{13}C-enriched compounds with respect to ANME biomarkers. During the GC-IRMS analyses, it was confirmed that co-elution of non-target small peaks did not modify the $\delta^{13}C$ values significantly. No considerable difference of the values was observed when several peak definitions were tested for calculation of the isotope ratios.

Compound-specific carbon isotopic compositions of the biomarkers for the ANME are shown in Fig. 1.7 and Table 1.3. The ANME biomarker PMI was detected in all samples except for those from the Fukusaki, Tanohama, Kanoura, and Nakanomata 2 seeps. At the ancient seeps, compound-specific $\delta^{13}C$ values of PMI are mostly lower than −100‰: −116‰ at Takinoue; −116‰ to −93‰ at Anazawa/Akanuda (n = 3); −100‰ at Sorimachi; −113‰ and −106‰ at Kuroiwa (n = 2); −113‰ and −108‰ at Nakanomata 1 (n = 2); −119‰ at Matsunoyama; and −137‰ at Anden. PMI extracted from a sample from the Takinoue seep is enriched in ^{13}C, with a $\delta^{13}C$ value of −57‰. In the sample from the Anden seep, unsaturated homologues of PMI, PMIΔ1 and PMIΔ2 with 1 and 2 double bonds, respectively, were detected. Similar to the PMI from the same sample, the two PMIΔ2 having two double bonds in different positions show extremely negative $\delta^{13}C$ values of −147‰ and −145‰. Another ANME biomarker crocetane was detected only in samples from the Anazawa/Akanuda, Nakanomata 1, and Anden seeps, with $\delta^{13}C$ values of −99‰, −101‰ in average (n =2), and −136‰, respectively. The $\delta^{13}C$ values of crocetane have to be used with caution in the following calculation (section 1.4.4), because the values are mixed with co-eluting phytane, which could be derived either from ANME, methanogenic archaea, or phototroph pigments. Acyclic biphytane was found in samples from the Anazawa/Akanuda and Nakanomata 1 seeps, the former

of which shows a $\delta^{13}C$ value of −115‰. The hydrocarbon fractions extracted from the heavily recrystallized carbonates from the Fukusaki, Tanohama, and Kanoura seeps contain only *n*-alkanes and minor amounts of isoprenoids pristane and phytane, and none of the biomarkers known for ANME was detected. For a sample from Tanohama, alternative lipid extraction method including the dissolution of the carbonate (see section 1.3.3) provided the same result. ANME biomarkers were not found also in samples from the Nakanomata 2 seep, which contain high amounts of pristane and phytane, steranes, and hopanes, as well as *n*-alkanes.

1.4.4. Estimated carbon isotopic compositions of methane at ancient seeps

The $\delta^{13}C$ values of methane at the ancient seep sites along the Japan Sea coast can be estimated by adding the carbon isotope offset calculated for the modern seep site ($\Delta\delta^{13}C_{methane - PMI}$ = 44‰, section 1.4.1) to the $\delta^{13}C$ values of PMI, as shown in upper panel of Fig. 1.7 and Table 1.3. The resulting $\delta^{13}C$ values of methane are mostly lower than −50‰: −72‰ at Takinoue; −59‰ in average at Anazawa/Akanuda (n = 3); −56‰ at Sorimachi; −66‰ in average at Kuroiwa (n = 2); −67‰ in average at Nakanomata 1 (n = 2); −75‰ at Matsunoyama; and −93‰ at Anden. Because the $\Delta\delta^{13}C_{methane - PMI}$ values obtained from literature range between 8‰ and 68‰ (Fig. 1.3A and Table 1.1),

the minimum and maximum $\delta^{13}C$ values of methane are also estimated using these values (upper panel of Fig. 1.7 and Table 1.3). The maximum $\delta^{13}C$ values of methane estimated in this way are lower than −40‰ except for four samples from Anazawa/Akanuda, Sorimachi, and Kuroiwa. PMI with a $\delta^{13}C$ value higher than −60‰ (−57‰) extracted from a Takinoue sample could be derived from methanogenic archaea, rather than ANME (e.g., Pancost and Sinninghe Damsté, 2003), and is excluded in this calculation. The $\delta^{13}C$ values of methane at the ancient seeps were estimated in the same way also using the isotopic compositions of crocetane. Since the carbon isotopic composition of crocetane in the Umitaka Spur sample could not be measured, the average carbon isotope offset between methane and crocetane ($\Delta\delta^{13}C_{methane - crocetane}$) obtained from literature (Fig. 1.3A and Table 1.1) was used. Using the $\Delta\delta^{13}C_{methane - crocetane}$ values ranging between 4‰ and 60‰ (39‰ in average), $\delta^{13}C$ values of methane at the Anazawa/Akanuda, Nakanomata 1, and Anden seeps can be estimated as lower than −40‰ (upper panel of Fig. 1.7 and Table 1.3). Although data for the carbon isotope offsets between methane and PMIΔ2 and acyclic biphytane are scarce relative to PMI and crocetane, some of the literature listed in Table 1.1 reported 52‰ in average (n = 5) and 50‰ offsets for the two biomarkers, respectively. These lead to the $\delta^{13}C$ values of methane of −65‰ at Anazawa/Akanuda and −94‰ in average

at Anden.

Using the calculated regression lines (section 1.4.1) and the measured $\delta^{13}C$ values of PMI and crocetane, the $\delta^{13}C$ values of methane were constrained between −82‰ and −51‰ at Takinoue, between −82‰ and −44‰ at Anazawa/Akanuda (n = 3), between −76‰ and −46‰ at Sorimachi, between −81‰ and −48‰ at Kuroiwa (n = 2), between −81‰ and −49‰ at Nakanomata 1 (n = 2), between −83‰ and −52‰ at Matsunoyama, and between −90‰ and −57‰ at Anden (lower panel of Fig. 1.7 and Table 1.3, minimum and maximum values indicate endpoints of 95% prediction intervals).

1.5. Discussion

1.5.1. Notes on carbon and oxygen isotopic compositions of carbonates

The isotopic compositions of the seep carbonates provide some insights into diagenetic histories of the carbonates and the origin of methane at the ancient seeps, although the latter cannot be specified only by $\delta^{13}C$ values of the carbonates as noted in section 1.1. The oxygen isotopic composition of the seep carbonates in this study becomes more depleted in ^{18}O with increasing age and degree of recrystallization, indicating diagenetic alterations during burial (Fig. 1.5). In contrast, the mean of the carbon isotopic composition of the carbonates is similar among the study sites, except

for those at Nakanomata 2 and Umitaka Spur, regardless of their age and degree of recrystallization. This is consistent with the assumption that carbon isotopes are less affected by late-diagenetic alterations than oxygen isotopes, as carbon is contained much less than oxygen in diagenetic fluids (e.g., Tong et al., 2016). The large scatter of the $\delta^{13}C$ values of the carbonates suggests, however, that the early-diagenetic phases analyzed in this study were precipitated not only from AOM-derived ^{13}C-depleted bicarbonate ions but also from more ^{13}C-enriched bicarbonate ions. The minimum $\delta^{13}C$ values of the carbonates could have at least originated from the methane oxidation, and therefore they could reflect carbon isotopic composition of methane contained in seep fluids. The minimum $\delta^{13}C$ values of the carbonates at the Tanohama and Anden seeps are lower than −50‰ (−52.8‰ and −64.7‰, respectively), indicating biogenic origins for methane. Carbonates at the remaining seep sites show $\delta^{13}C$ values higher than −50‰, indicating either biogenic or thermogenic, or both origins for methane. The carbonate $\delta^{13}C$ values at the Umitaka Spur seep, where thermogenic methane is known to be seeping, are not lower than −20‰ and generally higher than the ancient seep carbonates. It is probable that methane at the ancient seep sites had lower $\delta^{13}C$ values than the methane at Umitaka Spur (−36.0‰ in average; Hachikubo et al., 2015).

1.5.2. The origin of methane at the ancient seeps estimated by carbon isotopic compositions of ANME biomarkers

The estimated $\delta^{13}C$ values of methane at the ancient seeps were mostly lower than −50‰ and indicate biogenic origins for the methane, based on the measured $\delta^{13}C$ values of PMI and the carbon isotope offset calculated for the modern Umitaka Spur seep (upper panel of Fig. 1.7 and Table 1.3). The same conclusion was obtained even if the $\Delta\delta^{13}C_{methane-lipid}$ values having great ranges (~60‰) calculated from the literature data (Table 1.1) are used; the estimated $\delta^{13}C$ values of methane were mostly lower than −40‰, indicating biogenic origins. Indeed, the maximum estimated values of $\delta^{13}C$ of methane are higher than −40‰ at Anazawa/Akanuda, Sorimachi, and Kuroiwa and seemingly indicate thermogenic origins for the methane. However, the maximum estimates for the three sites seem overestimates for the following two reasons. First, the $\Delta\delta^{13}C_{methane-lipid}$ values are mostly within 30‰ to 60‰ and the isotope offset larger than 60‰ seems rare (Fig. 1.3). Second, the examined ancient seeps could have been dominated by an archaeal clade showing a small isotope offset. Niemann and Elvert (2008) showed that the isotope offset between methane and lipid depends on phylogenetic clades of ANME: ANME-2 archaea show a large offset (~50‰) while ANME-1 archaea show a smaller offset (~30‰). Crocetane is a specific biomarker for

ANME-2 archaea (Blumenberg et al., 2004; Niemann and Elvert, 2008), which was not detected from most of the ancient seep carbonates including the Anazawa/Akanuda, Sorimachi, and Kuroiwa samples. The ancient Japan Sea seeps were thus probably dominated by ANME-1 archaea. The $\delta^{13}C$ values of methane estimated using the isotope offset calculated for the Umitaka Spur could be also overestimates. The modern Umitaka Spur seep is inhabited by ANME-2 archaea, as supported by the presence of crocetane in the seep carbonate (section 1.4.1) and molecular phylogeny (Yanagawa et al., 2011). However, determination of taxonomic composition of ANME needs further analyses on other lipid signatures such as the hydroxyarchaeol to archaeol ratio (Niemann and Elvert, 2008). The prediction of the $\delta^{13}C$ values of methane by the regression analysis also supports the biogenic origin at the ancient seeps. As a result of the regression analysis, the difference between minimum and maximum $\delta^{13}C$ values of methane was about 30‰ (lower panel of Fig. 1.7 and Table 1.3). The regression analysis can thus constrain the origin of methane more strictly compared with the simple addition of the isotope offset.

Since ANME biomarkers were not detected from the examined samples from the Fukusaki, Tanohama, Kanoura, and Nakanomata 2 seeps, the isotopic composition of methane at these sites could not be constrained from the biomarkers. The hydrocarbon

fractions from the Fukusaki, Tanohama, and Kanoura seep carbonates are characterized by a predominance of short-chained *n*-alkanes and minor amounts of isoprenoids (Fig. 1.6), indicating that the carbonates are thermally mature (Tissot et al., 1971; Tissot and Welte, 1984; Peters et al., 2005; see also Part 2). It is thus possible that isoprenoid biomarkers such as PMI and crocetane were lost due to thermal cracking at these sites (Kiel et al., 2013, 2014). This is supported by the recrystallized nature and highly negative $\delta^{18}O$ values of the carbonates (Fig. 1.5). Since the average $\delta^{13}C$ values of the carbonates are similar between the above three and the other study sites, it is likely that methane at the three sites also had $\delta^{13}C$ values around −70‰ to −60‰ as estimated by biomarkers at the other sites. The hydrocarbon fractions from the Nakanomata 2 seep carbonates are mainly composed of isoprenoid hydrocarbons such as pristane and phytane which are typical of phototrophs, eukaryotic biomarkers steranes, and bacterial biomarkers hopanes. They are preserved more abundantly than *n*-alkanes. This feature and the positive $\delta^{18}O$ values of the carbonates indicate that the Nakanomata 2 seep carbonates were not affected by high temperature and resultant thermal cracking (see also Part 2). The relatively high $\delta^{13}C$ values of the Nakanomata 2 carbonates (−24.8‰ in minimum) might have originated from the oxidation of thermogenic methane. However, it is also possible that the carbonates were precipitated out of the AOM zone,

in which ANME biomarkers are commonly concentrated, or they were precipitated via the sulfate reduction of sedimentary organic matter rather than via methane seepage.

Based on the above, the origins of methane at the studied ancient seeps could have been mostly biogenic, although mixing with thermogenic methane cannot fully be ruled out. The study sites are underlain by sediment piles of over 1 km thick (Fig. 1.2). The underlying formations such as the middle to upper Miocene Nambayama, Nanatani, Lower Teradomari, and Onnagawa formations are the present source rocks of oil and gas and characterized by high total organic carbon contents of up to >3% (Hata and Sekiguchi, 1992; Monzawa et al., 2006; Kano et al., 2011). If the heat flow prevailing in the study area during the Miocene to Pleistocene was similar to that at present, it is possible that thermogenic methane was generated in the organic-rich sediments at the deep subsurface at the depositional time of the seep carbonates. Nevertheless, the Miocene to Pleistocene seeps in this study could have been sustained mainly by biogenic methane generated via microbial methanogenesis in the shallow subsurface. This suggests that migration and seepage of thermogenic gases through subsurface conduits such as deep-rooted faults were minor in the study area until Pleistocene. Okui et al. (2008) claimed that thermogenic gas generation began around 2–1 Ma in the Naoetsu Basin, offshore Niigata Prefecture, based on simulations of generation and

migration of the oil and gas using geophysical, geological, and geochemical data. This hypothesis is concordant with the present conclusion that generation and migration of thermogenic methane in the study area were minor at least in the Miocene. The seepage of biogenic methane produced in the shallow subsurface could be caused either by diffusion from the sediments, discharge of shallow- or deep-sourced fluids through faults accompanying with tectonic compression, decrease in sea level and hydraulic pressure, or submarine groundwater discharge (Ge et al., 2002; Wiedicke et al., 2002; Toki et al., 2014; Himmler et al., 2015; Crémière et al., 2016; Prouty et al., 2016; Pierre et al., 2017). The latter two possibilities might be ruled out in the case of some study sites, based on the water depth (upper to middle bathyal) and the positive $\delta^{18}O$ values of the seep carbonates. However, it is necessary to estimate the origin of seep fluids to know the processes in which biogenic methane seeped out in the study area. The examined seep carbonates are, in most cases, hosted within massive silty sediments with no indication of erosional events. Therefore, it can be ruled out that the seepage in the study area was caused by breaching of fine-grained sedimentary cover by mass wasting or erosion, which exposed high permeable horizons (Naudts et al., 2006).

This study assumes that the carbon isotopic composition of the ANME lipids is controlled by that of the source methane and net isotopic fractionation during

biosynthesis. Some previous culture experiments suggest that both methane and carbon dioxide are incorporated into the lipid synthesis (Nauhaus et al., 2007; Wegener et al., 2008; Kellermann et al., 2012). These experiments also suggest that the strong ^{13}C depletion in ANME lipids is not simply the result of the direct transfer of ^{13}C-depleted methane carbon into the lipid synthesis. More improved estimation of the carbon isotopic compositions of methane using that of ANME biomarkers requires better understanding of the process of the lipid biosynthesis by ANME and accompanying isotope fractionation.

1.6. Summary

1) Carbon isotope fractionations (offsets) between ANME biomarkers (PMI and crocetane) and methane were estimated as differences between the $\delta^{13}C$ values of them measured at modern methane seeps.
2) Regression lines were obtained to predict the carbon isotopic composition of methane based on that of the biomarkers with 95% prediction intervals.
3) ANME biomarkers including PMI and crocetane were extracted from the Miocene to Pleistocene methane-seep carbonate rocks collected along the Japan Sea coast. The compound-specific $\delta^{13}C$ values of the biomarkers were measured as mostly

lower than −90‰.

4) Using the calculated isotope offsets and regression lines, the origin of methane at the examined ancient seeps was estimated to have been mainly biogenic, with $\delta^{13}C$ values less than −50‰ or −40‰.

References

Akahane, S., Kato, H., 1989. Geology of the Takada-Seibu district. With Geological Sheet Map at 1:50,000, Geological Survey of Japan, 89 pp. (in Japanese with English abstract)

Alperin, M.J., Hoehler, T.M., 2009. Anaerobic methane oxidation by archaea/sulfate-reducing bacteria aggregates: 2. isotopic constraints. American Journal of Science 309, 958–984

Alperin, M.J., Reeburgh, W.S., Whiticar, M.J., 1988. Carbon and hydrogen isotope fractionation resulting from anaerobic methane oxidation. Global Biogeochemical Cycles 2, 279–288.

Birgel, D., Feng, D., Roberts, H.H., Peckmann, J., 2011. Changing redox conditions at cold seeps as revealed by authigenic carbonates from Alaminos Canyon, northern Gulf of Mexico. Chemical Geology 285, 82–96.

Blumenberg, M., 2010. Microbial chemofossils in specific marine hydrothermal and methane cold seep settings. In: Kiel, S. (Ed.), The Vent and Seep Biota, Topics in Geobiology 33. Springer, Heidelberg, pp. 73–106.

Blumenberg, M., Seifert, R., Nauhaus, K., Pape, T., Michaelis, W., 2005. In vitro study of lipid biosynthesis in an anaerobically methane-oxidizing microbial mat. Applied and Environmental Microbiology 71, 4345–4351.

Blumenberg, M., Seifert, R., Reitner, J., Pape, T., Michaelis, W., 2004. Membrane lipid patterns typify distinct anaerobic methanotrophic consortia. Proceedings of the National Academy of Sciences of the United States of America 101, 11111–11116.

Bojanowski, M.J., Bagiński, B., Guillermier, C., Franchi, I.A., 2015. Carbon and oxygen isotope analysis of hydrate-associated Oligocene authigenic carbonates using NanoSIMS and IRMS. Chemical Geology 416, 51–64.

Brooks, J.M., Field, M.E., Kennicutt II, M.C., 1991. Observations of gas hydrates in marine sediments, offshore northern California. Marine Geology 96, 103–109.

Burton, E.A., Walter, L.M., 1987. Relative precipitation rates of aragonite and Mg calcite from seawater: temperature or carbonate ion control? Geology 15, 111–114.

Campbell, K.A., Farmer, J.D., Des Marais, D., 2002. Ancient hydrocarbon seeps from the Mesozoic convergent margin of California: carbonate geochemistry, fluids and

palaeoenvironments. Geofluids 2, 63–94.

Chevalier, N., Bouloubassi, I., Birgel, D., Crémière, A., Taphanel, M.-H., Pierre, C., 2011. Authigenic carbonates at cold seeps in the Marmara Sea (Turkey): a lipid biomarker and stable carbon and oxygen isotope investigation. Marine Geology 288, 112–121.

Chevalier, N., Bouloubassi, I., Birgel, D., Taphanel, M.-H., López-García, P., 2013. Microbial methane turnover at Marmara Sea cold seeps: a combined 16S rRNA and lipid biomarker investigation. Geobiology 11, 55–71.

Chevalier, N., Bouloubassi, I., Stadnitskaia, A., Taphanel, M.-H., Lorre, A., Sinninghe Damsté, J., Pierre, C., 2010. Distributions and carbon isotopic compositions of lipid biomarkers in authigenic carbonate crusts from the Nordic margin (Norwegian Sea). Organic Geochemistry 41, 885–890.

Chevalier, N., Bouloubassi, I., Stadnitskaia, A., Taphanel, M.-H., Sinninghe Damsté, J., 2014. Lipid biomarkers for anaerobic oxidation of methane and sulphate reduction in cold seep sediments of Nyegga pockmarks (Norwegian margin): discrepancies in contents and carbon isotope signatures. Geo-Marine Letters 34, 269–280.

Crémière, A., Lepland, A., Chand, S., Sahy, D., Kirsimäe, K., Bau, M., Whitehouse, M.J., Noble, S.R., Martma, T., Thorsnes, T., Brunstad, H., 2016. Fluid source and

methane-related diagenetic processes recorded in cold seep carbonates from the Alvheim channel, central North Sea. Chemical Geology 432, 16–33.

Crémière, A., Pierre, C., Blanc-Valleron, M.-M., Zitter, T., Çağatay, M.N., Henry, P., 2012. Methane-derived authigenic carbonates along the North Anatolian fault system in the Sea of Marmara (Turkey). Deep-Sea Research I 66, 114–130.

Elvert, M., Greinert, J., Suess, E., Whiticar, M.J., 2001. Carbon isotopes of biomarkers derived from methane-oxidizing microbes at Hydrate Ridge, Cascadia convergent margin. In: Paull, C.K., Dillon, W.P. (Eds.), Natural Gas Hydrates: Occurrence, Distribution, and Detection. American Geophysical Union Geophysical Monograph 124, Washington, DC, pp. 115–129.

Elvert, M., Suess, E., Whiticar, M.J., 1999. Anaerobic methane oxidation associated with marine gas hydrates: superlight C-isotopes from saturated and unsaturated C_{20} and C_{25} irregular isoprenoids. Naturwissenschaften 86, 295–300.

Formolo, M.J., Lyons, T.W., Zhang, C., Kelley, C., Sassen, R., Horita, J., Cole, D.R., 2004. Quantifying carbon sources in the formation of authigenic carbonates at gas hydrate sites in the Gulf of Mexico. Chemical Geology 205, 253–264.

Ge, S., Bekins, B., Bredehoeft, J., Brown, K., Davis, E.E., Gorelick, S.M., Henry, P., Kooi, H., Moench, A.F., Ruppel, C., Sauter, M., Screaton, E., Swart, P.K., Tokunaga,

T., Voss, C.I., Whitaker, F., 2002. Hydrology program planning group final report. JOIDES Journal 28, 24–29.

Griffin, G.M., 1971. Interpretation of X-ray diffraction data. In: Carver, R.E. (Ed.), Procedures in Sedimentary Petrology. University of Georgia, Athens, pp. 541–565.

Haas, A., Peckmann, J., Elvert, M., Sahling, H., Bohrmann, G., 2010. Patterns of carbonate authigenesis at the Kouilou pockmarks on the Congo deep-sea fan. Marine Geology 268, 129–136.

Hachikubo, A., Yanagawa, K., Tomaru, H., Lu, H., Matsumoto, R., 2015. Molecular and isotopic composition of volatiles in gas hydrates and in sediment from the Joetsu Basin, eastern margin of the Japan Sea. Energies 8, 4647–4666.

Harayama, S., Otsuka, T., Sakai, J., Kosaka, T., Komazawa, M., 2009. Geology of the Matsumoto District. Quadrangle Series, 1:50,000, Geological Survey of Japan, AIST, 63 pp. (in Japanese with English abstract)

Hata, S., Sekiguchi, K., 1992. Geochemical study on the Kubiki Area, Niigata. Journal of the Japanese Association for Petroleum Technology 57, 67–76. (in Japanese with English abstract)

Himmler, T., Birgel, D., Bayon, G., Pape, T., Ge, L., Bohrmann, G., Peckmann, J., 2015. Formation of seep carbonates along the Makran convergent margin, northern

Arabian Sea and a molecular and isotopic approach to constrain the carbon isotopic composition of parent methane. Chemical Geology 415, 102–117.

Holler, T., Wegener, G., Knittel, K., Boetius, A., Brunner, B., Kuypers, M.M.M., Widdel, F., 2009. Substantial $^{13}C/^{12}C$ and D/H fractionation during anaerobic oxidation of methane by marine consortia enriched *in vitro*. Environmental Microbiology Reports 1, 370–376.

Hovland, M., 2002. On the self-sealing nature of marine seeps. Continental Shelf Research 22, 2387–2394.

Hovland, M., Svensen, H., Forsberg, C.F., Johansen, H., Fichler, C., Fosså, J.H., Jonsson, R., Rueslåtten, H., 2005. Complex pockmarks with carbonate-ridges off mid Norway: products of sediment degassing. Marine Geology 218, 191–206.

Hoyanagi, K., Miyasaka, S., Watanabe, Y., Kimura, G., Matsui, M., 1986. Depositions of turbidites in the Miocene collision zone, central Hokkaido. Monograph of the Association for the Geological Collaboration in Japan 31, 265–284.

Jolivet, L., Tamaki, K., 1992. Neogene kinematics in the Japan Sea region and volcanic activity of the northeast Japan arc. In: Tamaki, K., Suyehiro, K., Allan, J., et al. (Eds.), Proceedings of the Ocean Drilling Program, Scientific Results, Vol. 127/128 (Part 2). Ocean Drilling Program, College Station, TX, pp. 1311–1331.

Joye, S.B., Boetius, A., Orcutt, B.N., Montoya, J.P., Schulz, H.N., Erickson, M.J., Lugo, S.K., 2004. The anaerobic oxidation of methane and sulfate reduction in sediments from Gulf of Mexico cold seeps. Chemical Geology 205, 219–238.

Kano, K., Kato, H., Yanagisawa, Y., Yoshida, F., 1991. Stratigraphy and geologic history of the Cenozoic of Japan. Report, Geological Survey of Japan 274, 1–114. (in Japanese with English abstract)

Kano, K., Ohguchi, T., Yanagisawa, Y., Awata, Y., Kobayashi, N., Sato, Y., Hayashi, S., Kitazato, H., Ogasawara, K., Komazawa, M., 2011. Geology of the Toga and Funakawa District. Quadrangle Series, 1:50,000, Geological Survey of Japan, AIST, 127 pp. (in Japanese with English abstract)

Kato, S., Hiramatsu, C., Miwa, M., Nobuhara, T., 2011. Geological age and sedimentary environment of the Anazawa Limestone in the Middle Miocene Bessho Formation, Nagano Prefecture, central Japan. Bulletin of Mizunami Fossil Museum 37, 135–147. (in Japanese with English abstract)

Kawakami, G., Shiono, M., Kawamura, A., Urabe, A., Koizumi, I., 2002. Stratigraphy and depositional age of the Miocene Kawabata Formation, Yubari Mountains, central Hokkaido, Japan. Journal of the Geological Society of Japan 108, 186–200. (in Japanese with English abstract)

Kellermann, M.Y., Wegener, G., Elvert, M., Yoshinaga, M.Y., Lin, Y.S., Holler, T., Mollar, X.P., Knittel, K., Hinrichs, K.-U., 2012. Autotrophy as a predominant mode of carbon fixation in anaerobic methane-oxidizing microbial communities. Proceedings of the National Academy of Sciences of the United States of America 109, 19321–19326.

Kiel, S., Birgel, D., Campbell, K.A., Crampton, J.S., Schiøler, P., Peckmann, J., 2013. Cretaceous methane-seep deposits from New Zealand and their fauna. Palaeogeography, Palaeoclimatology, Palaeoecology 390, 17–34.

Kiel, S., Glodny, J., Birgel, D., Bulot, L.G., Campbell, K.A., Gaillard, C., Graziano, R., Kaim, A., Lazăr, L., Sandy, M.R., Peckmann, J., 2014. The paleoecology, habitats, and stratigraphic range of the enigmatic Cretaceous brachiopod *Peregrinella*. PLoS ONE 9(10), e109260.

Kikuchi, Y., Tono, S., Funayama, M., 1991. Petroleum resources in the Japanese island-arc setting. Episodes 14, 236–241.

Kubota, S., Motoyama, I., Kawamura, K., Kamikuri, S., Ogasawara, K., 2010. Radiolarian biostratigraphy of the Miocene rocks in the vicinity of the Horomui River, Iwamizawa City, Hokkaido. Journal of the Japanese Association for Petroleum Technology 75, 371–381. (in Japanese with English abstract)

Lein, A., Vogt, P., Crane, K., Egorov, A., Ivanov, M., 1999. Chemical and isotopic evidence for the nature of the fluid in CH_4-containing sediments of the Håkon Mosby Mud Volcano. Geo-Marine Letters 19, 76–83.

Londry, K.L., Dawson, K.G., Grover, H.D., Summons, R.E., Bradley, A.S., 2008. Stable carbon isotope fractionation between substrates and products of *Methanosarcina barkeri*. Organic Geochemistry 39, 608–621.

Martens, C.S., Albert, D.B., Alperin, M.J., 1999. Stable isotope tracing of anaerobic methane oxidation in the gassy sediments of Eckernförde Bay, German Baltic Sea. American Journal of Science 299, 589–610.

Michaelis, W., Seifert, R., Nauhaus, K., Treude, T., Thiel, V., Blumenberg, M., Knittel, K., Gieseke, A., Peterknecht, K., Pape, T., Boetius, A., Amann, R., Jørgensen, B.B., Widdel, F., Peckmann, J., Pimenov, N.V., Gulin, M.B., 2002. Microbial reefs in the Black Sea fueled by anaerobic oxidation of methane. Science 297, 1013–1015.

Miyajima, Y., Watanabe, Y., Yanagisawa, Y., Amano, K., Hasegawa, T., Shimobayashi, N., 2016. A late Miocene methane-seep deposit bearing methane-trapping silica minerals at Joetsu, central Japan. Palaeogeography, Palaeoclimatology, Palaeoecology 455, 1–15.

Monzawa, N., Kaneko, M., Osawa, M., 2006. A review of petroleum system in the deep

water area of the Toyama Trough to the Sado Island in the Japan Sea, based on the results of the METI Sado Nansei Oki drilling. Journal of the Japanese Association for Petroleum Technology 71, 618–627. (in Japanese with English abstract)

Naudts, L., Greinert, J., Artemov, Y., Staelens, P., Poort, J., Van Rensbergen, P., De Batist, M., 2006. Geological and morphological setting of 2778 methane seeps in the Dnepr paleo-delta, northwestern Black Sea. Marine Geology 227, 177–199.

Nauhaus, K., Albrecht, M., Elvert, M., Boetius, A., Widdel, F., 2007. *In vitro* cell growth of marine archaeal-bacterial consortia during anaerobic oxidation of methane with sulfate. Environmental Microbiology 9, 187–196.

Niemann, H., Elvert, M., 2008. Diagnostic lipid biomarker and stable carbon isotope signatures of microbial communities mediating the anaerobic oxidation of methane with sulphate. Organic Geochemistry 39, 1668–1677.

Niemann, H., Elvert, M., Hovland, M., Orcutt, B., Judd, A., Suck, I., Gutt, J., Joye, S., Damm, E., Finster, K., Boetius, A., 2005. Methane emission and consumption at a North Sea gas seep (Tommeliten area). Biogeosciences 2, 335–351.

Ninomiya, T., Shimoyama, S., Watanabe, K., Horie, K., Dunkley, D.J., Shiraishi, K., 2014. Age of the Taishu Group, southwestern Japan, and implications for the origin and evolution of the Japan Sea. Island Arc 23, 206–220.

Ogihara, S., Ishizaki, O., Matsumoto, R., 2009. Organic geochemical analysis of push core sediment samples collected from NT-06-19 (Umitaka Spur and Joetsu Knoll off Naoetsu). Journal of Geography 118, 128–135. (in Japanese with English abstract)

Ogihara, S., Matsumoto, R., Jenkins, R.G., Machiyama, H., 2003. Organic geochemical study of bacterial mats collected from Kuroshima Knoll. JAMSTEC Deep Sea Research 22, 107–114. (in Japanese with English abstract)

Okui, A., Kaneko, M., Nakanishi, S., Monzawa, N., Yamamoto, H., 2008. An integrated approach to understanding the petroleum system of a frontier deep-water area, offshore Japan. Petroleum Geoscience 14, 223–233.

Orphan, V.J., Hinrichs, K.-U., Ussler III, W., Paull, C.K., Taylor, L.T., Sylva, S.P., Hayes, J.M., Delong, E.F., 2001. Comparative analysis of methane-oxidizing archaea and sulfate-reducing bacteria in anoxic marine sediments. Applied and Environmental Microbiology 67, 1922–1934.

Pancost, R.D., Sinninghe Damsté, J.S., 2003. Carbon isotopic compositions of prokaryotic lipids as tracers of carbon cycling in diverse settings. Chemical Geology 195, 29–58.

Peckmann, J., Birgel, D., Kiel, S., 2009. Molecular fossils reveal fluid composition and flow intensity at a Cretaceous seep. Geology 37, 847–850.

Peckmann, J., Thiel, V., 2004. Carbon cycling at ancient methane-seeps. Chemical Geology 205, 443–467.

Peters, K.E., Walters, C.C., Moldowan, J.M., 2005. The biomarker guide, second edition. Cambridge University Press, New York, 1155 pp.

Pierre, C., Demange, J., Blanc-Valleron, M.-M., Dupré, S., 2017. Authigenic carbonate mounds from active methane seeps on the southern Aquitaine Shelf (Bay of Biscay, France): evidence for anaerobic oxidation of biogenic methane and submarine groundwater discharge during formation. Continental Shelf Research 133, 13–25.

Prouty, N.G., Sahy, D., Ruppel, C.D., Roark, E.B., Condon, D., Brooke, S., Ross, S.W., Demopoulos, A.W.J., 2016. Insights into methane dynamics from analysis of authigenic and chemosynthetic mussels at newly-discovered Atlantic Margin seeps. Earth and Planetary Science Letters 449, 332–344.

Reeburgh, W.S., 2007. Oceanic methane biogeochemistry. Chemical Reviews 107, 486–513.

Ritger, S., Carson, B., Suess, E., 1987. Methane-derived authigenic carbonates formed by subduction-induced pore-water expulsion along the Oregon/Washington margin. Geological Society of America Bulletin 98, 147–156.

Sato, H., 1994. The relationship between late Cenozoic tectonic events and stress field

and basin development in northeast Japan. Journal of Geophysical Research 99, 22261–22274.

Stadnitskaia, A., Muyzer, G., Abbas, B., Coolen, M.J.L., Hopmans, E.C., Baas, M., van Weering, T.C.E., Ivanov, M.K., Poludetkina, E., Sinninghe Damsté, J.S., 2005. Biomarker and 16S rDNA evidence for anaerobic oxidation of methane and related carbonate precipitation in deep-sea mud volcanoes of the Sorokin Trough, Black Sea. Marine Geology 217, 67–96.

Suess, E., Whiticar, M.J., 1989. Methane-derived CO_2 in pore fluids expelled from the Oregon subduction zone. Palaeogeography, Palaeoclimatology, Palaeoecology 71, 119–136.

Summons, R.E., Franzmann, P.D., Nichols, P.D., 1998. Carbon isotopic fractionation associated with methylotrophic methanogenesis. Organic Geochemistry 28, 465–475.

Takahashi, K., Taniguchi, H., Watanabe, J., Ishimaru, S., 2002. Explanatory text of the Geological Map of Japan 1:50,000, Momijiyama. Geological Survey of Hokkaido, 116 pp. (in Japanese with English abstract)

Takeuchi, K., Yoshikawa, T., Kamai, T., 2000. Geology of the Matsunoyama Onsen District. With Geological Sheet Map at 1:50,000, Geological Survey of Japan, 76

pp. (in Japanese with English abstract)

Takeuchi, K., Yoshimura, T., Kato, H., 1996. Geology of the Kakizaki District. With Geological Sheet Map at 1:50,000, Geological Survey of Japan, 48 pp. (in Japanese with English abstract)

Tissot, B., Califet-Debyser, Y., Deroo, G., Oudin, J.L., 1971. Origin and evolution of hydrocarbons in early Toarcian shales, Paris Basin, France. American Association of Petroleum Geologists Bulletin 55, 2177–2193.

Tissot, B.P., Welte, D.H., 1984. Petroleum Formation and Occurrence. Springer-Verlag, New York, 699 pp.

Toki, T., Higa, R., Ijiri, A., Tsunogai, U., Ashi, J., 2014. Origin and transport of pore fluids in the Nankai accretionary prism inferred from chemical and isotopic compositions of pore water at cold seep sites off Kumano. Earth, Planets and Space 66:137.

Tong, H., Wang, Q., Peckmann, J., Cao, Y., Chen, L., Zhou, W., Chen, D., 2016. Diagenetic alteration affecting $\delta^{18}O$, $\delta^{13}C$ and $^{87}Sr/^{86}Sr$ signatures of carbonates: a case study on Cretaceous seep deposits from Yarlung-Zangbo Suture Zone, Tibet, China. Chemical Geology 444, 71–82.

Wegener, G., Niemann, H., Elvert, M., Hinrichs, K.-U., Boetius, A., 2008. Assimilation

of methane and inorganic carbon by microbial communities mediating the anaerobic oxidation of methane. Environmental Microbiology 10, 2287–2298.

Whiticar, M.J., Faber, E., 1986. Methane oxidation in sediment and water column environments—isotope evidence. Organic Geochemistry 10, 759–768.

Wiedicke, M., Sahling, H., Delisle, G., Faber, E., Neben, S., Beiersdorf, H., Marchig, V., Weiss, W., von Mirbach, N., Afiat, A., 2002. Characteristics of an active vent in the fore-arc basin of the Sunda Arc, Indonesia. Marine Geology 184, 121–141.

Yanagawa, K., Sunamura, M., Lever, M.A., Morono, Y., Hiruta, A., Ishizaki, O., Matsumoto, R., Urabe, T., Inagaki, F., 2011. Niche separation of methanotrophic archaea (ANME-1 and -2) in methane-seep sediments of the eastern Japan Sea offshore Joetsu. Geomicrobiology Journal 28, 118–129.

Yanagisawa, Y., Amano, K., 2003. Diatom biostratigraphy and paleoceanography of the Pliocene sequence in the western part of Joetsu City, Niigata Prefecture, central Japan. Bulletin of the Geological Survey of Japan 54, 63–93. (in Japanese with English abstract)

Zhang, C.L., Pancost, R.D., Sassen, R., Qian, Y., Macko, S., 2003. Archaeal lipid biomarkers and isotopic evidence of anaerobic methane oxidation associated with gas hydrates in the Gulf of Mexico. Organic Geochemistry 34, 827–836.

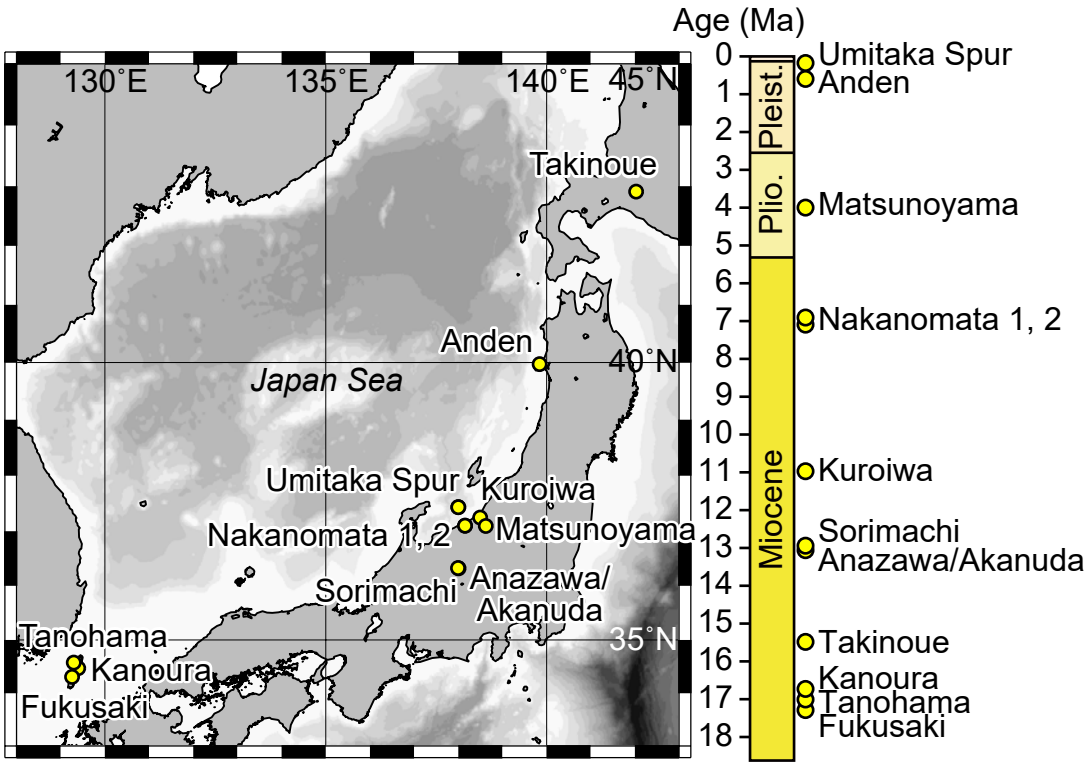

Fig. 1.1. Locations and approximate ages of the seep sites examined in this study. The Sorimachi and Anazawa/Akanuda sites are located in close proximity to each other, which is also the case with the Nakanomata 1 and 2 sites. Pleist., Pleistocene; Plio., Pliocene.

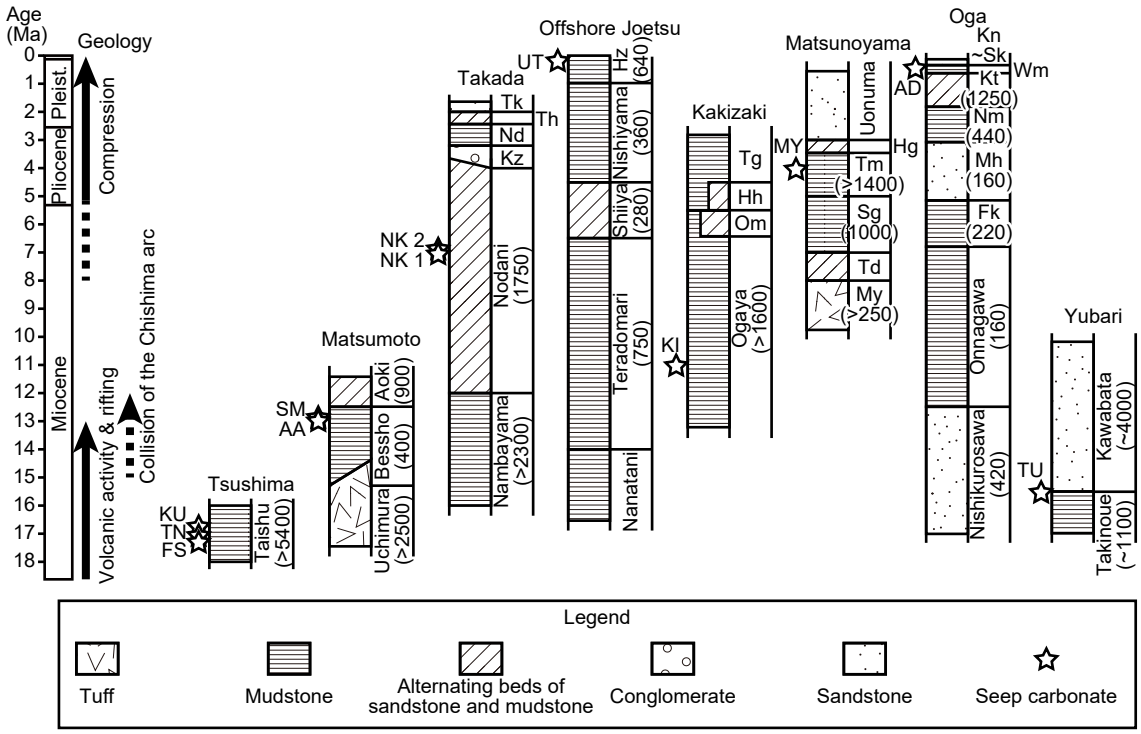

Fig. 1.2. Stratigraphy of the study area, with stratigraphic positions of the examined seep carbonates (stars). Major geological events in the Japan Sea region (Hoyanagi et al., 1986; Kano et al., 1991; Jolivet and Tamaki, 1992; Sato, 1994) are also shown. In each column, the formation name and thickness (m in parentheses) are shown next to the lithology. The stratigraphy and chronology are based on Akahane and Kato (1989), Kikuchi et al. (1991), Takeuchi et al. (1996, 2000), Takahashi et al. (2002), Kawakami et al. (2002), Yanagisawa and Amano (2003), Monzawa et al. (2006), Harayama et al. (2009), Kubota et al. (2010), Kano et al. (2011), Kato et al. (2011), and Ninomiya et al. (2014). Abbreviations: Pleist., Pleistocene; Plio., Pliocene; AA, Anazawa/Akanuda; AD, Anden; Fk, Funakawa; FS, Fukusaki; Hg, Higashigawa; Hh, Hijirigahana; Hz, Haizume; KI, Kuroiwa; Kn, Katanishi; Kt, Kitaura; KU, Kanoura; Kz, Kawazume; Mh, Minamihirasawa; MY and My, Matsunoyama; Nd, Nadachi; NK1, Nakanomata 1; NK2, Nakanomata 2; Nm, Nishimizuguchi; Om, Oshimizu; Sg, Sugawa; Sk, Shibikawa; SM, Sorimachi; Td, Taruda; Tg, Takegahana; Th, Tanihama; Tk, Torigakubi; Tm, Tamugigawa; TN, Tanohama; TU, Takinoue; UT, Umitaka Spur; Wm, Wakimoto.

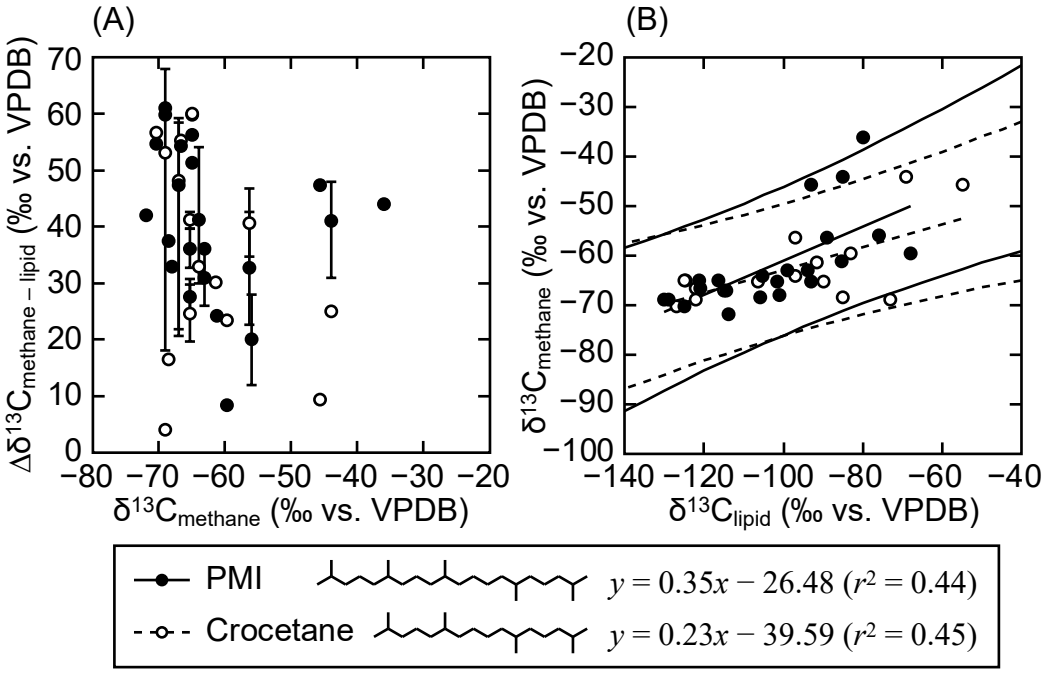

Fig. 1.3. Relationships between the carbon isotopic composition of the source methane and lipid biomarkers of anaerobic methane-oxidizing archaea, PMI and crocetane. The source of the data is shown in Table 1.1. (A) The carbon isotope offset between the source methane and the lipids ($\Delta\delta^{13}C_{methane - lipid}$) as a function of the $\delta^{13}C$ value of the source methane. Plots and error bars indicate the mean and observed range of the $\Delta\delta^{13}C_{methane - lipid}$ values. (B) Plot of the $\delta^{13}C$ values of the source methane (y) and lipid biomarkers (x), i.e., PMI and crocetane. Regression lines between the $\delta^{13}C$ values of methane and those of lipids are shown with 95% prediction intervals by solid and dashed lines for PMI and crocetane, respectively. r^2 value indicates the coefficient of determination.

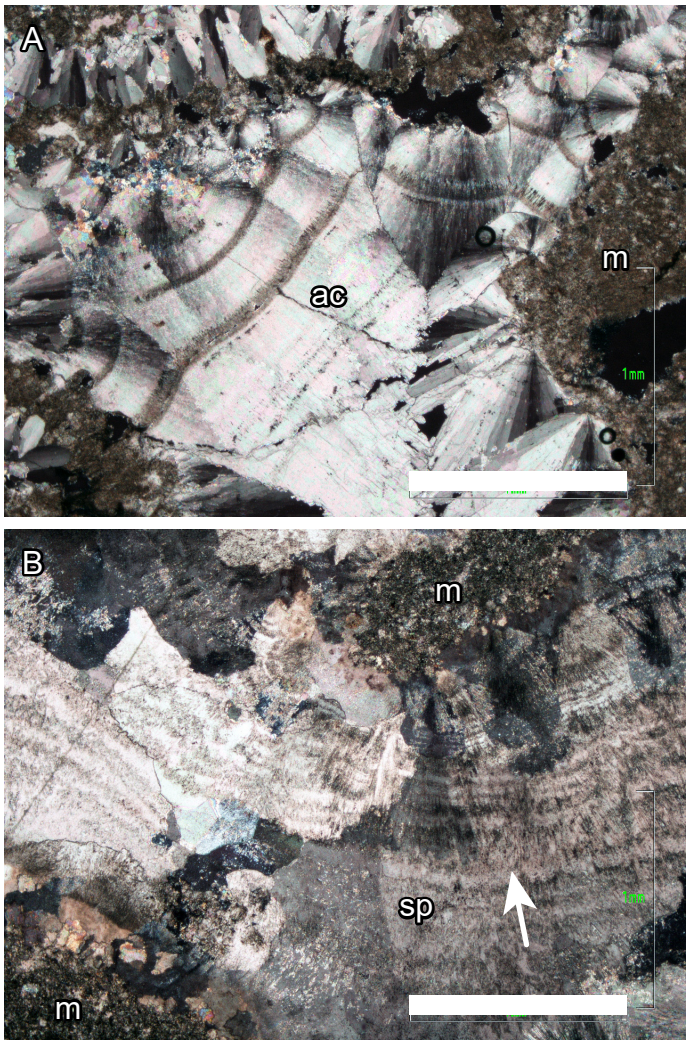

Fig. 1.4. Representative microphotographs showing void-filling cement fabrics of the seep carbonates. Cross-polarized light. Scale bar = 1 mm. (A) Layered acicular rim cements (ac) showing a radial extinction. Nakanomata 1. m, microcrystalline matrix. (B) Recrystallized void cements composed of a mosaic of sparry calcite (sp) with irregular crystal boundaries. Note the ghost structures after layered acicular rim cements (arrow). Kuroiwa.

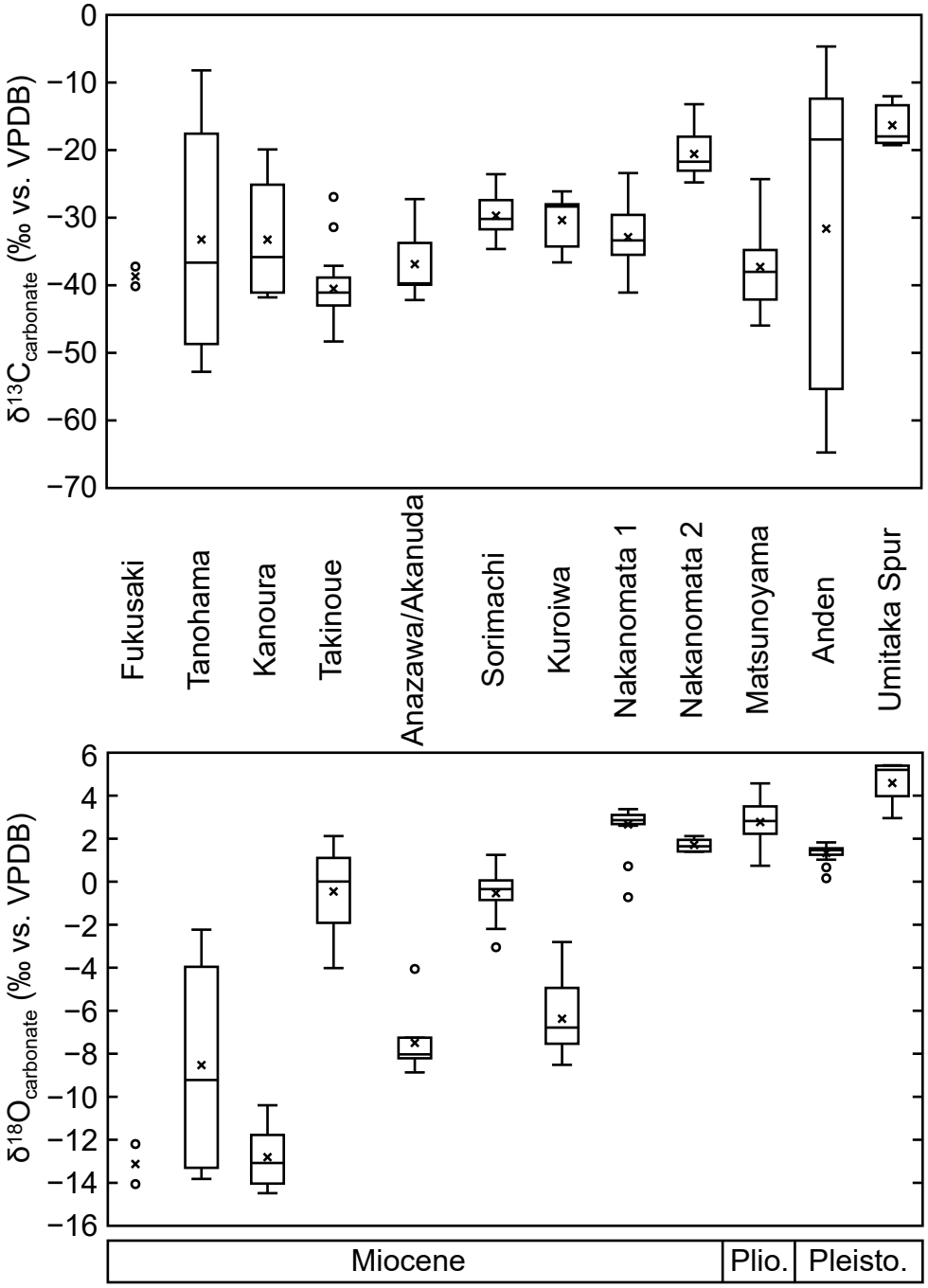

Fig. 1.5. Box plots showing stable carbon (upper) and oxygen (bottom) isotopic compositions of the early-diagenetic phases of the seep carbonates. In each box, horizontal bar and × indicate median and average, respectively. Open circle indicates outlier. Ordered from the oldest (left) to youngest (right) site. Pleisto., Pleistocene; Plio., Pliocene.

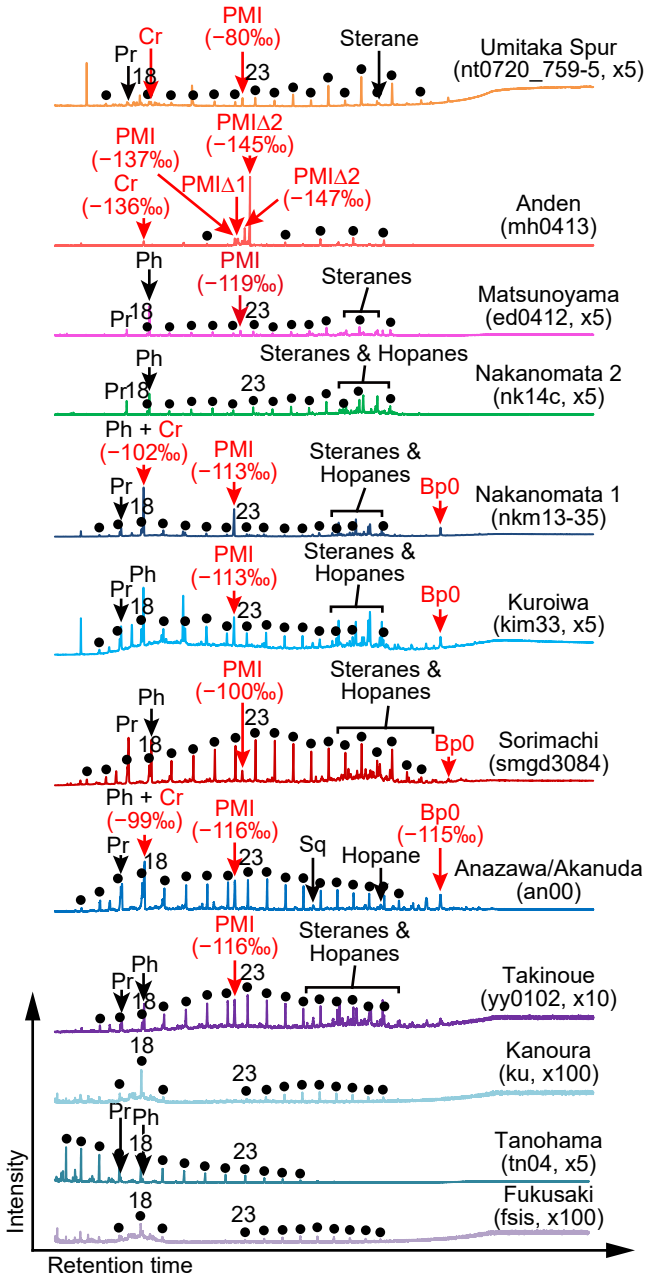

Fig. 1.6. Total ion chromatograms of the hydrocarbon fractions extracted from the seep carbonates. Compound-specific carbon isotopic composition is indicated as $\delta^{13}C$ ‰ vs. VPDB in parentheses. Chromatograms with low intensities are enlarged vertically. Ordered from the oldest (lower) to youngest (upper) site. *n*-Alkanes are indicated by filled circles with numbers representing total number of carbon atoms. Bp0, acyclic biphytane; Cr, crocetane; Ph, phytane; PMI, pentamethylicosane; PMIΔ1 and 2, unsaturated PMIs with one and two double bonds, respectively; Pr, pristane; Sq, squalane.

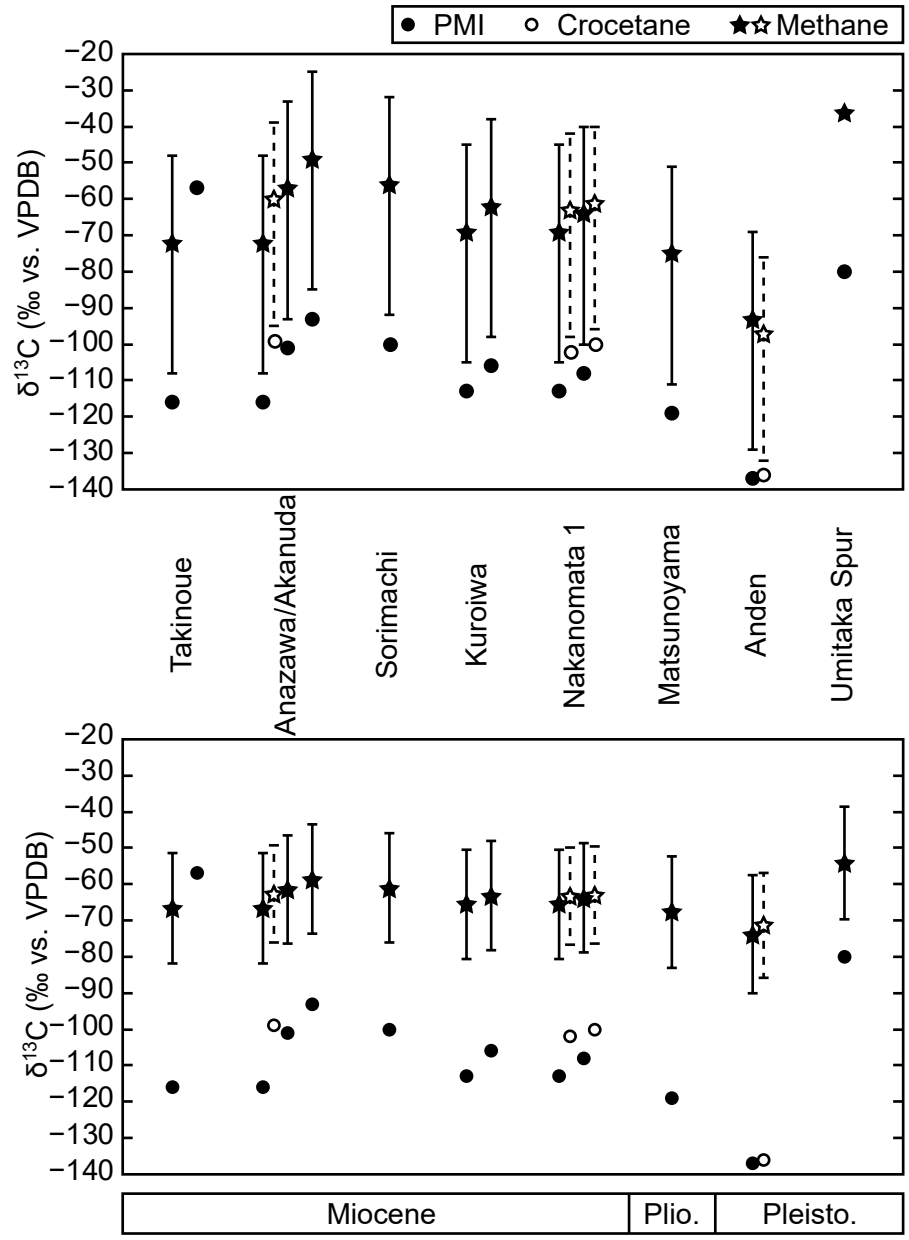

Fig. 1.7. Stable carbon isotopic compositions of the lipid biomarkers for anaerobic methane-oxidizing archaea, PMI and crocetane, extracted from the seep carbonates (filled and open circles). Stars indicate the carbon isotopic compositions of the source methane, which were estimated based on the carbon isotope offset ($\Delta\delta^{13}C_{methane - lipid}$, Fig. 1.3A) in the upper panel and on the regression lines (Fig. 1.3B) in the lower panel. Filled and open stars indicate the values estimated using the isotopic compositions of PMI and crocetane, respectively. In both panels, error bars indicate the range of the estimated values. Ordered from the oldest (left) to youngest (right) site. Pleisto., Pleistocene; Plio., Pliocene.

Table 1.1. Stable carbon isotopic compositions of methane and lipid biomarkers of anaerobic methane-oxidizing archaea (PMI and crocetane), and the carbon isotope offset between methane and the lipids. The data were compiled from the cited literatures on modern methane-seep sites, following the layout and style of Niemann and Elvert (2008).

Site	Sample type	$\delta^{13}C_{methane}$			$\delta^{13}C_{PMI}$			$\delta^{13}C_{crocetane}$			$\Delta\delta^{13}C_{methane-PMI}$			$\Delta\delta^{13}C_{methane-crocetane}$		
		Min.	Ave.	Max.	Min.	Ave.	Max.	Min.	Ave.	Max.	Min.	Ave.	Max.	Min.	Ave.	Max.
Microbial reef, type II, northwestern Black Sea [1, 2]	mt	−68	−65	−62	−96	−93	−90	−95	−90	−85	25	28	31	20	25	30
Microbial reef, type I, northwestern Black Sea [1, 2]	mt	−68	−65	−62	−105	−102	−98	−108	−107	−105	33	36	40	40	41	43
Odessa Mud Volcano, northwestern Black Sea [3]	cb	−68	−68	−68	−101	−101	−101	n.a.	n.a.	n.a.	33	33	33	-	-	-
NIOZ Mud Volcano, northeastern Black Sea [3]	cb	−63	−63	−63	−99	−94	−89	n.a.	n.a.	n.a.	26	31	36	-	-	-
Kazakov Mud Volcano, northeastern Black Sea [3]	mb	−56	−56	−56	−84	−76	−68	n.a.	n.a.	n.a.	12	20	28	-	-	-
Northern summit of Hydrate Ridge [4, 5]	sd	−72	−67	−62	−126	−114	−89	−126	−115	−88	22	47	59	21	48	59
Southern summit of Hydrate Ridge [4, 5]	sd	−65	−65	−65	−116	−116	−116	−125	−125	−125	51	51	51	60	60	60
Southern summit of Hydrate Ridge [4, 5]	cb	−65	−65	−65	−122	−121	−121	−125	−125	−125	56	56	57	60	60	60
Eel River Basin, northern California [6, 7]	sd	−69	−61	−58	n.a.	n.a.	n.a.	−92	−92	−92	-	-	-	30	30	30
Umitaka Spur, northern site, eastern Japan Sea [8]	sd	−72	−72	−72	−114	−114	−114	n.a.	n.a.	n.a.	42	42	42	-	-	-
Joetsu Knoll, eastern Japan Sea [8]	sd	−61	−61	−61	−85	−85	−85	n.a.	n.a.	n.a.	24	24	24	-	-	-

Table 1.1 (*continued*)

Makran continental margin, site 15, Arabian Sea [9]	cb	−70	−70	−70	−125	−125	−125	−127	−127	−127	55	55	55	57	57	57
Makran continental margin, site 7, Arabian Sea [9]	cb	−67	−67	−67	−121	−121	−121	−122	−122	−122	54	54	54	55	55	55
Makran continental margin, site 2, Arabian Sea [9]	cb	−69	−69	−69	−106	−106	−106	−85	−85	−85	38	38	38	17	17	17
Alaminos Canyon, northern Gulf of Mexico [10]	cb	−56	−56	−56	−99	−89	−79	−103	−97	−91	23	33	43	35	41	47
Bush Hill, northern Gulf of Mexico [11]	sd	−63	−63	−63	*−99	*−99	*−99	n.a.	n.a.	n.a.	36	36	36	-	-	-
Haakon Mosby Mud Volcano, Norwegian Sea [12, 13]	cb	−64	−60	−51	−68	−68	−68	−83	−83	−83	8	8	8	23	23	23
Tommeliten, North Sea [14, 15]	cb	−46	−46	−46	**−93	**−93	**−93	−55	−55	−55	47	47	47	9	9	9
Central High, Marmara Sea [16]	cb	−44	−44	−44	*−92	*−85	*−75	−69	−69	−69	31	41	48	25	25	25
Çinarcik Basin, Marmara Sea [17]	sd	−64	−64	−64	*−118	*−105	*−94	**−97	**−97	**−97	30	41	54	33	33	33
Nyegga pockmark G11, Norwegian Sea [13, 18]	cb	−69	−69	−69	−130	−130	−130	−122	−122	−122	61	61	61	53	53	53
Nyegga pockmark G11, Norwegian Sea [19]	sd	−69	−69	−69	*−137	*−129	*−87	−73	−73	−73	18	60	68	4	4	4
Umitaka Spur, central site, eastern Japan Sea [20, 21]	cb	−37	−36	−35	−80	−80	−80	n.a.	n.a.	n.a.	44	44	44	-	-	-

Values are in ‰ vs. VPDB. *Unsaturated homologues (PMIΔs). **Approximate value. cb, carbonate; mb, mud breccia; mt, microbial mat; sd, sediment; n.a., data not available. [1] Michaelis et al. (2002); [2] Blumenberg et al. (2004); [3] Stadnitskaia et al. (2005); [4] Elvert et al. (1999); [5] Elvert et al. (2001); [6] Brooks et al. (1991); [7] Orphan et al. (2001); [8] Ogihara et al. (2009); [9] Himmler et al. (2015); [10] Birgel et al. (2011); [11] Zhang et al. (2003); [12] Lein et al. (1999); [13] Chevalier et al. (2010); [14] Hovland (2002); [15] Niemann et al. (2005); [16] Chevalier et al. (2011); [17] Chevalier et al. (2013); [18] Hovland et al. (2005); [19] Chevalier et al. (2014); [20] Hachikubo et al. (2015); [21] This study.

Table 1.2. Stable carbon and oxygen isotopic compositions of the early-diagenetic phases of the seep carbonates.

Site	Sample	Phase	$\delta^{13}C$	$\delta^{18}O$
Fukusaki	fs01	Recrystallized matrix	−37.2	−14.1
Fukusaki	fs05	Recrystallized matrix	−40.2	−12.2
Tanohama	tn06	Micrite	−15.3	−13.3
Tanohama	tn08	Micrite	−26.5	−12.6
Tanohama	tn14	Micrite	−17.9	−13.3
Tanohama	tn10	Recrystallized matrix	−32.3	−12.9
Tanohama	tn19	Recrystallized matrix	−41.0	−5.9
Tanohama	tn02	Sparry calcite	−8.2	−13.8
Tanohama	tn04	Sparry calcite	−17.8	−13.1
Tanohama	tn07	Radial calcite	−50.5	−2.5
Tanohama	tn09	Sparry calcite	−48.4	−2.2
Tanohama	tn11	Sparry calcite (acicular ghost)	−45.2	−5.1
Tanohama	tn12	Sparry calcite	−46.3	−3.5
Tanohama	tn13	Sparry calcite	−17.3	−13.4
Tanohama	tn17	Sparry calcite	−13.6	−13.4
Tanohama	tn18	Sparry calcite	−52.8	−2.4
Tanohama	tn20	Sparry calcite	−49.6	−4.4
Tanohama	tn21	Sparry calcite (acicular ghost)	−49.0	−4.8
Kanoura	ku01	Recrystallized matrix	−25.1	−14.0
Kanoura	ku03	Recrystallized matrix	−30.7	−14.5
Kanoura	ku04	Recrystallized matrix	−19.9	−14.0
Kanoura	ku02	Sparry calcite	−41.1	−11.8
Kanoura	ku07	Sparry calcite	−41.8	−10.4
Kanoura	ku08	Sparry calcite	−41.0	−12.2
Takinoue	yy0129	Matrix micrite	−26.9	−2.9
Takinoue	yy0124	Matrix micrite	−31.4	−2.9
Takinoue	yy0101	Matrix micrite	−39.7	0.1
Takinoue	yy0108	Matrix micrite	−38.9	−0.5
Takinoue	yy0112	Matrix micrite	−37.1	−1.1
Takinoue	yy0114	Matrix micrite	−41.1	0.2
Takinoue	yy0116	Matrix micrite	−43.0	0.0
Takinoue	yy0122	Matrix micrite	−41.7	0.0
Takinoue	yy0125	Matrix micrite	−41.1	0.3
Takinoue	yy0102	Pinkish cement (spherical crystals)	−40.3	−3.3
Takinoue	yy0103	Pinkish cement (pure micrite)	−46.1	1.3
Takinoue	yy0104	Pinkish cement (microsparite)	−39.5	−4.0
Takinoue	yy0105	Pinkish cement (microsparite)	−45.7	1.1
Takinoue	yy0107	Pinkish cement (pure micrite)	−48.3	1.5
Takinoue	yy0109	Pinkish cement (pure micrite)	−40.2	0.5
Takinoue	yy0113	Pinkish cement (pure micrite)	−37.3	−0.3
Takinoue	yy0117	Pinkish cement (pure micrite)	−42.8	1.1
Takinoue	yy0120	Pinkish cement (pure micrite)	−42.1	−1.9

Table 1.2 (*continued*)

Takinoue	yy0121	Pinkish cement (pure micrite)	−47.0	2.1
Anazawa/Akanuda	ak01	Micrite	−33.7	−7.3
Anazawa/Akanuda	ak04	Micrite	−27.3	−8.2
Anazawa/Akanuda	az01	Micrite	−35.5	−8.0
Anazawa/Akanuda	az03	Micrite	−39.9	−8.2
Anazawa/Akanuda	ak03	Sparry calcite	−39.9	−4.1
Anazawa/Akanuda	az04	Sparry calcite	−39.7	−8.9
Anazawa/Akanuda	az05	Sparry calcite	−42.2	−7.8
Sorimachi	smcn00	Micrite	−26.8	−0.5
Sorimachi	smpn00-1	Micrite	−32.6	−0.2
Sorimachi	smpn00-2	Micrite	−33.1	−0.2
Sorimachi	smpn00-3	Micrite	−26.3	−2.2
Sorimachi	smpn00-4	Micrite	−31.1	−0.9
Sorimachi	smpn00-5	Micrite	−30.5	−0.3
Sorimachi	smpn01	Micrite	−30.5	0.1
Sorimachi	smpn02	Micrite	−31.5	0.2
Sorimachi	smpn03	Micrite	−29.6	0.1
Sorimachi	smpn04	Micrite	−29.3	−0.1
Sorimachi	smpn05	Micrite	−31.7	−0.5
Sorimachi	smpn06	Micrite	−32.5	0.1
Sorimachi	smpn07	Micrite	−29.8	−0.4
Sorimachi	smpn08	Micrite	−31.2	−0.2
Sorimachi	smpn09	Micrite	−30.7	−0.7
Sorimachi	smpn10	Micrite	−23.6	−3.0
Sorimachi	smpn11	Micrite	−27.1	−0.6
Sorimachi	smpn12	Micrite	−31.8	−0.9
Sorimachi	smpn13	Micrite	−29.6	−1.0
Sorimachi	smpn14	Micrite	−33.3	−0.4
Sorimachi	smpn15	Micrite	−27.4	−0.3
Sorimachi	smcn01-1	Micrite	−29.6	0.2
Sorimachi	smcn01-2	Micrite	−29.9	0.2
Sorimachi	smcn02	Micrite	−24.4	−1.4
Sorimachi	smcn04	Micrite	−23.7	−2.1
Sorimachi	smpn17	Micrite	−34.6	1.2
Kuroiwa	ki05	Micrite	−34.3	−8.5
Kuroiwa	ki09	Micrite	−26.1	−6.8
Kuroiwa	ki11	Micrite	−28.0	−7.5
Kuroiwa	ki13	Micrite	−28.4	−7.5
Kuroiwa	ki02	Acicular aragonite + calcite	−36.6	−2.8
Kuroiwa	ki12	Acicular aragonite + calcite	−28.0	−6.5
Kuroiwa	ki15	Acicular aragonite + calcite	−31.2	−4.9
Nakanomata 1*	nk1302	Microcrystalline aragonite	−31.9	2.8
Nakanomata 1*	nk1306	Microcrystalline aragonite	−35.5	2.7
Nakanomata 1*	nk1307	Microcrystalline aragonite	−27.9	0.7
Nakanomata 1*	nk1310	Microcrystalline aragonite	−35.3	2.7

Table 1.2 (*continued*)

Nakanomata 1*	nk1315	Microcrystalline aragonite	−34.8	2.7
Nakanomata 1*	nk1318	Microcrystalline aragonite	−33.6	2.7
Nakanomata 1*	nk1322	Microcrystalline aragonite	−23.4	3.2
Nakanomata 1*	nk1324	Microcrystalline aragonite	−31.6	2.7
Nakanomata 1*	nk1335	Microcrystalline aragonite	−29.6	3.0
Nakanomata 1*	nk1339	Microcrystalline aragonite	−24.9	3.0
Nakanomata 1*	nk1301	Acicular aragonite	−33.4	2.9
Nakanomata 1*	nk1305	Acicular aragonite	−34.1	3.0
Nakanomata 1*	nk1309	Acicular aragonite	−38.8	2.7
Nakanomata 1*	nk1313	Acicular aragonite	−35.0	3.1
Nakanomata 1*	nk1321	Acicular aragonite	−32.1	3.2
Nakanomata 1*	nk1325	Acicular aragonite	−38.4	−0.7
Nakanomata 1*	nk1327	Acicular aragonite	−41.1	2.9
Nakanomata 1*	nk1328	Acicular aragonite	−38.6	3.3
Nakanomata 1*	nk1329	Acicular aragonite	−37.9	2.7
Nakanomata 1*	nk1334	Acicular aragonite	−28.2	3.4
Nakanomata 1*	nk1337	Acicular aragonite	−28.0	3.1
Nakanomata 1*	nk1341	Acicular aragonite	−31.3	2.6
Nakanomata 1*	nk1342	Acicular aragonite	−30.8	2.9
Nakanomata 2	nk1401	Micrite	−21.7	1.6
Nakanomata 2	nk1403	Micrite	−18.0	1.6
Nakanomata 2	nk1407	Micrite	−20.6	1.4
Nakanomata 2	nk1408	Micrite	−13.2	1.8
Nakanomata 2	nk1410	Micrite	−23.1	1.4
Nakanomata 2	nk1402	Bladed calcite	−22.6	1.9
Nakanomata 2	nk1411	Fibrous calcite	−24.8	2.1
Matsunoyama	ed01	Micrite	−42.5	2.3
Matsunoyama	ed02	Micrite	−36.9	2.0
Matsunoyama	ed06	Micrite	−43.3	2.5
Matsunoyama	ed07	Micrite	−27.1	0.7
Matsunoyama	ed08	Micrite	−34.2	1.3
Matsunoyama	ed09	Micrite	−39.1	2.8
Matsunoyama	ed12	Micrite	−34.8	2.0
Matsunoyama	ed0401	Micrite	−36.6	3.6
Matsunoyama	ed0404	Micrite	−25.6	3.8
Matsunoyama	ed0406	Micrite	−38.2	3.8
Matsunoyama	ed0407	Micrite	−36.1	3.4
Matsunoyama	ed0410	Micrite	−24.3	1.5
Matsunoyama	ed0411	Micrite	−37.8	4.6
Matsunoyama	ed0412	Micrite	−29.9	1.7
Matsunoyama	ed0415	Micrite	−31.4	2.6
Matsunoyama	ed0416	Micrite	−36.2	2.2
Matsunoyama	ed0418	Micrite	−40.0	3.6
Matsunoyama	ed0420	Micrite	−42.1	3.8
Matsunoyama	ed0421	Micrite	−37.6	2.9

Table 1.2 (*continued*)

Matsunoyama	ed0423	Micrite	−44.7	3.2
Matsunoyama	ed0424	Micrite	−46.0	2.8
Matsunoyama	ed0425	Micrite	−43.6	2.8
Matsunoyama	ed0426	Micrite	−42.1	2.8
Matsunoyama	ed0428	Micrite	−39.7	2.9
Matsunoyama	ed0430	Micrite	−40.9	3.5
Matsunoyama	ed0433	Micrite	−38.3	3.1
Anden	mh01	Gray micrite	−14.9	1.5
Anden	mh02	Gray micrite	−16.5	1.6
Anden	mh03	Gray micrite	−20.4	1.4
Anden	mh04	Dark−gray micrite	−64.7	1.8
Anden	mh05	Gray micrite	−12.4	0.2
Anden	mh06	Dark−gray micrite	−54.8	1.4
Anden	mh07	Dark−gray micrite	−58.4	1.3
Anden	mh08	Gray micrite	−4.7	1.6
Anden	mh10	Gray micrite	−10.4	0.7
Anden	mh11	Gray micrite	−5.6	1.5
Anden	mh12	Dark−gray micrite	−55.3	1.5
Anden	mh13	Gray micrite	−14.2	1.8
Anden	mh14	Dark−gray micrite	−55.6	1.4
Anden	mh15	Dark−gray micrite	−54.9	1.0
Umitaka Spur	ut01	Micrite	−13.4	3.0
Umitaka Spur	ut02	Micrite	−12.0	4.0
Umitaka Spur	ut03	Micrite	−18.0	5.2
Umitaka Spur	ut04	Micrite	−18.9	5.4
Umitaka Spur	ut05	Micrite	−19.3	5.4

Values are in ‰ vs. VPDB. *Data from Nakanomata 1 were previously reported in Miyajima et al. (2016).

Table 1.3. Stable carbon isotopic compositions of lipid biomarkers for anaerobic methane-oxidizing archaea extracted from the seep carbonates. The estimated isotopic compositions of the source methane are also shown. The isotopic compositions of methane were estimated using isotope offset ($\Delta\delta^{13}C_{methane\ -\ lipid}$ values) and regression lines (see text).

							Methane estimated from isotope offset for PMI			Methane estimated from isotope offset for crocetane			Methane predicted from regression line for PMI			Methane predicted from regression line for crocetane		
Site	Sample	Phase	Cr	PMI	Δ2	Bp0		Min.	Max.		Min.	Max.		Min.	Max.		Min.	Max.
Takinoue	yy0102	m	n.d.	−116	n.d.	n.d.	−72	−108	−48	-	-	-	−67	−82	−51	-	-	-
Takinoue	yy0103	m + v	n.d.	−57	n.d.	n.d.	-	-	-	-	-	-	-	-	-	-	-	-
Anazawa/Akanuda	an00	m + v	−99	−116	n.d.	−115	−72	−108	−48	−60	−95	−39	−67	−82	−51	−63	−76	−49
Anazawa/Akanuda	ak0103	m	n.d.	−93	n.d.	n.d.	−49	−85	−25	-	-	-	−59	−74	−44	-	-	-
Anazawa/Akanuda	ak02	m	n.d.	−101	n.d.	n.a.	−57	−93	−33	-	-	-	−61	−76	−46	-	-	-
Sorimachi	smgd3084	m	n.d.	−100	n.d.	n.a.	−56	−92	−32	-	-	-	−61	−76	−46	-	-	-
Kuroiwa	k0132	m	n.d.	−106	n.d.	n.d.	−62	−98	−38	-	-	-	−63	−78	−48	-	-	-
Kuroiwa	kim33	m + v	n.d.	−113	n.d.	n.a.	−69	−105	−45	-	-	-	−66	−81	−50	-	-	-
Nakanomata 1	nk13	m	−100	−108	n.d.	n.d.	−64	−100	−40	−61	−96	−40	−64	−79	−49	−63	−76	−49
Nakanomata 1	nkm13-35	m + v	−102	−113	n.d.	n.a.	−69	−105	−45	−63	−98	−42	−66	−81	−50	−63	−77	−50
Matsunoyama	ed0412	m	n.d.	−119	n.d.	n.d.	−75	−111	−51	-	-	-	−68	−83	−52	-	-	-
Anden	mh0413	m	−136	−137	*−147	n.d.	−93	−129	−69	−97	−132	−76	−74	−90	−58	−71	−86	−57
Umitaka Spur	nt0720_7 59-5	m	n.a.	−80	n.d.	n.d.	−36	-	-	-	-	-	−54	−70	−39	-	-	-

Values are in $\delta^{13}C$‰ vs. VPDB. *Average of two peaks, which differ in the position of double bonds. PMI extraxted from the sample yy0103 at Takinoue was not used for calculation of the isotopic composition of methane because its high $\delta^{13}C$ value indicates methanogenic archaea rather than methane-oxidizing archaea. m, matrix of microcrystalline calcite or aragonite; m + v, microcrystalline matrix containing >40% void-filling cement such as acicular aragonite, sparry calcite, and pinkinsh cement (for details of the carbonate phases, see Appendix); Bp0, acyclic biphytane; Cr, crocetane; Δ2, unsaturated PMI with two double bonds; PMI, pentamethylicosane; n.a., not analyzed due to low concentration; n.d., not detected.

Part 2. Residual gases in methane-seep carbonates

2.1. Introduction

Hydrocarbon gases within sediments and minerals have been analyzed to examine subsurface microbial activity such as methanogenesis and to detect subsurface petroleum generation (e.g., Abrams, 2005; Inagaki et al., 2015). Gases exist either in the interstitial pore spaces as a free or dissolved phase, bound to mineral or organic surfaces, or entrapped in crystal inclusions (Abrams, 2005). Multiple methods have been performed to extract hydrocarbon gases from the sediments, although the physical binding state of the hydrocarbons is poorly understood. The interstitial gases have been liberated traditionally using a standard headspace method (Kvenvolden and McDonald, 1986) or mechanical destruction of sediments (reviewed in Abrams, 2005). Gases bound to mineral and organic surfaces or entrapped within crystal inclusions have been liberated by acid treatment (e.g., Whiticar et al., 1994; Knies et al., 2004), heating (e.g., Sugimoto et al., 2003; Toki et al., 2007), and vacuum desorption (Zhang, 2003). Hydrocarbon and noble gases trapped within mineral inclusions and volcanic glasses have been liberated by crushing the minerals and glasses in a ball mill (e.g., Nishio et al., 1998; Ueno et al., 2006). As noted in Abrams (2005), these procedures should not be considered as representative of the actual physical state of the gases in sediments.

It has been reported that methane is probably adsorbed on clay minerals in sediments by physical adsorption, and can be liberated by heating (Sugimoto et al., 2003; Toki et al., 2007). Ijiri et al. (2009) reported that methane and ethane could be liberated by acid treatment from authigenic carbonate concretions recovered from the deep-sea subseafloor sediments. The contents of the methane liberated from the carbonate concretions were two orders of magnitude higher than those in the bulk sediments, and increased with increasing carbonate content of the bulk sediments (Ijiri et al., 2009). Although the mechanism of storage of the hydrocarbon gases in the authigenic carbonates was unclear, Ijiri et al. (2009) considered that the methane was preserved in the carbonates by simple physical adsorption. Their results suggested that authigenic carbonate concretions have an important role as adsorbents of methane in sediments. The methane liberated from the concretions showed stable carbon isotopic compositions nearly identical to, or lower than the methane contained in the surrounding bulk sediments. It was thus considered that the methane in the carbonate concretions and that in the surrounding sediments are of the same origin (Ijiri et al., 2009).

Submarine methane seeps are characterized by elevated contents of methane and heavier hydrocarbons compared with the normal seafloor (e.g., Toki et al., 2007, 2012;

Pape et al., 2010, 2014). The previous studies mentioned above indicate a possibility that methane contained in the seep fluids is preserved within authigenic methane-seep carbonates, which formed via an alkalinity increase induced by the anaerobic oxidation of methane (AOM). Recently, Blumenberg et al. (2017) extracted methane and heavier hydrocarbons in low concentrations (up to 257 ppb) from modern seep carbonates by acid treatment. This results showed that the carbon isotopic composition of the carbonate-entrapped methane reflects that of the seep methane, while the molecular composition ($C_1/(C_2 + C_3)$) and carbon isotopic compositions of the ethane and propane appear to be modified in the carbonate-entrapped gases. Since there have been only a few attempts to extract the residual methane and other gases from the methane-seep carbonates (Ijiri, 2003; D. Maeyama, pers. comm.), the storage mechanisms and modification processes of the residual gases within the seep carbonates remain to be understood. Effects of thermal maturity on the residual gases within ancient methane-seep carbonates hosted in sedimentary strata are also unknown.

In this chapter, residual gases were extracted from both ancient and modern methane-seep carbonates using several methods. The origin of the extracted gases is estimated based on their concentrations and stable carbon isotopic compositions. Whether the extracted gases were originally contained in the seep fluids or originated

from secondary processes is discussed, based on carbon isotopic distributions among the residual gases and organic matter within the carbonates and maturity assessment of the samples. It is known that the carbon isotopic distribution among hydrocarbons depends on mixing of hydrocarbons from different sources as well as on their origins (thermogenic, biogenic, or abiotic) (e.g., Chung et al., 1988; Jenden et al., 1993; Tilley et al., 2011). This chapter also focuses on the isotopic distribution among methane, ethane, and propane in the residual gases from the view point of mixing of different gas components.

2.2. Material

For residual gas analyses, the same samples as used for the stable isotope and biomarker analyses were prepared. As described in Part 1, they were collected from the Miocene to Pleistocene sediments and a modern seep site along the Japan Sea coast (Fig. 1.1). Heating and crushing experiments described below were performed only on samples from the Tortonian or Messinian Nakanomata 1 site. The carbonates at Nakanomata 1 are composed of microcrystalline aragonite and acicular aragonite crystals, which are <10 μm or a few tens of μm in diameter.

2.3. Analytical methods

To extract residual gases in seep carbonates, this study performed three experiments: 1) acid-digestion; 2) heating; and 3) crushing experiments.

2.3.1. Acid-digestion experiment

Powdered samples were collected from cut slabs or blocks of the carbonate rocks using a hand-held rotary micromill. Some samples were prepared by grinding crushed chips using a tungsten mortar and pestle. Samples were collected from early-diagenetic carbonate phases, microcrystalline matrix and void-filling cements such as acicular aragonite or sparry calcite (see Part 1). Hydrocarbon gases were extracted from the carbonates using the same method described in Ijiri et al. (2009). The powders (~50–100 mg) were placed into a glass vial (inner volume 5 cm^3), which was then sealed with a butyl rubber septum and aluminum cap. The vial was evacuated and orthophosphoric acid (~0.5 mL) was added to dissolve the carbonates. After complete dissolution of the carbonates at 50°C, 10 mL of the liberated gas was extracted with a gas-tight syringe and introduced into a gas chromatograph-isotope ratio mass spectrometer (GC-IRMS: Thermo Scientific Trace GC-Delta plus XP) at the Kochi Institute for Core Sample Research (KOCHI), Japan Agency for Marine-Earth Science and Technology

(JAMSTEC), Nankoku, Japan. Produced CO_2 and water were removed by adsorbents before entering the GC. The extracted hydrocarbons were quantified in nmol/g of the carbonate, assuming that all of the gases present originated from the carbonate. The concentrations of hydrocarbons were calculated by comparing the $^{44}CO_2$ output of the IRMS with those measured during analyses of a working standard gas containing 0.513% methane, 0.492% ethane, 0.490% propane, and 0.502% *n*-butane. Measured values of *i*-butane are not shown in this study, because *i*-butane can be liberated from the butyl rubber septum by acid treatment. All isotope values are reported as a per-mil difference between the sample and a Vienna Pee Dee Belemnite (VPDB) standard in conventional delta (δ) notation.

Stable carbon isotopic compositions of the carbonate powders used for the acid-digestion experiment were measured by a Thermo Scientific GasBench II/Delta V Advantage IRMS at the Laboratory of Evolution of Earth Environment, Kanazawa University (LEEKU), Kanazawa, Japan and a Thermo Scientific Kiel III/MAT253 IRMS at the KOCHI. To produce CO_2, the powders of ~300–500 μg and ~50–70 μg were reacted in the online GasBench II and Kiel III carbonate devices, respectively, with orthophosphoric acid in a glass vial under vacuum at 70°C. Isotope compositions are given in δ notation (‰ vs. VPDB). The standard deviations of replicate analyses of

NBS19 and working standards LSVEC and JLs-1 by GasBench II/Delta V Advantage were better than 0.06‰ and 0.12‰ for $\delta^{13}C$ and $\delta^{18}O$, respectively. The standard deviations of replicate analyses of NBS19 and a working standard ANU-m2 by Kiel III/MAT253 were better than 0.07‰ and 0.08‰ for $\delta^{13}C$ and $\delta^{18}O$, respectively.

2.3.2. Heating experiment

Chipped samples (226–243 mg) were prepared by mechanically crushing the early-diagenetic carbonate phases, microcrystalline aragonite and acicular aragonite crystal aggregates. The chips were placed in the bottom of a crusher device composed of Pyrex glass (internal volume 5 cm^3), which was designed in Uemura et al. (2016). The crusher device was then heated at 90°C for 2 h under vacuum, using a mantle heater regulated by a temperature controller. The concentration of the released gas was monitored by a manometer. The released gases were collected at −196°C (liquid nitrogen) in a U-shaped trap, which contained silica gel (Fig. 2.1). To introduce the collected gases into the GC-IRMS, the trap was warmed to ~100°C (hot water) and the liberated gases were transferred by the helium flow. Water was removed by an adsorbent before entering the GC. The instrument used for the GC-IRMS analyses was the same as the acid-digestion experiment. It has been reported that methane was not formed by pyrolysis when fresh

sediment was heated at 121°C for 60 min using an autoclave in laboratory (Sugimoto et al., 2003).

2.3.3. Crushing experiment

After the heating and evacuation of the line, the chipped samples in the crusher device were crushed under vacuum at 90°C. Heating was continued during the crushing to minimize possible adsorption of gases onto the newly created surfaces. Crushing was performed by pressing the glass rod onto the samples by rotating the grip at the top of the threaded valve stem of the crusher as Uemura et al. (2016). A filter was installed between the crusher and the line to prevent contamination of the line by crushed particles (Fig. 2.1). The released gases were collected in the trap and then analyzed by the GC-IRMS as described in section 2.3.2. After the experiment, the crushed samples were removed from the crusher, powdered, and then dissolved by phosphoric acid in glass vials to liberate gases that were analyzed by the GC-IRMS, as described in section 2.3.1.

2.3.4. Stable carbon isotope analyses of total organic carbon

To get insights into the source of the hydrocarbons extracted from the seep

carbonates, the stable carbon isotopic compositions of total organic carbon (TOC) within the carbonates were analyzed. For the carbon isotope analyses of TOC, the same powdered samples used for biomarker analyses (Part 1) were prepared. The carbonates were completely dissolved by reacting with 5N HCl for 24 h at room temperature. Acid was then removed by repeated centrifugation and washing with deionized water. After freeze-drying, the residues (~1–4 mg, depending on the TOC content) were analyzed with a Thermo Quest NA2500NCS elemental analyzer (EA) connected to a Thermo Scientific Delta V Advantage IRMS at the LEEKU. Samples were oxygenated at 1000°C to make CO_2 gas. Carbon isotopic compositions are given in δ notation ($\delta^{13}C$‰ vs. VPDB). The standard deviations of replicate analyses of a working standard (L-alanine, LAL) and the international standard ANU sucrose were better than 0.06‰ and 0.11‰, respectively.

2.3.5. Maturity assessment using biomarkers

To assess thermal maturity of the carbonate samples, biomarker analyses were performed as described in Part 1. Maturity-related biomarker parameters were measured using peak areas of the relevant compounds in the total ion and mass chromatograms. The odd-to-even predominance (OEP) of *n*-alkanes and isomerization between S and R

configurations at C-20 in the C_{29} 5α(H),14α(H),17α(H)-steranes and at C-22 in the C_{31} and C_{32} 17α(H)-hopanes were measured as:

$$OEP_1 = (C_{21} + 6C_{23} + C_{25})/(4C_{22} + 4C_{24})$$

$$20S/(20S + 20R)$$

$$22S/(22S + 22R).$$

The OEP_1 value in a thermally mature oil or rock extract is near 1.0. With increasing maturity, the $20S/(20S + 20R)$ and $22S/(22S + 22R)$ ratios rise from 0 to equilibrium values 0.55 and 0.60, respectively (Peters et al., 2005). The $22S/(22S + 22R)$ ratios of the hopanes reach equilibrium earlier than the $20S/(20S + 20R)$ ratios of the steranes. These parameters can be correlated with the vitrinite reflectance $\%R_o$ to estimate the maturity level of oils or rock extracts (Peters et al., 2005).

2.3.6. Gas mixing model

To simulate the carbon isotope distribution observed in the hydrocarbon gases extracted by acid digestion, two-component mixing models were used. Assuming that two gases, A and B, mix to form a third gas, M, the concentration of *i* hydrocarbon in the mixed gas M (C_i^M) is given by simple mass balance as:

$$C_i^M = f \times C_i^A + (1 - f) \times C_i^B$$

where C_i^A and C_i^B are the concentrations of the *i* hydrocarbon in A and B, respectively, and *f* is the fraction of the component A in the mixed gas ($0 \leq f \leq 1$). The carbon isotopic composition ($\delta^{13}C$) of the *i* hydrocarbon in the mixed gas M (I_i^M) is then given by:

$$I_i^M = [f \times C_i^A \times I_i^A + (1 - f) \times C_i^B \times I_i^B]/C_i^M$$

using the isotopic compositions of the *i* hydrocarbon in A and B (I_i^A and I_i^B).

As an endmember component, average concentrations and isotopic compositions of methane to propane in Japanese natural gases were used (normal thermogenic gas): $C_1 = 83.8\%$, $C_2 = 4.7\%$, and $C_3 = 1.4\%$; $\delta^{13}C_1 = -34.6‰$, $\delta^{13}C_2 = -23.6‰$, and $\delta^{13}C_3 = -20.7‰$ (Waseda et al., 2002). The normal thermogenic gas was generated from marine/terrestrial kerogens whose $\delta^{13}C$ values are around −20‰ (Igari, 1999). As a biogenic gas, concentrations reported in Vogel et al. (1982) were used: $C_1 = 99.9757\%$, $C_2 = 0.0017\%$, and $C_3 = 0.0058\%$. Since reports on the isotopic compositions of biogenic ethane and propane are scarce, the isotopic compositions of the biogenic gas were assumed as $\delta^{13}C_1 = -70.0‰$, $\delta^{13}C_2 = -60.0‰$, and $\delta^{13}C_3 = -55.0‰$.

As another endmember of the mixing model, a secondary thermogenic gas (see section 2.5.4) was assumed. The isotopic compositions of hydrocarbons in the secondary thermogenic gas were calculated using formulae in Berner and Faber (1996). In their formulae, the isotopic compositions of hydrocarbons expected from thermal

cracking of a source kerogen with certain $\delta^{13}C$ value can be calculated as a function of thermal maturity (%R_o). A $\delta^{13}C$ value of a source was assumed so as to reproduce the isotopic compositions of the residual hydrocarbons extracted from the seep carbonates. For the hydrocarbon concentrations of the secondary gases, the results of open-system pyrolysis experiments of algal kerogens under different temperatures shown in Berner et al. (1995) were used.

2.4. Results

2.4.1. Hydrocarbon gases extracted by acid digestion

Methane and heavier hydrocarbons were successfully extracted from the examined seep carbonates by acid digestion. The concentrations and the stable carbon isotopic compositions of hydrocarbon gases extracted from the carbonates are shown in Table 2.1. Methane was extracted from all the samples, whose content ranges between 7 and 1354 nmol/g. A very high amount of methane (3650 nmol/g) was liberated from a sample from the Burdigalian Tanohama site. The methane content roughly increases with age of the carbonates (Fig. 2.2), and only trace amounts of methane (<13 nmol/g) was released from the samples taken from the Pleistocene and modern seep sites (Anden and Umitaka Spur, respectively). Ethane was extracted from the carbonates excluding

those at the Anden and Umitaka Spur seeps. Propane was liberated from the Tanohama, Takinoue, Anazawa/Akanuda, Sorimachi, Kuroiwa, Nakanomata 1 and 2, and Matsunoyama samples. *n*-Butane was liberated only from the Takinoue, Sorimachi, Anazawa/Akanuda, and Nakanomata 1 samples (Table 2.1). The methane to ethane plus propane ratios ($C_1/(C_2 + C_3)$) of the extracted gases range between 2 and 518, and are mostly lower than 50 except for the gases from the Fukusaki and Kanoura carbonates (Fig. 2.3A).

The $\delta^{13}C$ values of the methane extracted from the carbonates show a large scatter, ranging between −69.6‰ and −26.9‰ (Fig. 2.3A and B). The isotopic composition of the methane could not be measured for the Anden and Umitaka Spur samples due to its low concentration. The methane liberated from the Kanoura and Anazawa/Akanuda carbonates has $\delta^{13}C$ values lower than −50‰, while the methane from the Sorimachi, Kuroiwa, Nakanomata 2, and Matsunoyama has $\delta^{13}C$ values higher than −50‰. The $\delta^{13}C$ values of the methane extracted from the carbonates at Fukusaki, Tanohama, Takinoue, and Nakanomata 1 range from −69.6‰ to −40.0‰. The $\delta^{13}C$ values of the liberated ethane range between −78.0‰ and −26.2‰, which are lower or higher than the coexisting methane (Table 2.1 and Figs. 2.3B and 2.4). The propane has $\delta^{13}C$ values ranging between −83.7‰ and −28.9‰, which are in some cases lower than the

coexisting methane and ethane (Table 2.1 and Figs. 2.3C and 2.4). The $\delta^{13}C$ values of the *n*-butane range between −49.5‰ and −35.4‰, which are higher than the coexisting propane (Table 2.1 and Fig. 2.4). Comparisons of the $\delta^{13}C$ values of the coexisting hydrocarbons revealed increases in $\delta^{13}C$ values with increasing carbon number ($\delta^{13}C_1 < \delta^{13}C_2 < \delta^{13}C_3$) for some data, but also found isotopic "reversals" such as $\delta^{13}C_1 > \delta^{13}C_2$ and $\delta^{13}C_2 > \delta^{13}C_3$ for other data (Fig. 2.4). The methane, ethane, and propane liberated from the void-filling cements such as acicular aragonite or calcite and sparry calcite tend to have low $\delta^{13}C$ values with respect to those from microcrystalline matrix of the carbonates, although it is not always the case (Fig. 2.3).

The carbon isotopic compositions of the methane and the carbonate powders from which the methane was liberated were compared at two sites, Nakanomata 1 and Anazawa/Akanuda. The $\delta^{13}C$ values of the methane and the carbonates show a significant positive correlation ($r = 0.64$, $p < 0.05$) at Nakanomata 1, whereas those at Anazawa/Akanuda show no correlation (Fig. 2.5).

2.4.2. Gases extracted by heating experiment

During heating of the chipped carbonates from Nakanomata 1, the gas concentration increased continuously (Fig. 2.6). The increase rate of the gas

concentration dropped with time. The degassed gases contain methane (~2 nmol/g) and carbon dioxide (265–490 nmol/g) (n = 3; Table 2.2 and Fig. 2.7). Ethane and heavier hydrocarbons were not detected in the gases released by heating. While the low concentrations of the methane retarded measurements of the carbon isotopic compositions, the $\delta^{13}C$ values of the carbon dioxide was measured as −13.1‰ to −11.2‰ (Table 2.2 and Fig. 2.8B).

2.4.3. Gases extracted by crushing experiment

Crushing of the carbonate chips liberated methane and carbon dioxide. Ethane and heavier hydrocarbons were not detected in the gases released by crushing. The amount of the methane liberated by crushing (4–10 nmol/g) is higher than that by heating (Table 2.2 and Fig. 2.7). In contrast, the amount of the carbon dioxide liberated by crushing (41–193 nmol/g) is lower than that by heating. The $\delta^{13}C$ values of the liberated methane range between −55.1‰ and −49.9‰ (Table 2.2 and Fig. 2.8A). The $\delta^{13}C$ values of the carbon dioxide range between −26.8‰ and −25.0‰, which are lower than those liberated by heating (Table 2.2 and Fig. 2.8B). Even higher amounts of methane (163–247 nmol/g) were extracted along with heavier hydrocarbons by acid digestion of the crushed carbonate samples (Table 2.2 and Fig. 2.7). The $\delta^{13}C$ values of the methane

released by acid digestion range between −63.5‰ and −55.8‰, which are similar to or lower than those by crushing (Table 2.2 and Fig. 2.8A). The concentrations and carbon isotopic compositions of the hydrocarbons extricated by acid digestion of the crushed samples are identical to those reported for the Nakanomata 1 samples in section 2.4.1.

2.4.4. Carbon isotopic compositions of total organic carbon within the seep carbonates

The $\delta^{13}C$ values of the total organic carbon (TOC) within the examined seep carbonates range between −49.1‰ (Tanohama) and −24.3‰ (Matsunoyama) (Table 2.3 and Fig. 2.4). These $\delta^{13}C$ values are lower than those of sedimentary organic carbon and the kerogen in the Miocene source rocks for oils in the study area (>−25‰, Waseda and Iwano, 2008; Freire et al., 2012).

2.4.5. Thermal maturity of organic matter within the seep carbonates

The OEP_1 values of *n*-alkanes within the carbonates older than 10 Ma (Fukusaki, Tanohama, Kanoura, Takinoue, Anazawa/Akanuda, Sorimachi, and Kuroiwa) are around 1.0, while those within the younger carbonates at the remaining sites are significantly larger than 1.0 (Table 2.4 and Fig. 2.9). The $20S/(20S + 20R)$ ratios of the

C_{29} steranes range between 0.18 and 0.60, and particularly the Anazawa/Akanuda carbonates showed greater ratios (around 0.55) than any other samples (Fig. 2.9). The 22*S*/(22*S* + 22*R*) ratios of the C_{31} hopanes range between 0.26 and 0.59, and the Takinoue, Sorimachi, and Anazawa/Akanuda carbonates showed higher ratios than 0.48. Measurements of the 22*S*/(22*S* + 22*R*) ratios of the C_{32} hopanes gave the similar results, ranging between 0.18 and 0.62, except that a sample from the Pleistocene Anden carbonate showed a high ratio of 0.55. Steranes and hopanes were not detected within the carbonates at Fukusaki, Tanohama, and Kanoura, which are oldest in age in this study. These compounds could have been thermally degraded at the three sites due to an even higher level of thermal maturity (Peters et al., 2005). This interpretation is supported by the recrystallized nature and the strongly ^{18}O-depleted signature of the carbonates (see Part 1 and Appendix). Based on these biomarker parameters, the maturity level of the organic matter within the seep carbonates can be correlated with the vitrinite reflectance %R_o as follows: $R_o < 0.5\%$ for the Nakanomata 1 and 2, Matsunoyama, Anden, and Umitaka Spur carbonates; $R_o = 0.5\%–0.6\%$ for the Takinoue, Sorimachi, and Kuroiwa carbonates; $R_o > 0.7\%$ for the Fukusaki, Tanohama, Kanoura, and Anazawa/Akanuda carbonates.

2.4.6. Isotope distribution in hydrocarbons simulated by gas mixing models

Ethane and propane extracted by the acid-digestion experiment (section 2.4.1) have $\delta^{13}C$ values as low as −84‰. They can be reproduced if organic matter with $\delta^{13}C$ value of −80‰ contained within the carbonates is assumed to be thermally cracked to generate secondary thermogenic hydrocarbons (section 2.5.4). The carbon isotopic compositions of such a secondary thermogenic gas component can be calculated as $\delta^{13}C_1 = -95.9‰$, $\delta^{13}C_2 = -87.8‰$, and $\delta^{13}C_3 = -84.4‰$ based on Berner and Faber (1996), assuming maturity level (R_o) of 0.5%. The hydrocarbon concentrations of this component are given as $C_1 = 53.3\%$, $C_2 = 27.2\%$, and $C_3 = 11.2\%$ based on Berner et al. (1995). Figure 2.10A shows the isotope distribution in hydrocarbons of a mixed gas produced when the secondary thermogenic gas is mixed with a normal thermogenic gas in different fractions of 0.0 to 1.0. This mixing model shows isotopic "reversals" such as $\delta^{13}C_1 > \delta^{13}C_2$ and $\delta^{13}C_2 > \delta^{13}C_3$ as observed in the hydrocarbons extracted by the acid digestion of the seep carbonates (Fig. 2.4). The full isotopic reversal, $\delta^{13}C_1 > \delta^{13}C_2 > \delta^{13}C_3$, is produced when the fraction of the secondary gas is assumed to be 0.1 and 0.2. The result of another mixing model between a biogenic gas and the secondary gas is shown in Fig. 2.10B. This model also shows isotopic reversals between methane and ethane, but not between ethane and propane.

When the secondary thermogenic gas is generated at higher maturity level (R_o) of 1.5%, the isotopic compositions of hydrocarbons can be calculated as $\delta^{13}C_1 = -88.6‰$, $\delta^{13}C_2 = -79.2‰$, and $\delta^{13}C_3 = -76.2‰$. Using the result of pyrolysis experiment in Berner et al. (1995), the hydrocarbon concentrations of the secondary gas generated at R_o of 1.5% are given as $C_1 = 84.4\%$, $C_2 = 11.6\%$, and $C_3 = 2.1\%$. In Fig. 2.10C, the isotope distribution in hydrocarbons of a mixed gas is calculated assuming the mixing between the normal thermogenic gas and the secondary thermogenic gas generated at R_o of 1.5%. In this mixing model, the isotopic reversals are observed between methane and ethane when the fraction of the secondary gas is 0.3 to 0.6. However, the difference in the $\delta^{13}C$ value between methane and ethane is much smaller compared with the previous mixing model between the normal and secondary gases generated at R_o of 0.5% (Fig. 2.10A). The isotopic reversals were not observed between ethane and propane in this model (Fig. 2.10C).

2.5. Discussion

2.5.1. Storage of residual gases within the seep carbonates

As in clastic sediments, possible mechanisms of storage of gases within carbonate rocks are either 1) entrapment within intercrystalline pore spaces, 2) physical adsorption

to surfaces of carbonates and other minerals or organic matter, or 3) inclusion within carbonate crystals (Abrams, 2005; Ijiri et al., 2009). Acid digestion of powdered carbonates (<30 μm) can liberate the gases both adsorbed to mineral surfaces and entrapped within crystals. Heating of chipped carbonates (<8 mm) can desorb the gases physically adsorbed to surfaces of carbonates, clay minerals, or organic matter by weak intermolecular forces such as van der Waals forces (Sugimoto et al., 2003). Crushing of the chipped carbonates can release the gases entrapped in intercrystalline pores. Because heating was continued during the crushing experiment in this study, it is also possible that the gases were thermally desorbed from crystal surfaces newly exposed by the crushing. Both the acid-digestion and heating experiments liberated >200 nmol/g of hydrocarbons and carbon dioxide in total, while the crushing experiment liberated less amounts of gases (Table 2.2 and Fig. 2.7). This fact suggests that the gases within intercrystalline pores could be minor in amount. With respect to the methane, smaller amounts of methane were liberated by the heating and crushing experiments, compared with those liberated by the acid digestion. This might be because the methane entrapped within intercrystalline pores and adsorbed to crystal surfaces is minor in amount, and the methane is mainly entrapped within small individual crystals of <10 μm to a few tens of μm in diameter. However, it is also possible that the subsequent crushing and

powdering after heating exposed fresh surfaces of individual crystals, and resulted in further desorption of the methane adsorbed to the crystal surfaces by acid digestion. The amounts of methane liberated by the acid digestion are ~100 times larger than those liberated by the heating (Fig. 2.7). If all of the methane were adsorbed to individual crystal surfaces, this result cannot be explained by an increase in exposed crystal surfaces and further desorption. For example, powdering of a 5-mm cubic chip to 10-μm cubic crystals results in a 500-times increase of surface area, which would overestimate the amount of methane further desorbed from the exposed surfaces.

2.5.2. Origin of methane extracted from the seep carbonates

The $\delta^{13}C$ values of the methane and the $C_1/(C_2 + C_3)$ ratios of the gases extracted from the seep carbonates by acid digestion indicate either thermogenic or biogenic, or both origins for the extracted methane (Fig. 2.3A). The methane liberated from the Sorimachi, Kuroiwa, Nakanomata 2, and Matsunoyama carbonates has $\delta^{13}C$ values higher than −50‰ and $C_1/(C_2 + C_3)$ ratios lower than 50, indicating a thermogenic origin. The methane liberated from the Fukusaki, Tanohama, Kanoura, Takinoue, Anazawa/Akanuda, and Nakanomata 1 carbonates have $\delta^{13}C$ values around and lower than −50‰ and the $C_1/(C_2 + C_3)$ ratios lower than 1000. This methane could represent

biogenic methane enriched in ^{13}C and depleted in content due to fractionation during the methane oxidation (Whiticar and Faber, 1986). However, its $\delta^{13}C$ values can also be explained by mixed origins. Preferential adsorption or encapsulation of high-molecular-weight hydrocarbons might also have contributed to the low $C_1/(C_2 + C_3)$ ratios (Cheng and Huang, 2004; Ijiri et al., 2009; Blumenberg et al.,2017).

It is possible that the liberated methane clearly indicating a thermogenic origin ($\delta^{13}C > -50‰$, $C_1/(C_2 + C_3) < 50$) was secondary trapped within or adsorbed to the carbonates after their precipitation and during their burial, rather than represents the methane originally contained in the seep fluids. The secondary entrapment of thermogenic methane is supported by the facts that the sediments hosting the seep carbonates act as reservoir rocks of oil and gas today (Monzawa et al., 2006; Okui et al., 2008) and that only trace amounts of methane were extracted from the Pleistocene and modern carbonates (Fig. 2.2). The host rock at the Tortonian Kuroiwa site is intruded by a Pliocene andesite dyke, which could have generated thermogenic hydrocarbons even in the sediments surrounding the seep carbonates. The carbon isotopic compositions of the carbonates and biomarkers indicate biogenic, rather than thermogenic, origins for the methane at the examined ancient seeps, except for the Nakanomata 2 seep (Part 1).

The biogenic origin of the liberated methane seems consistent with the results

obtained from the biomarker isotopes (Part 1). However, it is also possible that thermal cracking of the ^{13}C-depleted organic matter preserved within the seep carbonates generated secondary thermogenic methane with $\delta^{13}C$ values lower than −50‰ (see below). It is nevertheless noteworthy that there is a positive significant correlation between the $\delta^{13}C$ values of the liberated methane and the carbonates at Nakanomata 1 (Fig. 2.5). The methane liberated from the acicular aragonite has relatively low $\delta^{13}C$ values as well as generally low $\delta^{13}C_{carbonate}$ values with respect to the microcrystalline aragonite. This correlation implies that the methane originally contained in the Miocene seep fluids was preserved within the host carbonate cements during their precipitation. The carbon isotope separation factor between carbon dioxide and methane (ε_C) was defined in Whiticar (1999) as:

$$\varepsilon_C \approx \delta^{13}C_{CO_2} - \delta^{13}C_{CH_4}.$$

The difference between the $\delta^{13}C$ values of the carbon dioxide and the methane released by the crushing of the Nakanomata 1 carbonates is consistent with the ε_C values resulting from the methane oxidation (Fig. 2.8C). This indicates that the biogenic methane contained in the seep fluids at the Nakanomata 1 seep became enriched in ^{13}C due to isotope fractionation during the AOM, and was preserved within the host carbonate cements along with the ^{13}C-depleted carbon dioxide. In contrast, there is no

significant correlation between the $\delta^{13}C$ values of the liberated methane and the carbonates at Anazawa/Akanuda (Fig. 2.5). This might be partly attributed to the dissolution and reprecipitation of the carbonates during recrystallization which caused the resetting of the isotopic compositions of the carbonates.

2.5.3. Origin of carbon dioxide extracted from the seep carbonates

The $\delta^{13}C$ values of the carbon dioxide extracted by heating from the Nakanomata 1 carbonates were higher than those by crushing (Table 2.2 and Fig. 2.8B). It is known for methane that gases adsorbed to sediments and coal are enriched in ^{13}C (Friedrich and Jüntgen, 1971; Whiticar et al., 1994; Knies et al., 2004; Toki et al., 2007). The ^{13}C-enriched carbon dioxide liberated by the heating could have thus resulted from the selective adsorption of ^{13}C-rich carbon dioxide on the carbonate surfaces. It is suspected that the ^{13}C-depleted carbon dioxide within the carbonate cements is attributed to the isotope fractionation during adsorption, as well as during methane oxidation.

2.5.4. Origin of hydrocarbons heavier than methane extracted from the seep carbonates

The hydrocarbons heavier than methane extracted by acid digestion have both low

$\delta^{13}C$ values as low as −83.7‰ and typical values for thermogenic gases ($\delta^{13}C$ > ~−40‰), indicating multiple sources (Fig. 2.3B and C). Biogenic ethane and propane with $\delta^{13}C$ values as low as −70‰ have been reported in natural environments, but they are <1% of methane (Vogel et al., 1982; Oremland et al., 1988; Waseda and Didyk, 1995; Whiticar, 1999). The biogenic origin for the ethane and propane is thus inconsistent with the $C_1/(C_2 + C_3)$ ratios lower than 100 (Fig. 2.3A).

The large amount of the ethane and propane liberated from the seep carbonates (Fig. 2.3A) indicates either decreases in the relative content of the methane due to the methane oxidation (Whiticar and Faber, 1986), thermogenic origins for the high-molecular-weight hydrocarbons, or combined results of them. If the extracted hydrocarbons were thermogenic in origin, the source for their low $\delta^{13}C$ values has to be explained. Calculation after the formulae in Berner and Faber (1996) indicated that the ^{13}C-depleted ethane and propane ($\delta^{13}C < -40$‰) extracted from the Tanohama, Takinoue, Anazawa/Akanuda, Sorimachi, Kuroiwa, Nakanomata 1, and Matsunoyama carbonates can be explained by the thermogenic generation from a source with a $\delta^{13}C$ value lower than −30‰ (Fig. 2.3B and C). One of the possible candidates for the ^{13}C-depleted source is TOC of the seep carbonates, with $\delta^{13}C$ values ranging between −49.1‰ (Tanohama) and −24.3‰ (Matsunoyama) (Table 2.3). The $\delta^{13}C_{TOC}$ values of

modern and ancient methane-seep carbonates are generally low due to inputs of methane-derived ^{13}C-depleted carbon into the biomass sustained by the seep fluids (e.g., Smrzka et al., 2016). Another candidate is even more ^{13}C-depleted compounds such as lipid biomarkers for methane-oxidizing archaea preserved within the carbonates (δ^{13}C value around −100‰, see Part 1). The unusually ^{13}C-depleted ethane and propane could have been produced by secondary thermal cracking of these organic compounds within the carbonates during burial and thermal maturation.

Hydrocarbon generation by the secondary thermal cracking of the ^{13}C-depleted compounds within the carbonates is possible in thermally mature samples. The organic matter within the Tanohama, Takinoue, Anazawa/Akanuda, Sorimachi, and Kuroiwa carbonates is mature (R_o > 0.5%, Table 2.4 and Fig. 2.9), and therefore such secondary process can be responsible for the ^{13}C-depleted ethane and propane extracted from these samples. The generation of the secondary thermogenic gas from immature organic matter within seep carbonates is controversial. The ^{13}C-depleted ethane and propane were liberated even from the Nakanomata 1 and Matsunoyama carbonates, in which organic matter is thermally immature (R_o < 0.5%, Table 2.4 and Fig. 2.9). These carbonates are unlikely to have been subjected to a high temperature of >100°C, as supported by the preservation of aragonitic phases and the positive δ^{18}O values of the

carbonates (Part 1; Miyajima et al., 2016). It is supposed that the secondary thermal cracking under relatively low temperatures produced low amounts of ^{13}C-depleted ethane and propane, while bulk organic matter remains immature within the seep carbonates. It can be ruled out that the secondary cracking was caused by the acid treatment and the subsequent heating at ~50°C during the experiments, because the acid-digestion experiments failed to extract ^{13}C-depleted ethane and propane from the Fukusaki, Anden, and Umitaka Spur carbonates.

Comparing the isotopic compositions of the coexisting hydrocarbons, the linear increase in $\delta^{13}C$ values of the liberated hydrocarbons with increasing carbon number, that is, $\delta^{13}C_1 < \delta^{13}C_2 < \delta^{13}C_3$ (Fig. 2.4), seems typical of thermogenic hydrocarbons formed by pyrolysis. This isotopic trend readily results from the kinetic isotope effect in which a $^{12}C–^{12}C$ bond is easier to break than a $^{12}C–^{13}C$ bond in kerogen molecules (Chung et al., 1988). A linear fit can be obtained when the $\delta^{13}C$ value of cogenetic hydrocarbons are plotted as a function of the inverse carbon number (called “Natural gas plot”). The $\delta^{13}C$ values of methane can deviate from the linear isotopic trend, due either to mixing of biogenic methane or to the methane oxidation (e.g., Pohlman et al., 2005). The isotopic trend of thermogenic gas was exhibited by the hydrocarbons liberated from the Tanohama, Anazawa/Akanuda, Nakanomata 1, and Nakanomata 2

carbonates. The methane at the Nakanomata 1 seep could have been mainly biogenic in origin (see Part 1 and section 2.5.2). In contrast, one trio of methane, ethane, and propane extracted from the Nakanomata 1 carbonate showed the thermogenic trend with $\delta^{13}C$ values higher than −43‰. This trio is possibly a thermogenic gas that migrated from the deep subsurface and was secondary entrapped within the carbonates. The secondary entrapment of thermogenic gas could also be the case for the hydrocarbons extracted from the Nakanomata 2 carbonates, since the Nodani Formation, which yielded the Nakanomata 1 and 2 carbonates, is known as a reservoir rock of oil and gas today (Akahane and Kato, 1989).

The hydrocarbons extracted from the Tanohama and Anazawa/Akanuda carbonates showed the linear isotopic trend of thermogenic gas (Fig. 2.4), but they include ethane and propane with significantly low $\delta^{13}C$ values compared with the typical thermogenic gases in the study area (>−42‰ for ethane and >−29‰ for propane: Sakata, 1991; Igari, 1999; Waseda et al., 2002). As discussed above, these ethane and propane with low $\delta^{13}C$ values could have originated from the secondary thermal cracking of the ^{13}C-depleted organic compounds within the seep carbonates. The source $\delta^{13}C$ values for the thermogenic hydrocarbons can be approximately estimated by the regression and extrapolation of the linear isotopic trend to the *y*-intercept in Fig. 2.4 (Chung et al.,

1988; Igari, 1999; Pohlman et al., 2005). When applied to the hydrocarbons liberated from the Tanohama and Anazawa/Akanuda carbonates, the source $\delta^{13}C$ values range between −47.4‰ and −23.3‰ (Fig. 2.4). These values are mostly lower than sedimentary organic carbon and are close to the $\delta^{13}C_{TOC}$ value of the Anazawa/Akanuda carbonate.

In addition to the isotopic trend of thermogenic gas, the hydrocarbons released from the seep carbonates at Takinoue, Anazawa/Akanuda, Sorimachi, Nakanomata 1, and Matsunoyama show isotopic "reversals", which are unusual for thermogenic and biogenic hydrocarbons. The "reverse" trends were found between the methane and ethane ($\delta^{13}C_1 > \delta^{13}C_2$) and also between the ethane and propane ($\delta^{13}C_2 > \delta^{13}C_3$) (Fig. 2.4). The ethane with $\delta^{13}C$ values lower than the coexisting methane was also extracted from the Kuroiwa carbonates, which did not yield propane (Table 2.1). In some extreme examples such as the hydrocarbons liberated from Nakanomata 1 and Matsunoyama, $\delta^{13}C$ values decrease linearly with increasing carbon number, namely, $\delta^{13}C_1 > \delta^{13}C_2 > \delta^{13}C_3$ (Fig. 2.4). The unusual "reverse" isotopic trends could be attributed either to abiotic generation of the hydrocarbons by polymerization reactions or to mixing of hydrocarbons with different origins and thus different isotopic and molecular compositions.

The isotopic trend showing depletion in ^{13}C for ethane to butane with respect to methane have been reported in abiogenic hydrocarbons. They are known from, for examples, products of spark discharge experiments (Des Marais et al., 1981), the Murchison meteorite (Yuen et al., 1984), crystalline rock mine of the Canadian shield (Sherwood Lollar et al., 2002), H_2-rich fumarolic gases from a shield basaltic volcano in the Eastern Pacific (Taran et al., 2010), natural gases derived from magma chambers in the Songliao Basin, China (Wang et al., 2009), and both on-land and seafloor serpentinite-hosted hydrothermal systems (Proskurowski et al., 2008; Charlou et al., 2010; Suda et al., 2017). The monotonous decrease in the $\delta^{13}C$ values of hydrocarbons with increasing carbon number, namely, $\delta^{13}C_1 > \delta^{13}C_2 > \delta^{13}C_3$, has been regarded as a result of polymerization reactions, such as production of higher-molecular-weight hydrocarbons from methane. In kinetically controlled synthesis, a reactant containing ^{12}C ($^{12}CH_4$) reacts more rapidly than that containing ^{13}C ($^{13}CH_4$), and thus ^{12}C is more likely to be incorporated into the synthesized larger hydrocarbon chains (Des Marais et al., 1981; Yuen et al., 1984; Sherwood Lollar et al., 2002). Therefore, the $^{13}C/^{12}C$ ratio in hydrocarbons synthesized from methane is lower than that of the reactant. Considering the common occurrences of the abiogenic hydrocarbons in hydrothermal systems and other extreme environments mentioned above, the abiotic formation by

polymerization reactions is unlikely for the hydrocarbons within methane-seep carbonates.

In addition to the possibility of the abiotic polymerization, the reverse isotopic trends of hydrocarbons can also be explained by input of the ethane and propane that were generated by secondary thermal cracking of the organic compounds within the carbonates. The positive correlations between the $\delta^{13}C$ values of the liberated methane, ethane, and propane (Fig. 2.3B and C) suggest mixing between normal thermogenic or biogenic gases and the unusually ^{13}C-depleted ethane and propane (Ijiri, 2003). "Isotopic reversals" caused by mixing of hydrocarbon gases of different origins have been reported by several studies. Jenden et al. (1993) reported isotopic reversals ($\delta^{13}C_1 > \delta^{13}C_2$) in thermogenic gases in northern Appalachian Basin and interpreted them as a result of mixing between early-mature wet gas with higher amounts of C_{2+} hydrocarbons and post-mature dry gas with lower amounts of C_{2+} hydrocarbons. Des Marais et al. (1988) also showed that isotopic reversals between ethane and propane ($\delta^{13}C_2 > \delta^{13}C_3$) result from mixing of hydrocarbons with different relative amounts of C_{2+} generated at different temperatures in laboratory by dry pyrolysis of lignite. Partial or full isotopic reversals have been also reported from shale gases of high maturity ($R_o >$ ~1.5%) (Burruss and Laughrey, 2010; Tilley et al., 2011; Zumberge et al., 2012; Xia et

al., 2013). The isotopic reversals in shale gases have been explained by a similar mechanism; primary gas from thermal cracking of kerogen mixed with secondary gas from cracking of oil or wet gas components, which is wetter than the primary gas (Xia et al., 2013). These previous studies indicate that if the secondary thermogenic hydrocarbons had low $C_1/(C_2 + C_3)$ ratios (high relative amounts of ethane and propane) as well as the low $\delta^{13}C$ values (<−40‰), they could cause the reverse isotopic trends when mixed with normal thermogenic or biogenic gases.

The result of the mixing model between a normal thermogenic gas and a secondary thermogenic gas (Fig. 2.10A) predicts that the isotopic reversals between methane, ethane, and propane depend on the mixing ratio. Here, the $C_1/(C_2 + C_3)$ ratio of the normal gas is 14, while that of the secondary gas is 1. This model also indicates that the extreme trend, namely, $\delta^{13}C_1 > \delta^{13}C_2 > \delta^{13}C_3$, can be generated when the ratio of the secondary thermogenic gas is low. It is thus supposed that even very low amounts of secondary thermogenic gas could produce the reverse isotopic trend. Another mixing model between a normal biogenic gas and the secondary thermogenic gas can also reproduce the reverse trends, but it cannot explain the observed $\delta^{13}C$ values of the residual gases (Fig. 2.10B).

To sum up, the reverse isotopic trends of the residual gases within the seep

carbonates are interpreted as a mixture of hydrocarbons with different origins; the normal thermogenic or biogenic hydrocarbons and the hydrocarbons generated by the secondary thermal cracking. Tilley et al. (2011) suggested that such isotopic reversals only occur in a closed system such as shales, where ^{12}C-enriched ethane generated from oil cracking accumulates along with mature, ^{13}C-enriched methane and little or no gas has been lost during its maturation history. Previous pyrolysis experiments of source rocks and coals showed that closed-system experiments generate a greater proportion of propane than do experiments by open-system at the same maturity (Andresen et al., 1995; Takahashi et al., 2014; Takahashi and Suzuki, 2017). The isotopic reversals observed in this study might be a result of accumulation of secondary gases enriched in ethane and propane with respect to normal gases within closed to semi-closed carbonate cements.

The isotopic trend of the residual gases within the seep carbonates seems to be related to thermal maturity of the organic matter within the carbonates. In the samples with $R_o < 0.6\%$ (Takinoue, Sorimachi, Nakanomata 1, and Matsunoyama), the residual gases showed mostly the reverse isotopic trends and the ethane had higher $\delta^{13}C$ values than the coexisting propane ($\delta^{13}C_2 > \delta^{13}C_3$) (Fig. 2.4). In contrast, in samples with $R_o >$ 0.7% (Tanohama and Anazawa/Akanuda), the ethane has lower $\delta^{13}C$ values than the

coexisting propane ($\delta^{13}C_2 < \delta^{13}C_3$) (Fig. 2.4). Berner et al. (1995)'s gas generation experiments by dry open-system pyrolysis of an algal-rich and a land-plant kerogen showed that at higher temperatures, the $C_1/(C_2 + C_3)$ ratio of the generated hydrocarbons increases, in other words, the relative amounts of ethane and propane decrease. Andresen et al. (1995) also showed increases in the $C_1/(C_2 + C_3)$ ratio with increasing temperature by hydrous closed-system pyrolysis of natural source rocks and coals. It is therefore suggested that the $C_1/(C_2 + C_3)$ ratios of the hydrocarbons generated by the secondary thermal cracking increase with increasing thermal maturity. The mixing model between the normal thermogenic gas and a secondary thermogenic gas generated at a higher maturity level (R_o = 1.5% and $C_1/(C_2 + C_3) = 6$) indicates that the isotopic reversals are not significant when the secondary gas has a high $C_1/(C_2 + C_3)$ ratio (Fig. 2.10C). The mixing models in Fig. 2.10 also indicate that the isotopic reversal becomes insignificant when the mixing ratio of the secondary gas endmember is high. Secondary thermal cracking can proceed within seep carbonates with increasing thermal stress, resulting in an increased mixing ratio of the secondary gas. The increase of the secondary-generated gases with increasing maturity is also indicated by the increase of the methane content with increasing age and maturity (Fig. 2.2).

In summary, the hydrocarbons liberated from the seep carbonates most likely

originated from the secondary entrapment of thermogenic or biogenic gases, which migrated through the host sediments during burial of the carbonates, and from the secondary thermal cracking of the ^{13}C-depleted organic compounds within the carbonates. The extent of the ^{13}C depletion in the hydrocarbons generated by the secondary thermal cracking could be controlled by the $\delta^{13}C$ values of the source, which depend on the relative abundance of the strongly ^{13}C-depleted compounds within the seep carbonates. The $\delta^{13}C$ values of the secondary hydrocarbons may also depend on the maturity; the generated hydrocarbons have higher $\delta^{13}C$ values with increasing maturity (Berner et al., 1995; Berner and Faber, 1996). The unusual "reverse" carbon isotope distribution among the residual gases can be attributed to mixing of the normal thermogenic or biogenic hydrocarbons with the hydrocarbons generated by the secondary thermal cracking. It is suggested that the mixing ratio and $C_1/(C_2 + C_3)$ ratio of the secondary-generated hydrocarbons depend on thermal maturity. Increase of maturity is probably associated either with the mixing ratio of the secondary-generated hydrocarbons to the normal gas or with the $C_1/(C_2 + C_3)$ ratio of them (Fig. 2.10). Several lines of evidence indicate that the original biogenic methane in the seep fluids was preserved within the carbonates at the Nakanomata 1 seep, whereas the ethane and propane there could have originated from the secondary processes.

2.6. Summary

1) By acid digestion of the carbonates, methane and heavier hydrocarbons were successfully extracted from the Miocene to Pliocene methane-seep carbonate rocks collected along the Japan Sea coast.
2) Methane and carbon dioxide were also liberated by heating and crushing of a Miocene seep carbonate at Nakanomata 1. The concentration of the methane liberated from this sample was highest in acid-digestion experiment, suggesting that the methane was mainly entrapped within micrometer-scaled crystals.
3) The carbon isotopic compositions and molecular compositions of the liberated methane indicate both thermogenic and biogenic origins. There is a possibility that the methane of thermogenic origin was entrapped within the seep carbonates during their burial.
4) A significant positive correlation was observed in the carbon isotopic compositions between carbonate and extracted methane at Nakanomata 1. Along with the isotopic composition of the methane and coexisting carbon dioxide, such correlation indicates that biogenic methane originally contained in the Miocene seep fluid was oxidized and preserved within the seep carbonate.

5) The ethane and propane extracted from the examined carbonates showed unusually ^{13}C-depleted isotopic compositions. These hydrocarbons are most likely generated by secondary thermal cracking of ^{13}C-depleted organic compounds within the seep carbonates during their burial.

6) Mixing between the normal thermogenic and/or biogenic gases and the secondary thermogenic gases could have produced the “reverse” carbon isotopic trends of the extracted hydrocarbons. The results of calculation based on a gas mixing model suggest that the isotopic trends of the hydrocarbons within the seep carbonates differ depending on the molecular composition or mixing ratio of the gas components, or thermal maturity of the carbonates.

References

Abrams, M.A., 2005. Significance of hydrocarbon seepage relative to petroleum generation and entrapment. Marine and Petroleum Geology 22, 457–477.

Akahane, S., Kato, H., 1989. Geology of the Takada-Seibu district. With Geological Sheet Map at 1:50,000, Geological Survey of Japan, 89 pp. (in Japanese with English abstract)

Andresen, B., Throndsen, T., Råheim, A., Bolstad, J., 1995. A comparison of pyrolysis

products with models for natural gas generation. Chemical Geology 126, 261–280.

Bernard, B.B., Brooks, J.M., Sackett, W.M., 1976. Natural gas seepage in the Gulf of Mexico. Earth and Planetary Science Letters 31, 48–54.

Berner, U., Faber, E., 1996. Empirical carbon isotope/maturity relationships for gases from algal kerogens and terrigenous organic matter, based on dry, open-system pyrolysis. Organic Geochemistry 24, 947–955.

Berner, U., Faber, E., Scheeder, G., Panten, D., 1995. Primary cracking of algal and landplant kerogens: kinetic models of isotope variations in methane, ethane and propane. Chemical Geology 126, 233–245.

Blumenberg, M., Pape, T., Seifert, R., Bohrmann, G., Schlömer, S., 2017. Can hydrocarbons entrapped in seep carbonates serve as gas geochemistry recorder? Geo-Marine Letters, 10.1007/s00367-017-0522-6.

Burruss, R.C., Laughrey, C.D., 2010. Carbon and hydrogen isotopic reversals in deep basin gas: evidence for limits to the stability of hydrocarbons. Organic Geochemistry 41, 1285–1296.

Charlou, J.L., Donval, J.P., Konn, C., Ondréas, H., Fouquet, Y., Jean-Baptiste, P., Fourré, E., 2010. High production and fluxes of H_2 and CH_4 and evidence of abiotic hydrocarbon synthesis by serpentinization in ultramafic-hosted hydrothermal

systems on the Mid-Atlantic Ridge. Diversity of Hydrothermal Systems on Slow Spreading Ocean Ridges, Geophysical Monograph Series 188, 265–296.

Cheng, A.-L., Huang, W.-L., 2004. Selective adsorption of hydrocarbon gases on clays and organic matter. Organic Geochemistry 35, 413–423.

Chung, H.M., Gormly, J.R., Squires, R.M., 1988. Origin of gaseous hydrocarbons in subsurface environments: theoretical considerations of carbon isotope distribution. Chemical Geology 71, 97–103.

Des Marais, D.J., Donchin, J.H., Nehring, N.L., Truesdell, A.H., 1981. Molecular carbon isotopic evidence for the origin of geothermal hydrocarbons. Nature 292, 826–828.

Des Marais, D.J., Stallarad, M.L., Nehring, N.L., Truesdell, A.H., 1988. Carbon isotope geochemistry of hydrocarbons in the Cerro Prieto geothermal field, Baja California Norte, Mexico. Chemical Geology 71, 159–167.

Freire, A.F.M., Matsumoto, R., Akiba, F., 2012. Geochemical analysis as a complementary tool to estimate the uplift of sediments caused by shallow gas hydrates in mounds at the seafloor of Joetsu Basin, eastern margin of the Japan Sea. Journal of Geological Research, 839840.

Friedrich, H.-U., Jüntgen, H., 1971. Some measurements of the $^{12}C/^{13}C$-ratio in methane

or ethane desorbed from hard coal or released by pyrolysis. In: Gaertner, H.R.V., Wehner, H., (Eds.), Advances in Organic Geochemistry 1971. Pergamon Press, 639–646.

Igari, S., 1999. Carbon isotopic ratios of methane, ethane and propane in natural gases from Niigata and Akita in Japan: factors affecting the parameters. Geochemical Journal 33, 127–132.

Ijiri, A., 2003. Stable Isotopic Studies on Fluid and Gas Migration in Forearc Sediments. Ph.D. Thesis 6575, Graduate School of Science, Hokkaido University, Sapporo, Japan, 100 pp.

Ijiri, A., Tsunogai, U., Gamo, T., Nakagawa, F., Sakamoto, T., Saito, S., 2009. Enrichment of adsorbed methane in authigenic carbonate concretions of the Japan Trench. Geo-Marine Letters 29, 301–308.

Inagaki, F., Hinrichs, K.-U., Kubo, Y., Bowles, M.W., Heuer, V.B., Hong, W.-L., Hoshino, T., Ijiri, A., Imachi, H., Ito, M., Kaneko, M., Lever, M.A., Lin, Y.-S., Methé, B.A., Morita, S., Morono, Y., Tanikawa, W., Bihan, M., Bowden, S.A., Elvert, M., Glombitza, C., Gross, D., Harrington, G.J., Hori, T., Li, K., Limmer, D., Liu, C.-H., Murayama, M., Ohkouchi, N., Ono, S., Park, Y.-S., Phillips, S.C., Prieto-Mollar, X., Purkey, M., Riedinger, N., Sanada, Y., Sauvage, J., Snyder, G.,

Susilawati, R., Takano, Y., Tasumi, E., Terada, T., Tomaru, H., Trembath-Reichert, E., Wang, D.T., Yamada, Y., 2015. Exploring deep microbial life in coal-bearing sediment down to ~2.5 km below the ocean floor. Science 349, 420–424.

Jenden, P.D., Drazan, D.J., Kaplan, I.R., 1993. Mixing of thermogenic natural gases in northern Appalachian Basin. American Association of Petroleum Geologists Bulletin 77, 980–998.

Knies, J., Damm, E., Gutt, J., Mann, U., Pinturier, L., 2004. Near-surface hydrocarbon anomalies in shelf sediments off Spitsbergen: evidences for past seepages. Geochemistry, Geophysics, Geosystems 5, Q06003.

Kvenvolden, K.A., McDonald, T.J., 1986. Organic Geochemistry on the *JOIDES Resolution*—an Assay. Technical Note of the Ocean Drilling Program 6, 147 pp.

Miyajima, Y., Watanabe, Y., Yanagisawa, Y., Amano, K., Hasegawa, T., Shimobayashi, N., 2016. A late Miocene methane-seep deposit bearing methane-trapping silica minerals at Joetsu, central Japan. Palaeogeography, Palaeoclimatology, Palaeoecology 455, 1–15.

Monzawa, N., Kaneko, M., Osawa, M., 2006. A review of petroleum system in the deep water area of the Toyama Trough to the Sado Island in the Japan Sea, based on the results of the METI Sado Nansei Oki drilling. Journal of the Japanese Association

for Petroleum Technology 71, 618–627. (in Japanese with English abstract)

Nishio, Y., Sasaki, S., Gamo, T., Hiyagon, H., Sano, Y., 1998. Carbon and helium isotope systematics of North Fiji Basin basalt glasses: carbon geochemical cycle in the subduction zone. Earth and Planetary Science Letters 154, 127–138.

Okui, A., Kaneko, M., Nakanishi, S., Monzawa, N., Yamamoto, H., 2008. An integrated approach to understanding the petroleum system of a frontier deep-water area, offshore Japan. Petroleum Geoscience 14, 223–233.

Oremland, R.S., Whiticar, M.J., Strohmaier, F.E., Kiene, R.P., 1988. Bacterial ethane formation from reduced, ethylated sulfur compounds in anoxic sediments. Geochimica et Cosmochimica Acta 52, 1895–1904.

Pape, T., Bahr, A., Rethemeyer, J., Kessler, J.D., Sahling, H., Hinrichs, K.-U., Klapp, S.A., Reeburgh, W.S., Bohrmann, G., 2010. Molecular and isotopic partitioning of low-molecular-weight hydrocarbons during migration and gas hydrate precipitation in deposits of a high-flux seepage site. Chemical Geology 269, 350–363.

Pape, T., Geprägs, P., Hammerschmidt, S., Wintersteller, P., Wei, J., Fleischmann, T., Bohrmann, G., Kopf, A.J., 2014. Hydrocarbon seepage and its sources at mud volcanoes of the Kumano forearc basin, Nankai Trough subduction zone. Geochemistry, Geophysics, Geosystems 15, 2180–2194.

Peters, K.E., Walters, C.C., Moldowan, J.M., 2005. The Biomarker Guide, Second Edition. Cambridge University Press, New York, 1155 pp.

Pohlman, J.W., Canuel, E.A., Ross Chapman, N., Spence, G.D., Whiticar, M.J., Coffin, R.B., 2005. The origin of thermogenic gas hydrates on the northern Cascadia Margin as inferred from isotopic ($^{13}C/^{12}C$ and D/H) and molecular composition of hydrate and vent gas. Organic Geochemistry 36, 703–716.

Poroskurowski, G., Lilley, M.D., Seewald, J.S., Früh-Green, G.L., Olson, E.J., Lupton, J.E., Sylva, S.P., Kelley, D.S., 2008. Abiogenic hydrocarbon production at Lost City Hydrothermal Field. Science 319, 604–607.

Sakata, S., 1991. Carbon isotope geochemistry of natural gases from the Green Tuff Basin, Japan. Geochimica et Cosmochimica Acta 55, 1395–1405.

Sherwood Lollar, B., Westgate, T.D., Ward, J.A., Slater, G.F., Lacrampe-Couloume, G., 2002. Abiogenic formation of alkanes in the Earth's crust as a minor source for global hydrocarbon reservoirs. Nature 416, 522–524.

Smrzka, D., Zwicker, J., Klügel, A., Monien, P., Bach, W., Bohrmann, G., Peckmann, J., 2016. Establishing criteria to distinguish oil-seep from methane-seep carbonates. Geology 44, 667–670.

Suda, K., Gilbert, A., Yamada, K., Yoshida, N., Ueno, Y., 2017. Compound- and

position-specific carbon isotopic signatures of abiogenic hydrocarbons from on-land serpentinite-hosted Hakuba Happo hot spring in Japan. Geochimica et Cosmochimica Acta 206, 201–215.

Sugimoto, A., Dan, J., Kumai, T., Murase, J., 2003. Adsorption as a methane storage process in natural lake sediment. Geophysical Research Letters 30(21), 2080.

Takahashi, K.U., Suzuki, N., 2017. Semi-open and closed system pyrolysis of Paleogene coal for evaluating the timing of hydrocarbon gas expulsion. International Journal of Coal Geology 178, 100–109.

Takahashi, K.U., Suzuki, N., Saito, H., 2014. Compositional and isotopic changes in expelled and residual gases during anhydrous closed-system pyrolysis of hydrogen-rich Eocene subbituminous coal. International Journal of Coal Geology 127, 14–23.

Taran, Y.A., Varley, N.R., Inguaggiato, S., Cienfuegos, E., 2010. Geochemistry of H_2- and CH_4-enriched hydrothermal fluids of Socorro Island, Revillagigedo Archipelago, Mexico. Evidence for serpentinization and abiogenic methane. Geofluids 10, 542–555.

Tilley, B., McLellan, S., Hiebert, S., Quartero, B., Veilleux, B., Muehlenbachs, K., 2011. Gas isotope reversals in fractured gas reservoirs of the western Canadian Foothills: mature shale gases in disguise. American Association of Petroleum Geologists

Bulletin 95, 1399–1422.

Toki, T., Tsunogai, U., Gamo, T., Tanahashi, M., 2007. Geochemical studies of pore fluid in surface sediment on the Daini Atsumi Knoll. Journal of Geochemical Exploration 95, 29–39.

Toki, T., Uehara, Y., Kinjo, K., Ijiri, A., Tsunogai, U., Tomaru, H., Ashi, J., 2012. Methane production and accumulation in the Nankai accretionary prism: results from IODP Expeditions 315 and 316. Geochemical Journal 46, 89–106.

Uemura, R., Nakamoto, M., Asami, R., Mishima, S., Gibo, M., Masaka, K., Jin-Ping, C., Wu, C.-C., Chang, Y.-W., Shen, C.-C., 2016. Precise oxygen and hydrogen isotope determination in nanoliter quantities of speleothem inclusion water by cavity ring-down spectroscopic techniques. Geochimica et Cosmochimica Acta 172, 159–176.

Ueno, Y., Yamada, K., Yoshida, N., Maruyama, S., Isozaki, Y., 2006. Evidence from fluid inclusions for microbial methanogenesis in the early Archaean era. Nature 440, 516–519.

Vogel, T.M., Oremland, R.S., Kvenvolden, K.A., 1982. Low-temperature formation of hydrocarbon gases in San Francisco Bay sediment (California, U.S.A.). Chemical Geology 37, 289–298.

Wang, X.B., Guo, Z.Q., Tuo, J.C., Guo, H.Y., Li, Z.X., Zhuo, S.G., Jiang, H.L., Zeng, L.W., Zhang, M.J., Wang, L.S., Liu, C.X., Yan, H., Li, L.W., Zhou, X.F., Wang, Y.L., Yang, H., Wang, G., 2009. Abiogenic hydrocarbons in commercial gases from the Songliao Basin, China. Sciences in China Series D: Earth Sciences 52, 213–226.

Waseda, A., Didyk, B.M., 1995. Isotope compositions of gases in sediments from the Chile continental margin. In: Lewis, S.D., Behrmann, J.H., Musgrave, R.J., Cande, S.C. (Eds.), Proceedings of the Ocean Drilling Program, Scientific Results 141. Ocean Drilling Program, College Station, TX, pp. 307–312.

Waseda, A., Iwano, H., 2008. Characterization of natural gases in Japan based on molecular and carbon isotope compositions. Geofluids 8, 286–292.

Waseda, A., Iwano, H., Takeda, N., 2002. Geochemical study on origin and maturity of natural gases. Journal of the Japanese Association for Petroleum Technology 67, 3–15. (in Japanese with English abstract)

Whiticar, M.J., 1999. Carbon and hydrogen isotope systematics of bacterial formation and oxidation of methane. Chemical Geology 161, 291–314.

Whiticar, M.J., Faber, E., 1986. Methane oxidation in sediment and water column environments—isotope evidence. Organic Geochemistry 10, 759–768.

Whiticar, M.J., Faber, E., Whelan, J.K., Simoneit, B.R.T., 1994. Thermogenic and

bacterial hydrocarbon gases (free and sorbed) in Middle Valley, Juan de Fuca Ridge, Leg 139. In: Mottl, M.J., Davis, E.E., Fisher, A.T., Slack, J.F. (Eds.), Proceedings of the Ocean Drilling Program, Scientific Results 139. Ocean Drilling Program, College Station, TX, pp. 467–477.

Xia, X., Chen, J., Braun, R., Tang, Y., 2013. Isotopic reversals with respect to maturity trends due to mixing of primary and secondary products in source rocks. Chemical Geology 339, 205–212.

Yuen, G., Blair, N., Des Marais, D.J., Chang, S., 1984. Carbon isotope composition of low molecular weight hydrocarbons and monocarboxylic acids from Murchison meteorite. Nature 307, 252–254.

Zhang, L., 2003. Vacuum desorption of light hydrocarbons adsorbed on soil particles: a new method in geochemical exploration for petroleum. American Association Petroleum Geochemical Exploration Bulletin 87, 89–97.

Zumberge, J., Ferworn, K., Brown, S., 2012. Isotopic reversal (‘rollover’) in shale gases produced from the Mississippian Barnett and Fayetteville formations. Marine and Petroleum Geology 31, 43–52.

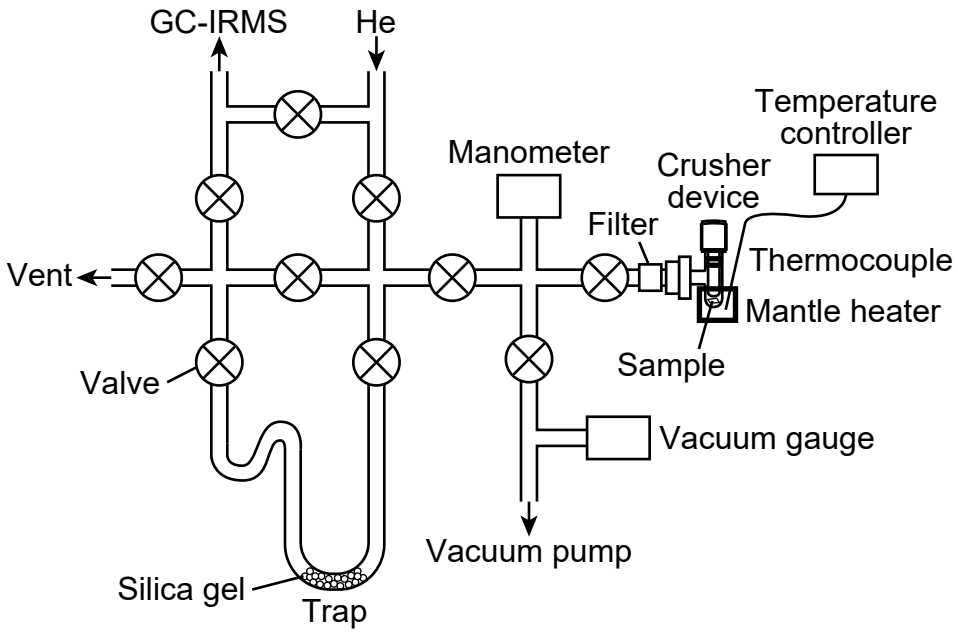

Fig. 2.1. Schematic view of the line used for the heating and crushing extraction of residual gases.

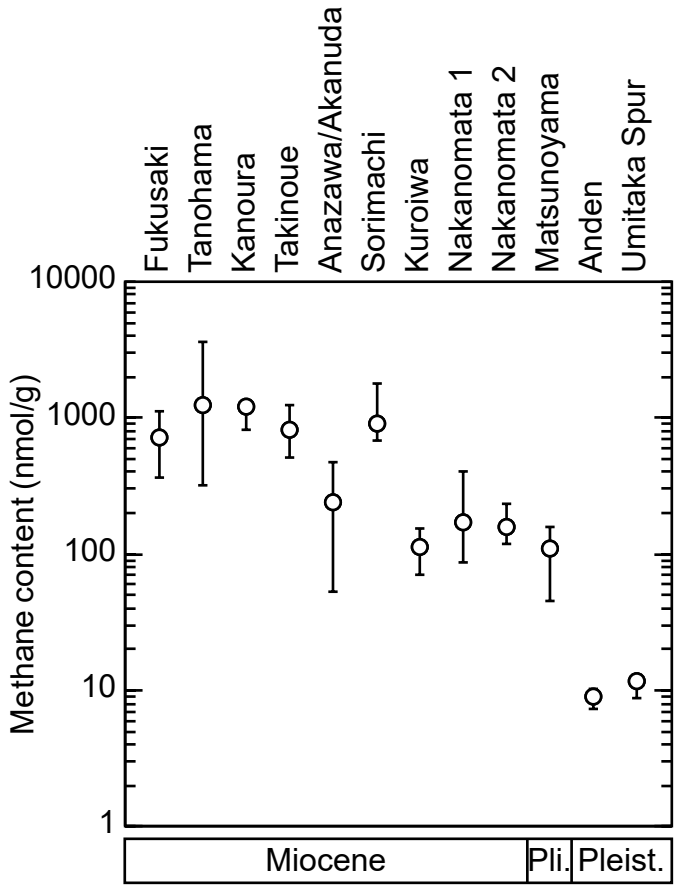

Fig. 2.2. Concentrations of the methane extracted from the seep carbonates by the acid-digestion experiment. Note the logarithmic scale. Open circles indicate the mean values, and error bars indicate the range of the observed values. Ordered from the oldest (left) to youngest (right) site. Pleist., Pleistocene; Pli., Pliocene.

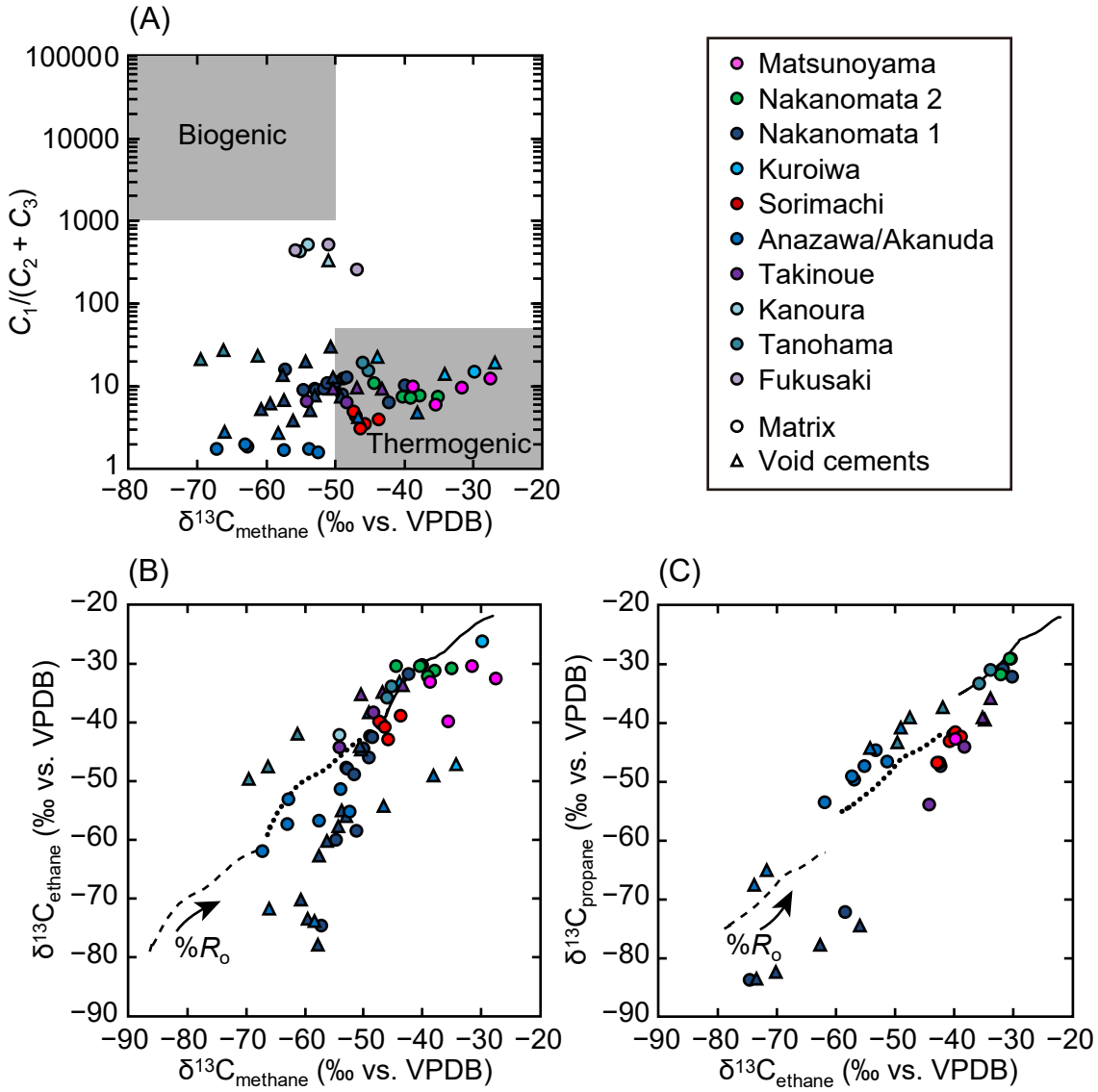

Fig. 2.3. Stable carbon isotopic compositions and molecular ratios of the hydrocarbons extracted from the seep carbonates by the acid-digestion experiment. Data from the Anden and Umitaka Spur seeps are not included. (A) "Bernard diagram" (Bernard et al., 1976) showing $\delta^{13}C$ values of the methane and the methane to (ethane+propane) ratios. Shaded areas indicate typical ranges for biogenic and thermogenic gases after Whiticar (1999). (B, C) Cross plots of $\delta^{13}C$ values of the methane and ethane (B) and the ethane and propane (C). Solid, dotted, and dashed lines indicate the $\delta^{13}C$ values expected from thermal cracking of source kerogens with $\delta^{13}C$ values of −30 ‰ , −50 ‰ , and −70 ‰ , respectively, as a function of the vitrinite reflectance (%R_o) (calculated after Berner and Faber, 1996).

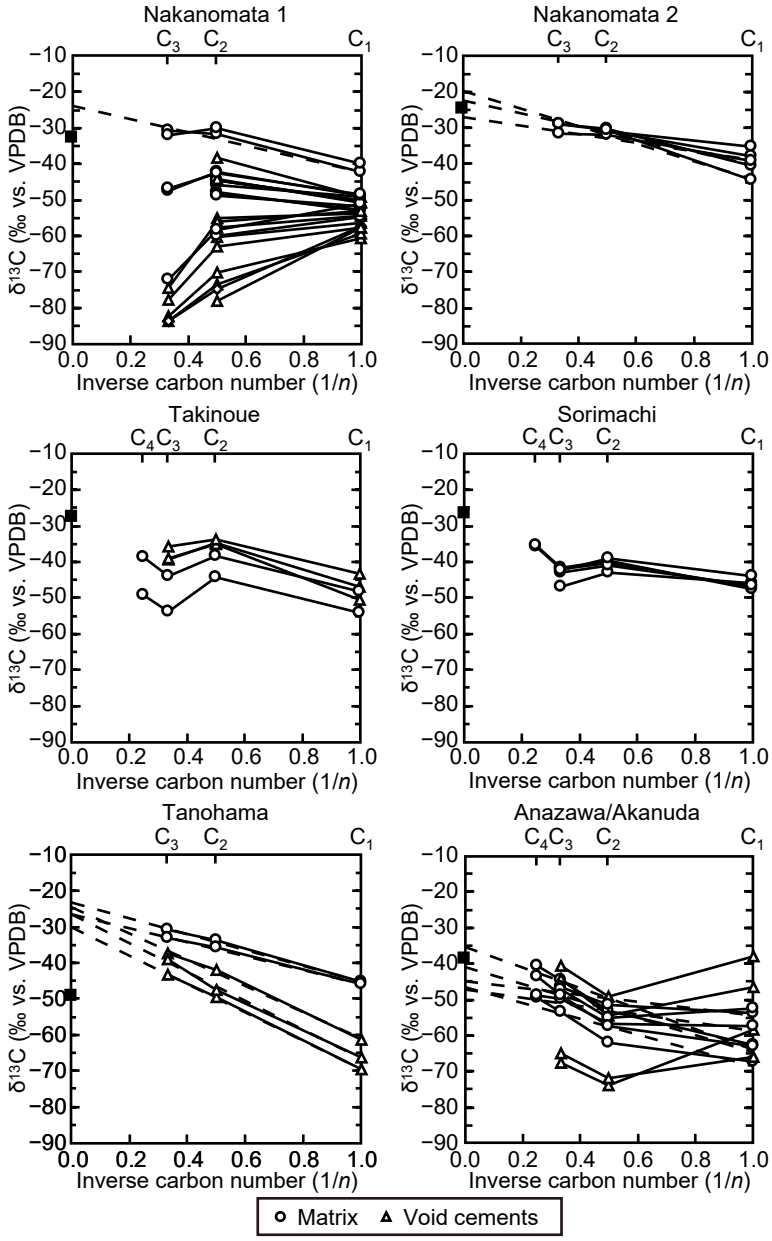

Fig. 2.4. Plots of stable carbon isotopic compositions against the inverse carbon number ($1/n$) for the methane (C_1) to *n*-butane (C_4) extracted from the seep carbonates by the acid-digestion experiment ("Natural gas plots" : Chung et al., 1988). Only data from representative sites are shown. Dashed lines indicate the linear regression lines for the data showing the isotopic trend of thermogenic gas, $\delta^{13}C_1 < \delta^{13}C_2 < \delta^{13}C_3$, the extrapolated intercepts of which indicate the $\delta^{13}C$ values of the source organic matter. For comparison, the $\delta^{13}C$ values of total organic carbon (TOC) within the carbonates are indicated by filled squares. Thermal maturity increases in the order of Nakanomata 1 and 2, Takinoue, Sorimachi, Anazawa/Akanuda, Tanohama.

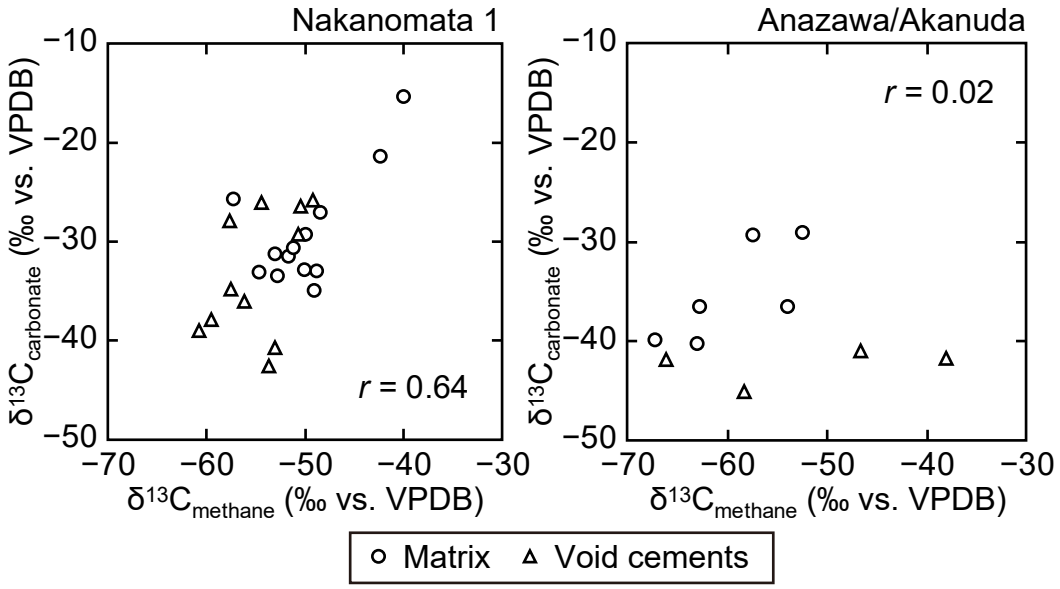

Fig. 2.5. Relationships between stable carbon isotopic compositions of the methane and the carbonate from which the methane was extracted by the acid-digestion experiment. *r* value indicates the correlation coefficient.

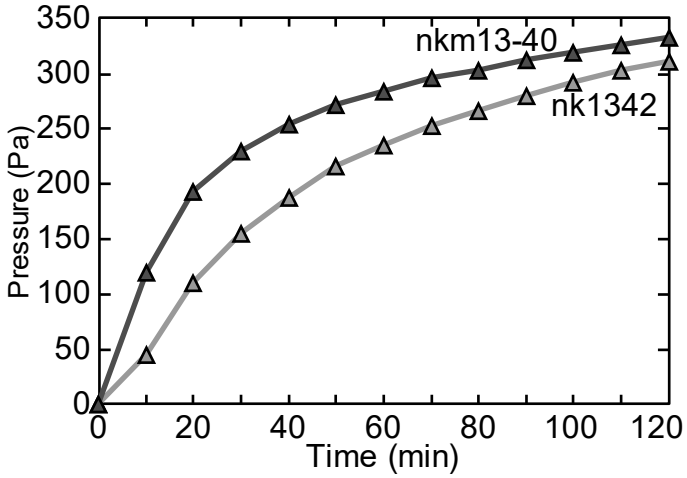

Fig. 2.6. Temporal changes of the pressure of gases desorbed from the Nakanomata 1 carbonates during the heating experiments (90°C, 2 h).

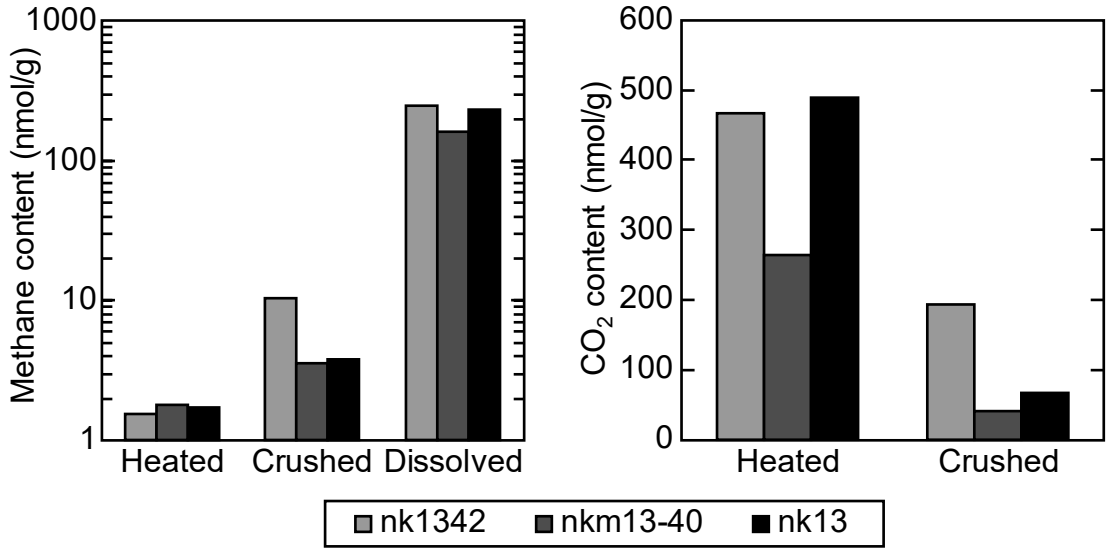

Fig. 2.7. Concentrations of the methane (left panel) and the carbon dioxide (right panel) extracted from the Nakanomata 1 carbonates by heating, crushing, and acid digestion of the crushed carbonates. Note the logarithmic scale for the methane content.

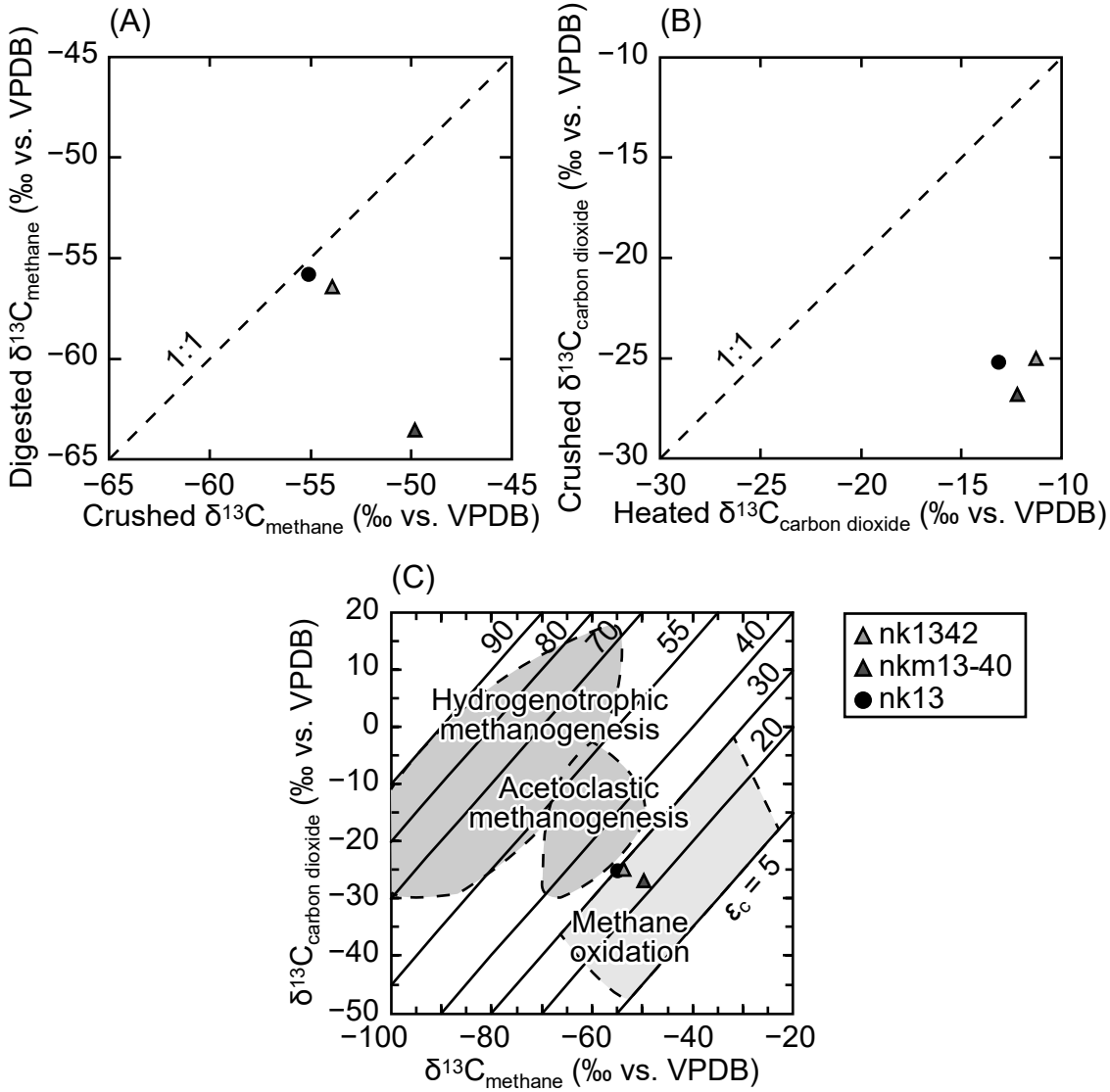

Fig. 2.8. Stable carbon isotopic compositions of the methane and carbon dioxide extracted from the Nakanomata 1 carbonates. (A) Cross plot of $\delta^{13}C$ values of the methane extracted by crushing and acid digestion of the crushed carbonates. Dashed line indicates a 1:1 relationship. (B) Cross plot of $\delta^{13}C$ values of the carbon dioxide extracted by the heating and crushing experiments. Dashed line indicates a 1:1 relationship. (C) Relationship between $\delta^{13}C$ values of the methane and carbon dioxide extracted by the crushing experiments. Diagonal lines indicate the carbon isotope separation factors ($\varepsilon_C \approx \delta^{13}C_{CO_2} - \delta^{13}C_{CH_4}$). Shaded areas indicate typical ranges of the ε_C values for methane and carbon dioxide resulting from methanogenesis and methane oxidation after Whiticar (1999).

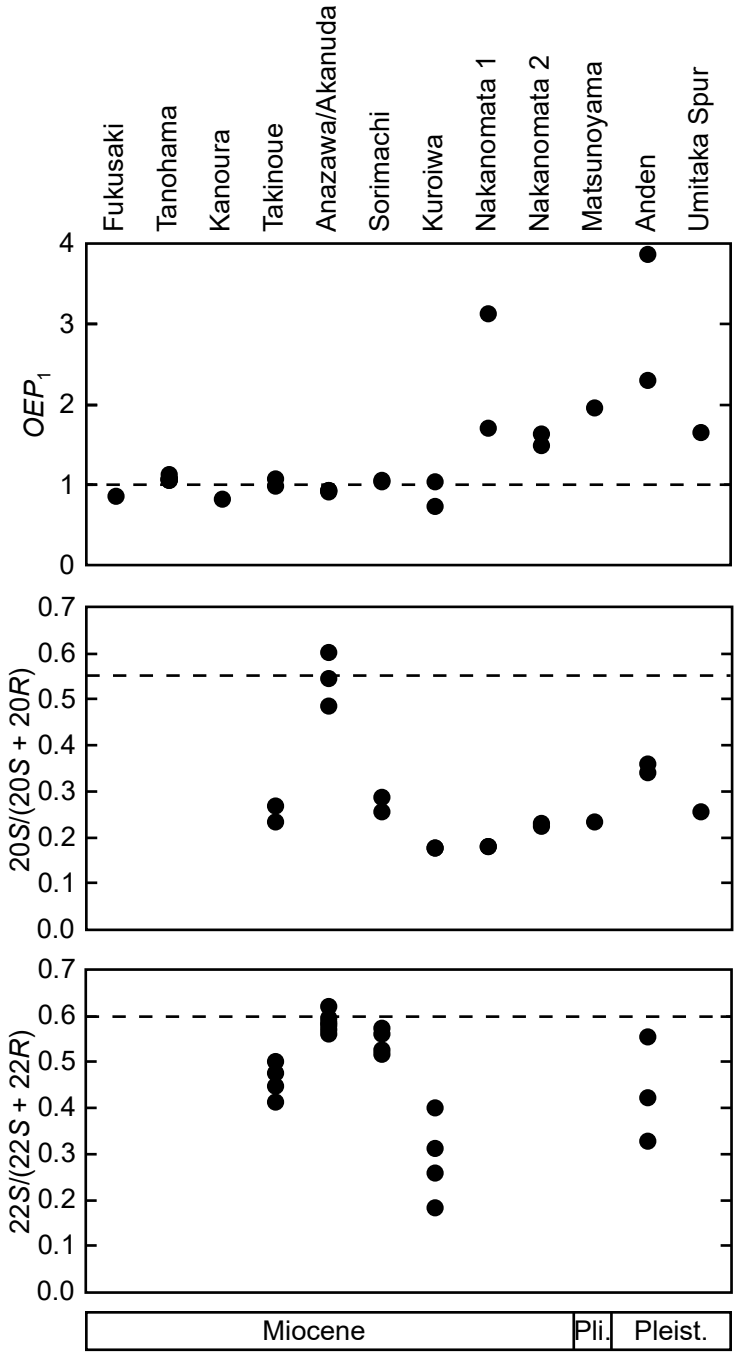

Fig. 2.9. Maturity-related biomarker parameters measured for the lipid extracts from the seep carbonates. OEP_1, odd-to-even predominance of *n*-alkanes. 20*S*/(20*S* + 20*R*), isomerization between S and R configurations at C-20 in the C_{29} 5α(H),14α(H),17α(H)-steranes. 22*S*/(22*S* + 22*R*), isomerization between S and R configurations at C-22 in the C_{31} and C_{32} 17α(H)-hopanes. Dashed lines indicate equilibrium values for mature samples with vitrinite reflectance R_o > 0.5%. Ordered from the oldest (left) to youngest (right) site. Pleist., Pleistocene; Pli., Pliocene.

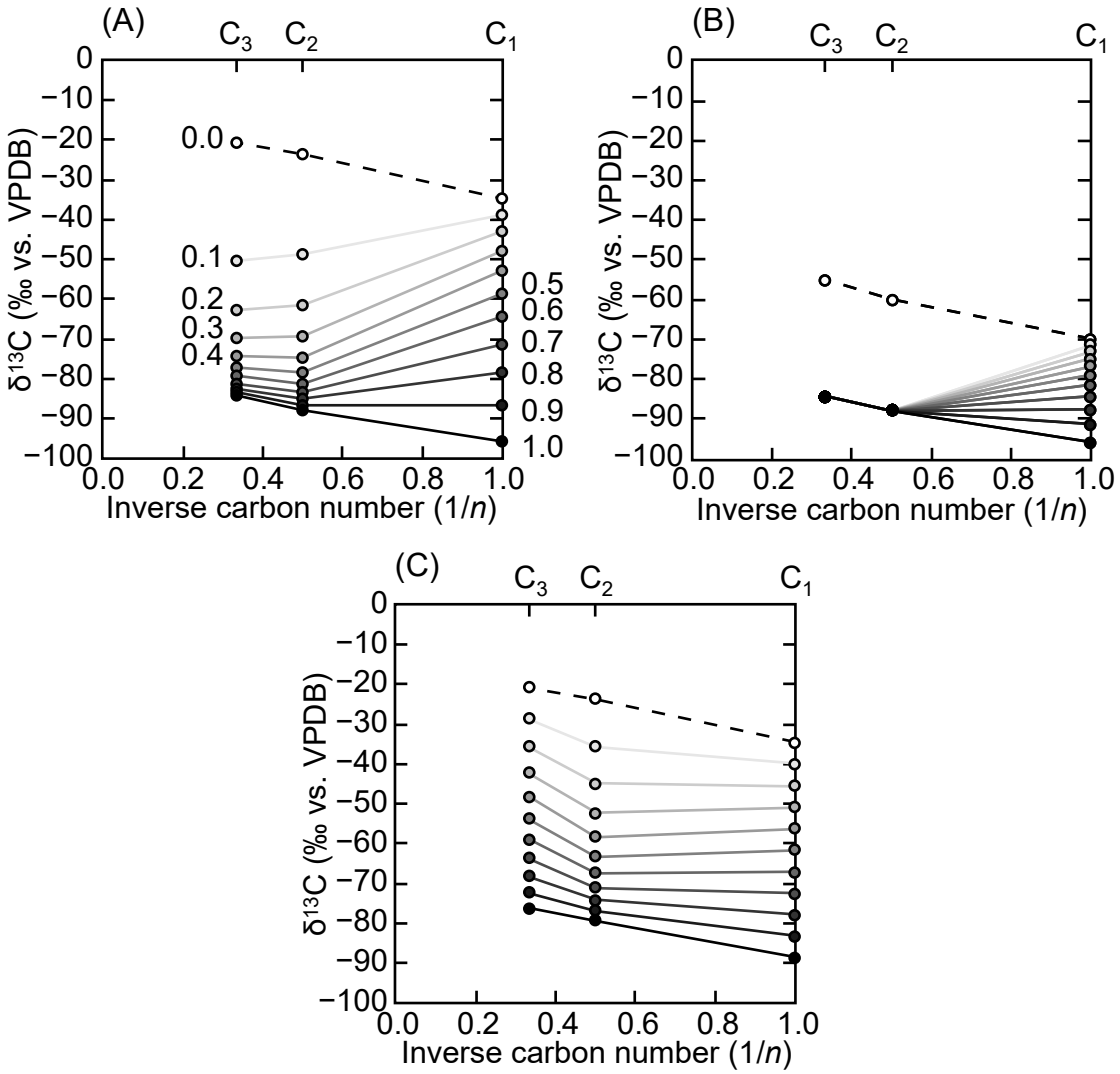

Fig. 2.10. Plots of stable carbon isotopic compositions against the inverse carbon number ($1/n$) for methane (C_1) to propane (C_3), calculated from mixing models between hydrocarbons of different origins. (A) Mixing between a normal thermogenic gas and a secondary thermogenic gas, generated from a source with $\delta^{13}C$ value of −80 ‰ at R_o of 0.5%. (B) Mixing between a biogenic gas and the secondary thermogenic gas assumed in (A). (C) Mixing between the normal thermogenic gas and a secondary thermogenic gas, generated from a source with $\delta^{13}C$ value of −80 ‰ at R_o of 1.5%. Dashed lines and open circles indicate the end-member values for the thermogenic or biogenic gas. The solid lines and filled circles become darker with increasing fraction (mixing ratio) of the secondary thermogenic gases, which is indicated with numbers 0.0 to 1.0 in (A). For isotopic compositions and concentrations of hydrocarbons in the endmember gases, see sections 2.3.6 and 2.4.6 in the text.

Table 2.1. Concentrations and stable carbon isotopic compositions of the hydrocarbons extracted from the seep carbonates by the acid-digestion experiment.

Site	Sample	Phase	Methane content	Ethane content	Propane content	Butane content	$C_1/(C_2+C_3)$	$\delta^{13}C_{methane}$	$\delta^{13}C_{ethane}$	$\delta^{13}C_{propane}$	$\delta^{13}C_{butane}$	$\delta^{13}C_{carbonate}$
Fukusaki	fsis	rm	1119.7	2.2	n.d.	n.d.	518.1	−51.1	n.a.	n.d.	n.d.	n.a.
Fukusaki	fs08	rm	640.8	1.4	n.d.	n.d.	445.3	−55.9	n.a.	n.d.	n.d.	n.a.
Fukusaki	fs10	rm	363.2	1.4	n.d.	n.d.	255.9	−46.9	n.a.	n.d.	n.d.	n.a.
Tanohama	tn04	sp	3649.6	132.2	42.8	n.d.	20.9	−69.6	−49.6	−43.3	n.d.	n.a.
Tanohama	tn0223	m	1013.6	41.6	23.3	n.d.	15.6	−45.3	−33.9	−30.9	n.d.	n.a.
Tanohama	tn0227	sp	321.3	9.1	4.6	n.d.	23.5	−61.3	−42.0	−37.4	n.d.	n.a.
Tanohama	tn0328	m + sp	580.6	21.6	8.3	n.d.	19.4	−46.0	−35.8	−33.2	n.d.	n.a.
Tanohama	tn0324	sp	514.8	13.5	5.6	n.d.	27.0	−66.3	−47.6	−39.0	n.d.	n.a.
Kanoura	ku09	rm	1335.6	2.6	n.d.	n.d.	511.7	−54.1	−42.2	n.d.	n.d.	n.a.
Kanoura	ku12	sp + rm	1354.1	4.0	n.d.	n.d.	337.3	−51.1	n.a.	n.d.	n.d.	n.a.
Kanoura	ku13	rm	814.6	1.9	n.d.	n.d.	431.9	−55.2	n.a.	n.d.	n.d.	n.a.
Takinoue	yy0102	m	1245.8	116.9	74.9	27.6	6.5	−54.1	−44.3	−53.8	−49.1	n.a.
Takinoue	yy010133	pk	588.6	44.5	17.0	n.d.	9.6	−46.9	−34.9	−39.5	n.d.	n.a.
Takinoue	yy010134	pk	607.7	47.9	16.5	n.d.	9.4	−50.5	−35.2	−39.1	n.d.	n.a.
Takinoue	yy010335	m	999.7	103.8	55.0	16.0	6.3	−48.4	−38.2	−44.0	−38.5	n.a.
Takinoue	yy010336	pk	508.1	40.5	13.6	n.d.	9.4	−43.4	−33.8	−35.8	n.d.	n.a.
Anazawa/Akanuda	an0006	m	262.2	105.0	45.1	12.0	1.7	−67.2	−61.9	−53.4	−49.5	−39.9
Anazawa/Akanuda	an0007	sp	187.8	45.7	22.7	6.7	2.7	−58.4	−74.0	−67.6	n.a.	−45.0
Anazawa/Akanuda	an0008	m	227.4	87.7	34.8	9.5	1.9	−62.8	−53.2	−44.6	−40.5	−36.5
Anazawa/Akanuda	an0009	sp + m	183.5	26.0	11.8	n.d.	4.9	−38.1	−49.1	−40.7	n.d.	−41.7

Table 2.1 (*continued*)

Anazawa/Akanuda	an0010	sp	114.2	19.2	7.9	2.5	4.2	−46.7	−54.3	−44.3	n.a.	−40.9
Anazawa/Akanuda	ak0103	m	170.1	65.5	32.8	8.6	1.7	−53.9	−51.4	−46.6	n.a.	−36.5
Anazawa/Akanuda	ak02	m	416.6	163.2	84.6	17.9	1.7	−57.5	−56.9	−49.7	−48.8	−29.3
Anazawa/Akanuda	ak05	m	216.8	93.7	45.7	10.7	1.6	−52.5	−55.3	−47.3	n.a.	−29.1
Anazawa/Akanuda	an0011	m	198.3	71.3	29.0	8.3	2.0	−63.1	−57.4	−49.0	−43.6	−40.2
Anazawa/Akanuda	an0012	sp	369.7	91.2	40.4	9.4	2.8	−66.1	−71.9	−65.0	n.a.	−41.8
Sorimachi	smgd3084	m	1075.5	147.3	96.4	34.9	4.4	−47.0	−40.2	−42.0	−35.8	n.a.
Sorimachi	smgd5130	m	1064.2	129.3	89.1	34.6	4.9	−47.4	−39.8	−41.6	−35.4	n.a.
Sorimachi	smgd1005	m	474.1	80.9	53.8	17.5	3.5	−45.8	−42.8	−46.8	n.a.	n.a.
Sorimachi	smgd2045	m	929.7	197.4	102.6	27.5	3.1	−46.4	−40.9	−43.1	n.a.	n.a.
Sorimachi	smgd4102	m	871.3	143.9	74.9	19.5	4.0	−43.8	−38.9	−42.4	n.a.	n.a.
Kuroiwa	k0132	m	146.5	7.4	2.4	n.d.	14.9	−29.9	−26.2	n.a.	n.d.	n.a.
Kuroiwa	ki17	sp	71.0	5.1	n.d.	n.d.	14.0	−34.3	−47.1	n.d.	n.d.	n.a.
Kuroiwa	ki3321	sp	73.6	3.9	n.d.	n.d.	19.1	−26.9	n.a.	n.d.	n.d.	n.a.
Kuroiwa	ki3323	sp	153.7	6.8	n.d.	n.d.	22.7	−43.9	−33.1	n.d.	n.d.	n.a.
Nakanomata 1	nk1301	ac + m	99.3	12.2	6.6	0.9	5.3	−60.7	−70.2	−82.4	n.a.	−39.0
Nakanomata 1	nk1302	m	108.6	7.9	3.6	0.2	9.4	−53.1	−47.7	n.a.	n.a.	−31.3
Nakanomata 1	nk1309	ac + m	102.8	15.8	10.7	n.d.	3.9	−56.2	−60.2	n.a.	n.d.	−36.0
Nakanomata 1	nk1312	m	285.9	33.0	11.7	n.d.	6.4	−42.4	−31.8	−30.7	n.d.	−21.3
Nakanomata 1	nk1315	m	120.1	10.6	4.7	n.d.	7.8	−49.1	−46.0	n.a.	n.d.	−34.9
Nakanomata 1	nk1321	ac + m	155.5	8.5	3.7	0.6	12.8	−50.4	−44.6	n.a.	n.a.	−26.4
Nakanomata 1	nk1329	ac	143.5	15.1	7.8	0.1	6.2	−59.5	−73.5	−83.6	n.a.	−37.9
Nakanomata 1	nk1343	m	402.3	16.3	8.9	2.7	15.9	−57.3	−74.7	−83.7	n.a.	−25.7

Table 2.1 (*continued*)

Nakanomata 1	nk1344	m	102.4	7.8	3.7	0.5	8.9	−52.8	−48.0	n.a.	n.a.	−33.4
Nakanomata 1	nk1345	ac	133.9	17.6	9.0	tr	5.0	−53.7	−55.1	n.a.	n.a.	−42.6
Nakanomata 1	nk1346	m	271.1	18.9	7.8	0.5	10.2	−40.0	−30.2	−32.0	n.a.	−15.4
Nakanomata 1	nk1347	ac	148.1	13.7	5.6	0.5	7.7	−53.1	−56.1	−74.5	n.a.	−40.7
Nakanomata 1	nk1348	m	215.5	12.1	5.4	tr	12.3	−48.9	−42.3	−47.4	n.a.	−32.9
Nakanomata 1	nk1349	ac	86.8	7.7	3.8	n.d.	7.5	−49.2	−38.4	n.a.	n.d.	−25.8
Nakanomata 1	nk1350	m	140.7	9.9	5.1	n.d.	9.4	−51.7	−49.0	n.a.	n.d.	−31.5
Nakanomata 1	nk1351	m	154.7	10.1	4.9	n.d.	10.3	−50.2	−44.5	n.a.	n.d.	−32.8
Nakanomata 1	nk1352	m	215.1	11.6	5.2	n.d.	12.8	−48.5	−42.6	−46.8	n.d.	−27.0
Nakanomata 1	nk1353	ac + m	181.2	6.2	3.0	n.d.	19.7	−54.4	−57.8	n.a.	n.d.	−26.0
Nakanomata 1	nk1354	m	226.4	14.4	6.3	n.d.	10.9	−51.2	−58.5	−72.2	n.d.	−30.6
Nakanomata 1	nk1355	m	104.4	7.5	4.0	n.d.	9.1	−54.7	−60.0	n.a.	n.d.	−33.1
Nakanomata 1	nk1356	ac	156.0	15.4	7.4	0.7	6.8	−57.6	−62.8	−77.7	n.a.	−34.8
Nakanomata 1	nk1357	m	118.1	7.2	3.2	n.d.	11.3	−50.0	−44.5	n.a.	n.d.	−29.3
Nakanomata 1	nk1358	ac	175.5	8.0	4.8	n.d.	13.8	−57.7	−78.0	n.a.	n.d.	−27.8
Nakanomata 1	nk1359	ac	166.4	5.5	n.d.	n.d.	30.5	−50.7	−44.1	n.d.	n.d.	−29.3
Nakanomata 2	nk1403	m	119.0	12.0	4.1	n.d.	7.4	−35.1	−30.8	n.a.	n.d.	n.a.
Nakanomata 2	nk1407	m	135.3	13.1	4.6	n.d.	7.6	−37.9	−31.1	n.a.	n.d.	n.a.
Nakanomata 2	nk1408	m	135.3	13.2	4.6	n.d.	7.6	−40.4	−30.4	−29.0	n.d.	n.a.
Nakanomata 2	nk1401	m	152.5	15.7	5.7	n.d.	7.1	−39.2	−32.1	−31.7	n.d.	n.a.
Nakanomata 2	nk14p	m	236.6	15.7	6.2	n.d.	10.8	−44.5	−30.5	−28.9	n.d.	n.a.
Matsunoyama	ed0412	m	158.5	15.9	n.d.	n.d.	9.9	−38.8	−33.1	n.d.	n.d.	n.a.
Matsunoyama	ed0402	m	81.7	8.6	n.d.	n.d.	9.5	−31.7	−30.4	n.d.	n.d.	n.a.
Matsunoyama	ed0404	m	45.0	3.6	n.d.	n.d.	12.3	−27.6	−32.5	n.d.	n.d.	n.a.
Matsunoyama	ed0433	m	142.6	17.6	6.5	n.d.	5.9	−35.6	−39.8	−42.6	n.d.	n.a.
Anden	mh0411	m	7.2	n.d.	n.d.	n.d.	n.c.	n.a.	n.d.	n.d.	n.d.	n.a.
Anden	mh0413	m	10.3	n.d.	n.d.	n.d.	n.c.	n.a.	n.d.	n.d.	n.d.	n.a.
Umitaka Spur	nt0720_759-5	m	8.8	n.d.	n.d.	n.d.	n.c.	n.a.	n.d.	n.d.	n.d.	n.a.

Table 2.1 (*continued*)

Umitaka Spur	ut0206	m	13.1	n.d.	n.d.	n.d.	n.c.	n.a.	n.d.	n.d.	n.d.	n.d.	n.a.
Umitaka Spur	ut0508	m	12.5	n.d.	n.d.	n.d.	n.c.	n.a.	n.d.	n.d.	n.d.	n.d.	n.a.

Concentrations are in nmol/g. $\delta^{13}C$ values are in ‰ vs. VPDB. All values for butane are those of *n* -butane. ac, acicular aragonite or calcite; m, microcrystalline aragonite or calcite; pk, pinkish cement; rm, recrystallized matrix; sp, sparry calcite (see Appendix for details of carbonate phases); n.a., not analyzed due to low concentration; n.c., not calculated; n.d., not detected; tr, trace (<0.1).

Table 2.2. Concentrations and stable carbon isotopic compositions of the methane and carbon dioxide extracted from the Nakanomata 1 carbonates by heating, crushing, and acid digestion of the crushed carbonates.

		Heating				Crushing				Acid digestion	
Sample	Phase	Methane content	Carbon dioxide content	$\delta^{13}C_{methane}$	$\delta^{13}C_{carbon\ dioxide}$	Methane content	Carbon dioxide content	$\delta^{13}C_{methane}$	$\delta^{13}C_{carbon\ dioxide}$	Methane content	$\delta^{13}C_{methane}$
nk1342	ac	1.6	466.1	n.a.	−11.3	10.4	193.0	−53.9	−25.0	247.0	−56.4
nkm13-40	ac	1.8	264.6	n.a.	−12.2	3.6	40.7	−49.9	−26.8	162.9	−63.5
nk13	m	1.7	490.2	n.a.	−13.1	3.8	66.0	−55.1	−25.2	234.9	−55.8

Concentrations are in nmol/g. $\delta^{13}C$ values are in ‰ vs. VPDB. ac, acicular aragonite; m, microcrystalline aragonite; n.a., not analyzed due to low concentration.

Table 2.3. Stable carbon isotopic compositions of total organic carbon (TOC) within the seep carbonates. Carbonate contents are also shown.

Site	Sample	Phase	Carbonate content (wt%)	$\delta^{13}C_{TOC}$ (‰ vs. VPDB)
Fukusaki	fsis	rm	94.0	−42.3
Tanohama	tn04	sp	98.3	−49.1
Kanoura	ku	rm	89.2	−35.6
Takinoue	yy0102	m	88.2	−27.4
Anazawa/Akanuda	an00	m + sp	93.1	−38.8
Sorimachi	smgd3084	m	91.0	−26.6
Kuroiwa	k0132	m	87.8	−29.0
Nakanomata 1	nk13	m	84.5	−32.6
Nakanomata 2	nk14p	m	85.9	−24.5
Matsunoyama	ed0412	m	74.8	−24.3
Anden	mh0413	m	78.9	−33.4
Umitaka Spur	nt0720_759-5	m	82.3	−25.9

Abbreviations for phase are the same as those in Table 2.1.

Table 2.4. Maturity-related biomarker parameters measured for the lipid extracts from the seep carbonates and the corresponding vitrinite-reflectance values ($\%R_o$).

Site	Sample	OEP_1	$20S/(20S + 20R)$ C_{29} steranes	$22S/(22S + 22R)$ C_{31} hopanes	$22S/(22S + 22R)$ C_{32} hopanes	R_o (%)
Fukusaki	fsis	0.87	n.d.	n.d.	n.d.	>0.7
Tanohama	tn01_50	1.07	n.d.	n.d.	n.d.	>0.7
Tanohama	tn02	1.06	n.d.	n.d.	n.d.	>0.7
Tanohama	tn03	1.06	n.d.	n.d.	n.d.	>0.7
Tanohama	tn04	1.08	n.d.	n.d.	n.d.	>0.7
Tanohama	tn05	1.13	n.d.	n.d.	n.d.	>0.7
Kanoura	ku	0.82	n.d.	n.d.	n.d.	>0.7
Takinoue	yy0102	1.07	0.23	0.50	0.45	0.5–0.6
Takinoue	yy0103_20	0.98	0.27	0.48	0.41	0.5–0.6
Anazawa/Akanuda	an00	0.94	0.60	0.56	0.58	>0.7
Anazawa/Akanuda	ak0103	0.93	0.55	0.59	0.62	>0.7
Anazawa/Akanuda	ak02	0.91	0.49	0.57	0.60	>0.7
Sorimachi	smgd3084	1.05	0.29	0.56	0.53	0.5–0.6
Sorimachi	smgd5130	1.04	0.26	0.57	0.52	0.5–0.6
Kuroiwa	k0132	0.73	0.18	0.26	0.18	0.5
Kuroiwa	kim33	1.03	0.18	0.40	0.31	0.5
Nakanomata 1	nk13	3.13	0.18	n.d.	n.d.	<0.5
Nakanomata 1	nkm13-35	1.71	0.18	n.d.	n.d.	<0.5
Nakanomata 2	nk14c	1.49	0.22	n.d.	n.d.	<0.5
Nakanomata 2	nk14p	1.63	0.23	n.d.	n.d.	<0.5
Matsunoyama	ed0412	1.95	0.23	n.d.	n.d.	<0.5
Anden	mh0411	2.30	0.36	0.33	n.d.	<0.5
Anden	mh0413	3.87	0.34	0.42	0.55	<0.5
Umitaka Spur	nt0720_759-5	1.65	0.25	n.d.	n.d.	<0.5

Correlation to the vitrinite reflectance ($\%R_o$) is based on Peters et al. (2005). OEP_1, odd-to-even predominance of *n*-alkanes; n.d., not detected.

Concluding remarks

The origin of methane cannot be identified unambiguously by stable carbon isotopic compositions of seep carbonates, because the compositions reflect mixing between bicarbonate ions from different sources as well as from AOM and show wide ranges of $\delta^{13}C$ values (Fig. 1.5). This study successfully constrained the carbon isotopic compositions of methane at ancient seeps using the isotopic compositions of the ANME biomarkers, on the assumption that they are determined by those of the source methane and isotopic fractionations during biosynthesis. It is unclear whether the carbon isotope offset between methane and the biomarker calculated for the modern seep of the Japan sea (Umitaka Spur) can be applied to other settings of the world. The isotope offset compiled from literature shows wide range (~60‰) and can result in ambiguous estimation of the origin of methane. In contrast, the regression formulae between the $\delta^{13}C_{methane}$ and $\delta^{13}C_{lipid}$ values could be widely applicable to better constrain the origin of methane at ancient seeps.

Since biogenic methane is produced in shallow subsurface, the biogenic origins for the methane at the examined seeps indicate that seepage of thermogenic gases through subsurface conduits such as deep-rooted faults were minor in the study area until Pleistocene. Identification of the origins of seep fluids helps to reveal the subsurface

migration pathways and mechanisms for the biogenic methane at the studied seeps.

This study revealed that all the three methods, i.e., acid digestion, heating, and crushing, can be used to extract and to analyze residual gases from ancient seep carbonates. These different methods help to reveal whether the residual gases are entrapped within intercrystalline pore spaces or crystal inclusions of the carbonates. Another possibility is that the residual gases were adsorbed to surfaces of the carbonate crystals, other minerals, or organic particles. Residual gases within ancient seep carbonates were possibly influenced seriously by thermal maturation of the host sediments (noted below) and probably by experimental procedures. Even if they all came from the seep fluids, their isotopic compositions could have been altered by the methane oxidation. Therefore, in assessing the origin of methane at ancient seeps, analytical results for residual gases should be carefully interpreted and be complemented by other signatures such as biomarkers. The $\delta^{13}C$ value of methane at the Nakanomata 1 seep estimated using the regression line for the biomarker PMI was ~−65‰ (Table 1.3). However, the methane liberated from the Nakanomata 1 carbonate showed a $\delta^{13}C$ value of −52.2‰ in average (Table 2.1). It is suspected that the methane entrapped within the carbonates is ^{13}C-enriched with respect to the original biogenic methane in the seep fluid due to the isotopic fractionation during AOM, as well as the

mixing with thermogenic methane (sections 2.5.3 and 2.5.4). Finding and analyzing intracrystalline inclusions would be helpful to strictly extract original isotopic signatures of methane.

Based on the data presented in parts 1 and 2, it is possible to systematically depict diagenetic history of methane-seep carbonates which has rarely been documented. The methane-seep carbonates examined in this study are from different ages in the late Cenozoic and have been subjected to different levels of diagenetic alteration and thermal maturity (Table 2.4). These are imprinted in the petrographic texture, stable oxygen isotopic composition, and biomarker composition of the carbonates. The early-diagenetic carbonate phases are preserved in the carbonates of low thermal maturity (R_o < 0.6%), while such phases are recrystallized in the highly mature samples (R_o > 0.7%). The $\delta^{18}O$ values of the carbonates are mostly positive or around 0‰ in average in the low maturity samples, and decrease to negative values as low as −14‰ with increasing maturity (Fig. 1.5). Fukusaki, Tanohama, and Kanoura carbonates lack isoprenoid hydrocarbons including biomarkers for methane-oxidizing archaea and cyclic hydrocarbons such as steranes and hopanes (Fig. 2.6). The chromatograms dominated by *n*-alkanes and the ^{13}C-depleted TOC from these carbonates indicate that the ^{13}C-depleted biomarkers have been broken down into *n*-alkanes during thermal maturity.

Therefore, the following processes are inferred to proceed with increasing burial and thermal maturity of seep carbonates: void-filling cements and subsequently microcrystalline matrix are recrystallized, the isotopic composition becomes depleted in ^{18}O, and isoprenoid and cyclic hydrocarbons are lost whereas *n*-alkanes become predominant. It should be noted that the depletion in ^{18}O could be ascribed to meteoric water input and the isotopic composition of the original seep fluid as well as to temperature increase during burial. The biomarker composition can also reflect the original organic compounds contained in the host sediments. Despite the diagenetic alterations mentioned above, the carbon isotopic compositions of the biomarkers for methane-oxidizing archaea (ANME) appear to be less affected by thermal maturity, assuming that the carbon isotopic compositions of the source methane were similar among the study sites (Fig. 1.7). This assumption is supported by the similar carbon isotopic compositions of the examined ancient carbonates, which are less affected by diagenetic alterations with respect to oxygen isotopes. However, if the ANME biomarkers are small in quantity, their isotopic compositions would be seriously masked by increased amounts of background compounds due to maturity.

In addition, the data presented in Part 2 indicate possible influence of thermal maturity on residual gases within seep carbonates. Thermal maturity could induce

secondary cracking of the ^{13}C-depleted organic matter within the seep carbonates, producing hydrocarbons with unusual isotopic compositions (Fig. 2.3). Nevertheless, the isotopic compositions of the liberated methane possibly represent the original signatures in immature samples such as the Nakanomata 1 carbonates. This interpretation is indicated by a positive correlation of the carbon isotopic compositions between methane and its host carbonate (Figs. 2.5 and 2.8). The isotopic trend of the residual hydrocarbons may be useful to assess the relative contribution (mixing ratio) of the secondary gases to the normal thermogenic or biogenic gases. It can also provide useful information on the molecular composition of the secondary gases, which depends on thermal maturity (Figs. 2.4 and 2.10). Pyrolysis experiments of immature organic compounds within seep carbonates would be helpful to simulate the generation of the secondary gases and changes in their amount and molecular composition with maturity.

This study is the first attempt to constrain the isotopic composition of "paleo methane" contained in ancient seep fluids, and took the first step to know subsurface environment in the geologic past using methane-seep carbonates. Such an attempt will be further advanced by reexamining seep carbonates of various ages in the world from the viewpoint of organic geochemistry and trace-element geochemistry in the future.

Appendix. Site descriptions

A.1. Burdigalian methane seeps in Tsushima Island

A.1.1. Geological setting

Tsushima Island is located between Kyushu Island and the Korean Peninsula in the southern Japan Sea. This island is composed entirely of Cenozoic marine sedimentary rocks of >5400 m in thickness, called the Taishu Group (Fig. A.1; The Ministry of International Trade and Industry, 1972, 1973, 1974; Yamada et al., 1990). The Taishu Group represents sediments accumulated in the Tsushima deep basin that formed during pull-apart processes in the right-lateral strike-slip system of the southwestern Japan Sea (Lallemand and Jolivet, 1985; Jolivet and Tamaki, 1992; Golozubov et al., 2017). The Taishu Group is subdivided into the Lower, Middle, and Upper formations, and they are composed mainly of mudstone, sandstone, and alternating beds of sandstone and mudstone. These sediments are regarded as materials supplied by landslide blocks from the shallow shelf to the base of the continental slope at a high sedimentation rate of ~2700 m/Ma (Golozubov et al., 2017). They are intruded by volcanic rocks including middle Miocene (~15 Ma) granite in the southern part of the island. The geological structure of the Taishu Group is characterized by multiple NE–SW-trending anticlines and synclines. These folded structures are related to postsedimentation NW-directed

shortening (Golozubov et al., 2017). Age of the Taishu Group had been regarded as early Eocene to early Miocene based on planktonic foraminifers, radiolarians, and K-Ar ages of a tuff bed (Ibaraki, 1994; Nakajo and Funakawa, 1996; Sakai and Yuasa, 1998). On the contrary, Ninomiya et al. (2014) reported U-Pb ages of 17.86 ± 0.07 Ma and 15.93 ± 0.20 Ma from tuff beds intercalated in the basal and uppermost parts of the Taishu Group, respectively. This study follows Ninomiya et al. (2014), which concluded that the Taishu Group was deposited in the Burdigalian to Langhian (17.9–15.9 Ma).

A.1.2. Carbonate occurrence

Several carbonate rocks have been reported from the Taishu Group, some of which are possibly methane-seep carbonates (The Ministry of International Trade and Industry, 1972; Ninomiya, 2011, 2012). This study focuses on three seep-related carbonate rocks at Kanoura (34°28′17″N, 129°23′38″E), Fukusaki (34°18′21″N, 129°15′12″E), and Tanohama (34°34′34″N, 129°17′49″E) (Fig. A.1).

A.1.2.1. Kanoura

At Kanoura, siltstone-rich alternation of the Middle Formation of the Taishu Group crops out along a bay coast (Fig. A.2A). A large carbonate body with densely-packed

bivalve fossils is intercalated in the dark-gray siltstone (Fig. A.2B–D). Although vegetation and weathered nature of the outcrop make it difficult to entirely observe the main carbonate body, it seems to be more than 4 m in length and about 1.5 m in thickness. According to Ninomiya (2012), the contact between the carbonate body and the surrounding mudstone is gradual, and the lower contact contains decimeter-sized nodular limestones. Samples for paleontological, petrographical and geochemical analyses were collected from boulders derived from the carbonate body. When cracked, these carbonate rocks emit strong sulfide odor.

A.1.2.2. Fukusaki

At Fukusaki, sandstone-rich alternation of the Lower Formation of the Taishu Group is well exposed along a coastline. Trace fossils and slumps are commonly observed (Fig. A.3A). At a gravel beach facing an outcrop composed entirely of dark-gray siltstone, well-rounded carbonate cobbles and boulders are found abundantly, which were most likely abraded by waves. The carbonates have whitish veins and contain bivalve fossils (Fig. A.3B). A large, ~5.6 m-long and ~0.3 m-thick carbonate lens is exposed in situ in the siltstone, and is almost barren of fossils (Fig. A.3C). Several-centimeter-sized concretions are scattered throughout the siltstone just below

this carbonate lens (Fig. A.3D). The concretion-bearing siltstone continues laterally about 50 m from the carbonate lens.

A.1.2.3. Tanohama

At Tanohama, siltstone-rich alternation of the Lower Formation of the Taishu Group is well exposed along a coastline (Fig. A.4A). A ~3.7 m-long and ~1 m-thick carbonate body is exposed in situ in the dark-gray siltstone with several-centimeter-sized concretions (Fig. A.4B and C). A pipe-shaped concretion is also found below the carbonate body. Based on the macroscopic texture, this carbonate body can be divided into three facies (Fig. A.4C). Facies A consists of dark-gray siltstone of less than 1 m thick that contains the centimeter-sized concretions (Fig. A.4D). The siltstone of Faces A also contains bivalve fossils. Facies B consists of carbonate with densely-packed bivalve fossils, and composes the lower part of the carbonate body (Fig. A.4E). Facies B also contains laminated, stromatolite-like texture, which is less common than Facies C. Facies C consists of carbonate with stromatolite-like laminae and composes the upper part of the carbonate body (Fig. A.4F). Facies C contains no bivalve fossils. The siltstone several meters below the carbonate body is intercalated with thick sandstones and associated with slumps.

A.1.3. Carbonate petrography

A.1.3.1. Kanoura

The dark-gray matrix of the carbonate body at Kanoura is recrystallized and composed of mosaics of sparry or microsparitic calcite (Fig. A.5A–C). The matrix commonly contains foraminifer tests, whereas it rarely contains detrital grains such as quartz (Fig. A.5D). Ninomiya (2012) reported pellets of about 0.3 mm in diameter contained in the matrix of the Kanoura carbonate. Gold-colored patches that have irregular contact with the recrystallized matrix are composed of dolomicrite (Fig. A.5E). Bivalve shells are replaced completely by sparry calcite, which also crosscuts the matrix as veins (Fig. A.5D). Aggregates of polygonal pyrite crystals line the bivalve shells (Fig. A.5F).

A.1.3.2. Fukusaki

The dark-gray matrix of the carbonates at Fukusaki is heavily recrystallized and composed almost entirely of sparry calcite mosaic (Fig. A.6A–C). Small round patches of clotted dolomicrite or irregular aggregates of ~100 μm dolomite crystals are contained in the matrix (Fig. A.6D and E). Pyrite crystals and detrital grains are rare in

the matrix. Euhedral quartz crystals are contained within veins of sparry calcite that crosscuts the matrix (Fig. A.6F). The small concretion collected below the carbonate lens is composed of dolomicrite and microsparite. The dolomicrite of the small concretion contains framboidal pyrite and peloids.

A.1.3.3. Tanohama

At Tanohama, the small concretion from Facies A is composed of dolomicrite, which contains ~40% low-Mg calcite (Fig. A.7A). The dolomicrite shows clotted fabric and contains bioclasts and pyrite, and no detrital grains (Fig. A.7B). Void spaces are lined with radial cements and filled with sparry calcite mosaic and globular chalcedony (Fig. A.7C and D). The carbonate of Facies B is mainly composed of micritic low-Mg calcite, which contains ~7% dolomite (Fig. A.8A). The micrite is partly recrystallized to microsparite to sparitic mosaic, and shows clotted fabric (Fig. A.8B). Detrital grains are rare, whereas foraminifer and echinoderm tests are contained in the micrite. Pyrite aggregates are contained in the micrite or line rims of void spaces. The void spaces in the micrite are filled with mosaic of sparry calcite and equant quartz crystals (Fig. A.8C). Some voids are rimmed with acicular or radial calcite cements, which are enclosed in sparite mosaic (Fig. A.8D and E). Bivalve shells are completely replaced by

sparry mosaic with their margins rimmed with pyrite aggregates. The stromatolite-like fabric of Facies C consists of dark-gray recrystallized matrix and grayish void-filling sparitic cements (Fig. A.9A). The recrystallized matrix consists of sparry calcite mosaic that shows brownish color under plane-polarized light (Fig. A.9B and C). The void-filling sparry calcite shows ghosts of acicular or radial crystal aggregates that line the recrystallized matrix (Fig. A.9C–E). The recrystallized matrix and the void-filling cements both contain no detrital grain and pyrite. Globular chalcedony and microcrystalline silica also fill the void spaces (Fig. A.9D and E).

A.1.4. Stable carbon and oxygen isotopes

The stable carbon isotopic composition of the carbonates from Kanoura, Fukusaki, and Tanohama is variable, with $\delta^{13}C$ values ranging from −52.8‰ to −4.7‰, while their $\delta^{18}O$ values vary between −14.5‰ to −2.2‰. Samples taken from the same carbonate phase generally show similar isotopic compositions (Fig. A.10; Table 1.2).

At Kanoura, the $\delta^{13}C$ values of the recrystallized matrix and the sparry calcite range between −30.7‰ and −19.9‰ (n = 3) and −41.8‰ and −41.0‰ (n = 3), respectively. Their $\delta^{18}O$ values range from −14.4‰ to −10.5‰, with those of the recrystallized matrix lower. In contrast to Kanoura, the recrystallized matrix from

Fukusaki has $\delta^{13}C$ values of −40.2‰ and −37.2‰ (n = 2), which are much lower than the sparry calcite (−12.9‰ and −12.6‰, n = 2). The $\delta^{18}O$ values of the carbonates from Fukusaki are less variable (−14.4‰ to −12.2‰) compared to the other two sites.

Carbon and oxygen isotopic compositions of the carbonates from Tanohama are much variable, and show a characteristic trend, in which higher $\delta^{13}C$ values are accompanied with lower $\delta^{18}O$ values (Fig. A.10). The sparry calcite of Facies A is most ^{13}C-enriched and ^{18}O-depleted among the carbonates from Tanohama, with $\delta^{13}C$ values of −13.6‰ and −8.2‰ (n = 2) and corresponding $\delta^{18}O$ values of −13.4‰ and −13.8‰, respectively. The micrite and the sparry calcite of Facies B show moderate ^{13}C-depletion, with $\delta^{13}C$ values of −26.5‰ to −15.3‰ (n = 5), although their $\delta^{18}O$ values are similar to or slightly higher than those of Facies A (−13.4‰ to −12.6‰). Two samples collected from the sparry and radial calcite of Facies B have extremely low $\delta^{13}C$ values (−48.4‰ and −50.5‰, respectively) and high $\delta^{18}O$ values (−2.2‰ and −2.5‰, respectively). The bivalve shell replaced by sparry calcite has an intermediate isotopic composition ($\delta^{13}C$ and $\delta^{18}O$ values of −32.4‰ and −8.5‰, respectively) or shows a strong ^{13}C-enrichment ($\delta^{13}C$ and $\delta^{18}O$ values of −4.7‰ and −4.6‰, respectively). The carbonate phases of Facies C are strongly ^{13}C-depleted and generally more ^{18}O-enriched than those of Facies A and B. The recrystallized matrix and the

sparry and radial calcite of Facies C have $\delta^{13}C$ values of −52.8‰ to −32.3‰ (n = 7), with the sparry and radial cements lower than the matrix. The $\delta^{18}O$ values of these phases range between −5.9‰ and −2.4‰, with an exception from the recrystallized matrix (−12.9‰).

A.1.5. Interpretation

The strong ^{13}C-depletion of the carbonate phases, with $\delta^{13}C$ values as low as −52.8‰, indicates that the carbonate rocks at Kanoura, Fukusaki, and Tanohama were formed via the anaerobic oxidation of methane (AOM, e.g., Peckmann and Thiel, 2004). It is supposed that terrigenous organic matter supplied rapidly by landslide blocks was a sufficient source of biogenic methane production in the sediments. The recrystallized matrix is interpreted as former cemented sediments that were recrystallized to sparry calcite mosaic. The presence of the ^{13}C-depleted veins of sparry calcite at Kanoura and the void-filling sparry and radial calcite at Tanohama suggest a high flux rate of methane-containing fluids (Peckmann et al., 2009; Kiel et al., 2014). The variation of the carbon and oxygen isotopic compositions of the carbonate phases might partly be explained by the mixing between a ^{13}C-depleted and ^{18}O-enriched seep-fluid endmember and a ^{13}C-enriched and ^{18}O-depleted diagenetic fluid endmember. The

mixing of the two endmembers could have created the characteristic isotopic trend in the Tanohama carbonates (Fig. A.10; Tong et al., 2016). In spite of no detection of lipid biomarkers of the anaerobic methane-oxidizing archaea, the significantly low $\delta^{13}C_{TOC}$ values of the carbonates as low as −49.1‰ also support the incorporation of methane-derived carbon into the bulk organic matter (parts 1 and 2). Facies A of the Tanohama seep contains small concretions that are scattered in the siltstone with sparse bivalve fossils, and is interpreted to have been formed by diffusive seepage of methane (Nesbitt et al., 2013). However, their $\delta^{13}C$ values are not low enough to exclude other possibility such as organoclastic sulfate reduction. Facies B with dense bivalve fossils could have been formed in a bivalve community or a thanatocoenosis. The stromatolite-like fabric that constitutes the upper part of the carbonate body at Tanohama (Facies C) suggest the microbially mediated cement formation in the cavities, which could have been caused by AOM-performing microbial mats (Greinert et al., 2002; Reitner et al., 2005). Therefore, Facies C could be interpreted as fossilized microbial mats.

A.2. A Langhian methane seep at Takinoue, western Hokkaido

A.2.1. Geological setting

In central Hokkaido, several NS trending Neogene sedimentary basins are widely

distributed, which are foreland basins formed by the collision of the Chishima and Honshu arcs during the middle Miocene (Hoyanagi et al., 1986). One of them, the Ishikari-Hidaka basin, comprises the western part of Yubari City. In this area, the Neogene sediments unconformably overlie the Cretaceous Yezo Group and the Paleogene Poronai and Momijiyama formations (Fig. A.11; Ishida et al., 1980; Nakagawa et al., 1996). The Neogene sediments become younger to the west, and they are subdivided into the Takinoue, Kawabata, Umaoiyama, and Yuni formations in ascending order (Matsuno and Hata, 1960; Takahashi et al., 2002). Several NW–SE-trending folds and faults affect these sediments. The methane-seep carbonates examined in this study are contained in the Takinoue Formation. The Takinoue Formation consists of sandstone-rich facies in the lower part and mudstone-rich facies in the upper part. The seep carbonates are contained in the latter mudstone-rich facies. Although the depositional environment of the Takinoue Formation remains unclear, Kanno and Ogawa (1964) has reported shallow-water molluscan fossils such as *Ostrea* and *Clinocardium* from the lower part and rather deeper-water-dwelling species such as *Akebiconcha* (later reidentified as *Adulomya* by Amano and Kiel, 2011) and *Portlandia* from the upper part of the formation. Kawakami et al. (2002) and Kubota et al. (2010) tentatively located the boundary between the Takinoue and Kawabata formations in the

Yubari area at around 15 Ma, based on the age of the Kawabata Formation determined by K-Ar dating of a tuff bed and diatom and radiolarian fossils within this formation.

A.2.2. Carbonate occurrence

Irregular-shaped carbonate concretions of a few to 300 mm in diameter are scattered within a 3.5 m-thick dark-gray siltstone of the Takinoue Formation on a stepped riverbed of Yamayosawa Creek, a branch of the Yubari River (Figs. A.12 and A.13, coordinates: 42°54′34″N, 142°01′49″E). A large concretion of ~1 m in diameter is also contained in the uppermost part of this concretion-bearing horizon. This horizon is probably located close to the boundary between the Takinoue and Kawabata formations, although many faults affecting the formations around this site make its stratigraphic position difficult to determine (Takahashi et al., 2002).

A.2.3. Associated molluscan fossils

Abundant shells of a small, elongated vesicomyid *Adulomya* sp. (up to >65 mm in shell length) are concentrated in the carbonate concretions or in the siltstone just above them (Figs. A.12D and A.13). Kanno and Ogawa (1964) has previously reported float blocks containing fossils of *Akebiconcha chitanii* around this site, which were later

reidentified as *Adulomya uchimuraensis* by Amano and Kiel (2011). The vesicomyid fossils collected in this study are, however, significantly smaller than *A. uchimuraensis*. The vesicomyid shells are articulated or disarticulated, and densely packed (Fig. A.12D). Although vesicomyid shells are chalky, some specimens are composed of aragonite with cross lamellar microstructure. In addition to the vesicomyid, only one specimen of articulated valves of *Lucinoma* sp. was found in one of the concretions.

A.2.4. Carbonate petrography

The matrix of the carbonate concretions is dark-gray micrite and crosscut by mm- to cm-scale cracks, which are filled with pinkish-colored cement (Fig. A.14A). The matrix micrite and pinkish cement are both composed of high-Mg calcite. The matrix micrite commonly contains glauconite, as well as pyrite and detrital grains. The pinkish cement is composed of detritus-poor pure micrite, microsparite, and spherical crystal aggregates (Fig. A.14B). The spherical crystals are about 50 μm in diameter, some of which consist of radially arranged aggregates of small calcite crystals (Fig. A.14C). The pinkish cements show laminated and mottled fabrics. The lamination encrusts the inner walls of the crack independently of the normal depositional process governed by gravity (Fig. A.14D). The mottled fabric is composed of various-sized peloids or clasts (up to 1

mm in diameter) of the pure micrite floated within a matrix of the microsparite (Fig. A.14E). In addition, the pinkish cement shows a “non-gravitational fabric” (Martire et al., 2010), characterized by incongruent geopetal infillings by the pure micrite within a single cavity (Fig. A.14F and G). The dark-gray matrix and pinkish cements are crosscut by fractures filled with brownish micrite, which contains angular clasts of the pinkish cement. The largest concretion contained in the uppermost part of the concretion-bearing horizon is composed of clotted micrite with recrystallized vesicomyid shells in the upper a few-cm part, and dolomicrite in the lower part.

A.2.5. Stable carbon and oxygen isotopes

The matrix micrite has $\delta^{13}C$ and $\delta^{18}O$ values ranging from −43.0‰ to −26.9‰ and from −2.9‰ to +0.3‰, respectively (n = 8, Fig. A.15 and Table 1.2). The pure micrite of the pinkish cement shows the strongest ^{13}C depletion and ^{18}O enrichment, with $\delta^{13}C$ values of −48.3‰ to −37.3‰ and $\delta^{18}O$ values of −1.9‰ to +2.1‰ (n = 7). Two samples collected from the microsparite of the cement yielded $\delta^{13}C$ values of −45.7‰ and −39.5‰, with $\delta^{18}O$ values of +1.1‰ and −4.0‰, respectively. A sample from the spherical crystal aggregates yielded a $\delta^{13}C$ value of −40.3‰ and a $\delta^{18}O$ value of −3.3‰. The *Adulomya* shells show higher $\delta^{13}C$ values of −21.2‰ to −12.5‰, although their

$\delta^{18}O$ values are similar to the carbonate phases mentioned above (−0.7‰ to 0.0‰). A recrystallized shell has a distinct isotopic composition, with $\delta^{13}C$ and $\delta^{18}O$ values of −16.3‰ and −9.2‰, respectively. The brownish micrite has the highest $\delta^{13}C$ value of −4.0‰ with a $\delta^{18}O$ value of −0.3‰. Except for the vesicomyid shells and the brownish micrite, the $\delta^{13}C$ and $\delta^{18}O$ values of the carbonate phases show a negative correlation, in which higher $\delta^{13}C$ values accompany lower $\delta^{18}O$ values (Fig. A.15).

A.2.6. Interpretation

The strongly ^{13}C-depleted isotopic compositions of the matrix micrite and the pinkish cement indicate that they originated from the anaerobic oxidation of methane. The cracks filled with the pinkish cement were formed probably by the displacement of the semi-consolidated sediment by focused fluid flows or the contraction of the cemented sediment. The morphology and size of the spherical crystals of the pinkish cement (Fig. A.14C) resemble those of *Baccanella*, a genus of enigmatic microfossils microproblematica (Flügel, 2010). *Baccanella* has been interpreted as a bacterially induced precipitate or a diagenetic product caused by recrystallization of micritic high-Mg calcite and aragonite on the seafloor. The laminated fabric lining inner walls of the cracks suggests the former presence of microbial mats in the cracks (Cavagna et al.,

1999; Campbell et al., 2002; Greinert et al., 2002; Martire et al., 2010). The mottled fabric of the pinkish cement, with peloids and clasts floating in the microsparite, could have originated from a microbial activity (e.g., Peckmann et al., 1999), or the erosion of the pure micrite by a fluid flow. Martire et al. (2010) interpreted the "non-gravitational fabric" in Miocene methane-seep carbonates from Marmorito, NW Italy, to have been formed through the following process: gas hydrates that initially filled the cavities were partially dissociated and authigenic carbonates or injected sediments subsequently filled the new spaces. However, the paleotemperature estimated from the $\delta^{18}O$ values of the aragonitic *Adulomya* shells is around 19°C (Lécuyer et al., 2012) and is too high for the common bottom-water temperature in which gas hydrates are stable (Kvenvolden, 1988). The $\delta^{13}C$ values of the vesicomyid shells are low with respect to seawater. A negative correlation between the $\delta^{13}C$ and $\delta^{18}O$ values of the carbonate phases (Fig. A.15) is commonly observed in methane-seep carbonates and is known as a diagenetic trend (e.g., Tong et al., 2016). These facts suggest that the oxygen isotopic composition of the *Adulomya* shells have been somewhat altered by diagenetic processes such as a temperature increase during burial and a meteoric input. It is therefore difficult to prove the presence of gas hydrates at the Takinoue seep.

A.3. Miocene to Pliocene methane seeps in the Shin'etsu area

In the Shin'etsu area, Miocene methane seeps were previously reported in detail by Amano et al. (2010) (Kuroiwa seep), Nobuhara (2010) (Anazawa/Akanuda seep), and Miyajima et al. (2016) (Nakanomata 1 seep). The Neogene seep sites in this area including these previously-reported sites are briefly described below.

A.3.1. Anazawa/Akanuda (Serravallian)

Large-sized carbonate bodies of up to ~20 m in diameter are intercalated within the middle Miocene Bessho Formation near the Anazawa and Akanuda villages, Nagano Prefecture (coordinates of the largest body called the "Anazawa Limestone": 36°19′25″N, 138°00′34″E). From the Anazawa Limestone, Kato et al. (2011) reported calcareous nannofossil assemblage of the CN5a zone of Okada and Burkry (1980), which corresponds to an absolute age of 13.6 to 13.1 Ma (Saito, 1999). Abundant and diverse fossils of vesicomyid, bathymodiolin, and other mollusks are contained in the carbonates (Tanaka, 1959; Nobuhara, 2010; Miyajima et al., 2017). The carbonates are composed of muddy micrite with sparitic veins and veinlets, both showing low $\delta^{13}C$ and $\delta^{18}O$ values ranging from −42.2‰ to −27.3‰ and from −8.9‰ to −4.1‰, respectively (measured in this study, see Table 1.2). The veins and veinlets consist of mosaics of

sparry calcite with ghosts of acicular crystals.

A.3.2. Sorimachi (Serravallian)

Small carbonate nodules of 10 to 170 mm in diameter are abundantly contained with vesicomyid fossils in the siltstone of the middle Miocene Bessho Formation at a riverside cliff of the Hofukuji River, Nagano Prefecture (coordinates: 36°19′37″N, 137°59′40″E). This locality is located about 1.3 to 1.5 km west of, and probably stratigraphically above the Anazawa/Akanuda seep (Seki, 1983). The nodules are composed entirely of micrite, which is strongly depleted in ^{13}C ($\delta^{13}C$ values as low as −34.6‰).

A.3.3. Kuroiwa (Tortonian)

Two large carbonate bodies are contained within the uppermost middle Miocene Ogaya Formation at a quarry of Kita-Kuroiwa, Niigata Prefecture (coordinates: 37°14′51″N, 138°30′04″). The carbonate bodies are in contact with a Pliocene andesite dyke (Takeuchi et al., 1996), and underlain by a tuff bed dated as latest Serravallian to earliest Tortonian (11.64 ± 0.65 Ma) using fission track method (Muramatsu, 1988). According to Amano et al. (2010), one of the carbonate bodies (southern body) was 10

m long, 4 m high with unknown width, but the original outcrop has been destroyed during recent quarrying and only float blocks of the carbonate could be collected for this study. As described in Amano et al. (2010), the collected carbonates contain abundant vesicomyid and provannid fossils and are composed mainly of micrite with several spots or veins of void-filling sparry calcite. The voids are also lined with acicular aragonite or calcite, which is enclosed in sparry calcite. Some of the collected carbonates are composed of mosaics of sparry calcite instead of micrite. All of these carbonate phases show low $\delta^{13}C$ and $\delta^{18}O$ values ranging from −36.6‰ to −26.1‰ and from −8.5‰ to −2.8‰, respectively (measured in this study, see Table 1.2). Another carbonate body (northern body), which was not examined in this study, is heavily recrystallized and contains fossils of bathymodiolins as well as vesicomyids.

A.3.4. Nakanomata 1 (Tortonian or Messinian)

Several float blocks of seep carbonates were found on a riverbed of the Nakanomata River, Niigata Prefecture. One of them, a ~30-cm block called the "Nakanomata Seep Deposit" (found at 37°05′50″N, 138°09′22″E), contains diatom fossils of the *Rouxia californica* zone (NPD7A) of Yanagisawa and Akiba (1998), which corresponds to the Tortonian to Messinian (7.5–6.5 Ma), and is most likely derived from

the upper Miocene Nodani Formation (Miyajima et al., 2016). This carbonate block contains vesicomyid, bathymodiolin, and provannid fossils, and consists of microcrystalline aragonite that is crosscut by vein-like networks of voids and cavities. The void spaces are rimmed with crystal aggregates of acicular aragonite. The microcrystalline and acicular aragonites are both strongly depleted in ^{13}C, with $\delta^{13}C$ values as low as −41.1‰.

A.3.5. Nakanomata 2 (Tortonian)

Several cm-sized carbonate nodules and fossils of a vesicomyid *Calyptogena pacifica* are contained in the siltstone of the upper Miocene Nodani Formation at a riverside cliff of the Nakanomata River (coordinates: 37°05′49″N, 138°09′26″E). The nodule-bearing horizon is about 200 m below a tuff bed dated as latest Tortonian to earliest Messinian (7.13 ± 0.42 Ma) using fission track method (Muramatsu, 1989). The nodules are spherical or pipe-shaped with a central void, and entirely composed of micrite. Millimeter- to centimeter-scale voids around the central cavity of the pipe-shaped nodules are rimmed with bladed or fibrous calcite. The micrite and bladed or fibrous calcite are moderately depleted in ^{13}C, with $\delta^{13}C$ values higher than −25‰ (−24.8‰ to −13.2‰, see Table 1.2). The $\delta^{18}O$ values of these phases are positive

(+1.4‰ to +2.1‰).

A.3.6. Matsunoyama (Zanclean)

Small carbonate nodules of 10 to 130 mm in diameter are abundantly contained in the siltstone of the Pliocene Tamugigawa Formation at a riverside cliff of the Koedo River, Niigata Prefecture (coordinates: 37°05′44″N, 138°37′42″E). This locality is stratigraphically located about 160 m above a tuff bed dated as Zanclean (5.06 Ma) using fission track method (Amano et al., 1991). The nodules are associated with vesicomyid and other diverse molluscan fossils and composed of strongly ^{13}C-depleted micrite ($\delta^{13}C$ values as low as −46.0‰).

A.4. A Middle Pleistocene methane seep at Anden, the Oga Peninsula

A.4.1. Geological setting

The Cenozoic sediments in the Oga Peninsula are unconformably underlain by the Cretaceous granitic basement and Cretaceous to Neogene volcanic rocks (Kano et al., 2011; Fig. A.16). The Miocene to Pleistocene sediments are exposed in the eastern part of the peninsula, which become younger to the east and generally show a shallowing-upward change of sedimentary environment (Kitazato, 1975; Shirai and Tada, 2000).

The Pleistocene sediments are affected by N–S and NNW–SSE trending reverse faults and folds in the easternmost part (Kano et al., 2011). At the Anden Coast located in the central part of the northern coast of the peninsula, the Pleistocene sediments subdivided into the Kitaura, Wakimoto, Shibikawa, and Katanishi formations in ascending order are well exposed along a seaside cliff. The methane-seep carbonates examined in this study are contained in the Wakimoto Formation, which consists of dark-gray sandy siltstone deposited on shelf (Shirai and Tada, 2000). The age of the Kitaura Formation is estimated as 1.8 to 0.6 Ma based on microfossils and tuff beds (reviewed in Kano et al., 2011). A fission track age of 0.39 ± 0.04 Ma was obtained for a tuff bed called “Oga” and intercalated within the lowermost part of the Shibikawa Formation (Kano et al., 2002). The age of the Wakimoto Formation is thus estimated as the Middle Pleistocene (0.6 to 0.4 Ma).

A.4.2. Carbonate occurrence

Carbonate concretions of up to ~240 mm in diameter and smaller, irregular or burrow-shaped nodules are scattered within a ~2.2 m-thick horizon of the sandy siltstone of the Wakimoto Formation at the Anden Coast (Figs. A.17 and A.18, coordinates: 39°58′12″N, 139°50′38″E). This horizon is located about 6.5 m below the

boundary between the Wakimoto and Shibikawa formations, and about 23 m below the "Oga" tuff bed. The sandy siltstone surrounding the carbonates contains abundant trace fossils.

A.4.3. Associated molluscan fossils

The carbonate concretions and surrounding sandy siltstone contain fossils of a large thyasirid bivalve, *Conchocele bisecta* (up to 96.1 mm in shell length, Fig. A.17C). Fossils of *C. bisecta* occur exclusively as articulated valves (n = 7), directing their umbones upward as in their life position (Hickman, 1984). The original aragonite mineralogy and cross lamellar microstructure of the shell is preserved. A protobranch bivalve *Neilonella* sp. is also contained within a ~240 mm-diameter concretion. The sandy siltstones surrounding the carbonates sparsely contain fragments or disarticulated valves of shallow-water bivalves, such as *Cyclocardia ferruginea* and *Clinocardium*? sp., and gastropods such as *Margarites laudatus*, *Turritella* (*Neohaustator*) *fortilirata*, *Lacuna* (*Epheria*) *turrita*, and *Euspira* sp.

A.4.4. Carbonate petrography

The carbonate concretions and nodules from the Anden locality consist of an

irregular mixture of cream-colored, gray, and dark-gray parts, showing burrow-like appearances (Fig. A.19A). The gray and dark-gray parts are tightly cemented by micritic low-Mg and high-Mg calcite, respectively, whereas the cream-colored parts are loosely cemented. The dark-gray micrite shows clotted fabric (Fig. A.19B).

A.4.5. Stable carbon and oxygen isotopes

The dark-gray micrite is strongly depleted in ^{13}C, with $\delta^{13}C$ values ranging between −64.7‰ and −54.8‰ (n = 6). In contrast, the gray micrite shows higher $\delta^{13}C$ values of −20.4‰ to −4.7‰ (n = 7). The $\delta^{18}O$ values of these phases overlap between +0.2‰ and +1.8‰, with those of the gray micrite ranging wider (Fig. A.20 and Table 1.2). A sample taken from an aragonitic shell of *Conchocele bisecta* has an isotopic composition similar to that of the gray micrite, with a $\delta^{13}C$ value of −4.2‰ and a $\delta^{18}O$ value of +0.7‰.

A.4.6. Interpretation

Thyasirid bivalves including *Conchocele bisecta* are typical inhabitants in sulfide-rich reducing environments such as methane seeps (Dufour, 2005; Taylor and Glover, 2010). The strongly ^{13}C-depleted isotopic composition of the dark-gray micrite, with

$\delta^{13}C$ values as low as −65‰, obviously indicates that this phase originated from the anaerobic oxidation of methane (AOM). The matrix of the carbonate concretions and surrounding sediments are bioturbated, and the burrow-like appearance of the concretions suggests that the methane-charged fluids diffused into the burrows and other pore spaces in the sandy silt. However, the $\delta^{13}C$ values not lower than −20‰ of the gray micrite that encloses the dark-gray micrite could have resulted from the sulfate reduction of the sedimentary organic matter, rather than the AOM (Irwin et al., 1977). The lower Mg content of the gray micrite compared with the dark-gray micrite might have resulted from a decrease in seawater-derived Mg in the pore water due to an increase in burial depth of the micrite. Based on the $\delta^{18}O$ values, the *Conchocele* shell and gray and dark-gray micrites could have been precipitated nearly in equilibrium with the ambient bottom water (~0‰), therefore close to the seafloor (Tarutani et al., 1969; Friedman and O'Neil, 1977; Lécuyer et al., 2012).

A.5. Umitaka Spur central seep site, offshore Joetsu

A.5.1. Geological setting

The Umitaka Spur is located about 40 km offshore from Joetsu City, Niigata Prefecture (Fig. A.21). The spur is one of the anticlinal axes extending NNE to SSW,

which are related to the compressional tectonics since the late Neogene in the Japan Sea (Matsumoto et al., 2009; also see Preface V). The spur is characterized by large pockmarks and mounds of ~500 m in diameter, which are arranged NNE to SSW on the summit of the spur at ~900 m water depth (Matsumoto et al., 2009). At the central part of the Umitaka Spur, methane plumes and emanating gas bubbles have been observed around two mounds, where abundant carbonate nodules and bacterial mats are distributed on the seafloor (Machiyama et al., 2009). The sulfate-methane interface is located shallower than 2.0 m below seafloor around the methane plume sites, indicating a very high methane flux (Hiruta et al., 2009). Gas hydrates are exposed on the seafloor and have been recovered from the subseafloor by piston coring at the mounds. The hydrate-bound methane at the mounds has $\delta^{13}C$ values ranging between −37.3‰ and −34.6‰ (−36.0‰ in average, $n = 6$) and is thermogenic in origin (Hachikubo et al., 2015). The seeping methane has similar isotopic composition to the hydrate-bound methane (R. Matsumoto pers. comm.). The thermogenic methane possibly originated from the Miocene Nanatani and Lower Teradomari formations deeper than 1 km below seafloor and migrated through subseafloor faults and carrier beds (Monzawa et al., 2006; Matsumoto et al., 2009; Freire et al., 2011).

A.5.2. Occurrence and age of carbonates

At the southern flat area of one of the two mounds in the Umitaka Spur central, several cm-sized and platy carbonate nodules are scattered on the seafloor, which is covered with bacterial mats. The carbonate samples examined in this study were recovered in this flat area at ~900 m water depth from two sites, which are Site 2 (coordinates: 37°25.981′N, 138°00.210′E) and Site 5 (coordinates: 37°25.991′N, 138°00.259′E) of the HPD_00759 dive survey by ROV Hyper-dolphin of the R/V Natsushima (Japan Agency for Marine-Earth Science and Technology, JAMSTEC) during the NT07-20 cruise (October 2007). These sites are located at less than ~100 m from the methane seep sites where gas bubbles were observed (Machiyama et al., 2009). Although the formation ages of the examined nodules are unknown, U-Th and ^{14}C dating of carbonate nodules collected from the seafloor and piston core sediments at another mound of the Umitaka Spur central site indicated formation ages ranging between ~40 and 10 ka (Watanabe et al., 2008; Hiruta et al., 2014). Watanabe et al. (2008) suggested that methane seepage was most intensive at ~20 ka, which accords with the lowest-stand sea level during the last glacial age. Therefore, the examined carbonates in this study could also have been formed at some time during the Late Pleistocene.

A.5.3. Carbonate petrography

The platy carbonate nodule collected at Site 2 shows an obscure lamination, while that collected at Site 5 shows a porous texture (Fig. A.22). The nodules are entirely composed of light-gray micritic high-Mg calcite (Fig. A.22). The micrite commonly contains foraminifera tests and shows clotted or peloidal fabrics (Fig. A.22C).

A.5.4. Stable carbon and oxygen isotopes

The micrite of the carbonate nodules at the Umitaka Spur central seep site is relatively less depleted in ^{13}C and most enriched in ^{18}O, compared with the other seep carbonates examined in this study (Table 1.2). Two samples from the micrite at Site 2 shows $\delta^{13}C$ values of −13.4‰ and −12.0‰, with $\delta^{18}O$ values of +3.0‰ and +4.0‰, respectively. The micrite from Site 5 has $\delta^{13}C$ values of −19.3‰ to −18.0‰ and $\delta^{18}O$ values of +5.2‰ to +5.4‰ (n = 3).

References

Amano, K., Hasegawa, Y., Imai, R., Kubota, Y., Watanabe, T., Oba, T., 1991. Geography and Geology. In: Editorial Committee on History of Matsunoyama-machi (Ed.),

History of Matsunoyama-machi. Chapter 1 Nature. Editorial Committee on History of Matsunoyama-machi, Niigata, pp. 7–76. (in Japanese, original title translated)

Amano, K., Jenkins, R.G., Aikawa, M., Nobuhara, T., 2010. A Miocene chemosynthetic community from the Ogaya Formation in Joetsu: evidence for depth-related ecologic control among fossil seep communities in the Japan Sea back-arc basin. Palaeogeography, Palaeoclimatology, Palaeoecology 286, 164–170.

Amano, K., Kiel, S., 2011. Fossil *Adulomya* (Vesicomyidae, Bivalvia) from Japan. Veliger 51, 76–90.

Campbell, K.A., Farmer, J.D., Des Marais, D., 2002. Ancient hydrocarbon seeps from the Mesozoic convergent margin of California: carbonate geochemistry, fluids and palaeoenvironments. Geofluids 2, 63–94.

Cavagna, S., Clari, P., Martire, L., 1999. The role of bacteria in the formation of cold seep carbonates: geological evidence from Monferrato (Tertiary, NW Italy). Sedimentary Geology 126, 253–270.

Dufour, S.C., 2005. Gill anatomy and the evolution of symbiosis in the bivalve family Thyasiridae. Biology Bulletin 208, 200–212.

Flügel, E., 2010. Microfacies of Carbonate Rocks. Analysis, Interpretation and Application. 2nd Edition. Springer, Heidelberg, 984 pp.

Freire, A.F.M., Matsumoto, R., Santos, L.A., 2011. Structural-stratigraphic control on the Umitaka Spur gas hydrates of Joetsu Basin in the eastern margin of the Japan Sea. Marine and Petroleum Geology 28, 1967–1978.

Friedman, I., O'Neil, J.R., 1977. Compilation of stable isotope fractionation factors of geochemical interest. In: Fleischer, M. (Ed.), Data of Geochemistry. Sixth Edition. United States Geological Survey Professional Paper, Washington, pp. KK1–KK12.

Golozubov, V.V., Kasatkin, S.A., Yokoyama, K., Tsutsumi, Y., Kiyokawa, S., 2017. Miocene dislocations during the formation of the Sea of Japan Basin: case study of Tsushima Island. Geotectonics 51, 412–427.

Greinert, J., Bohrmann, G., Elvert, M., 2002. Stromatolitic fabric of authigenic carbonate crusts: result of anaerobic methane oxidation at cold seeps in 4,850 m water depth. International Journal of Earth Sciences 91, 698–711.

Hachikubo, A., Yanagawa, K., Tomaru, H., Lu, H., Matsumoto, R., 2015. Molecular and isotopic composition of volatiles in gas hydrates and in sediment from the Joetsu Basin, eastern margin of the Japan Sea. Energies 8, 4647–4666.

Hickman, C.S., 1984. Composition, structure, ecology, and evolution of six Cenozoic deep-water mollusk communities. Journal of Paleontology 58, 1215–1234.

Hiruta, A., Snyder, G.T., Tomaru, H., Matsumoto, R., 2009. Geochemical constraints for

the formation and dissociation of gas hydrate in an area of high methane flux, eastern margin of the Japan Sea. Earth and Planetary Science Letters 279, 326–339.

Hiruta, A., Wang, L.-C., Ishizaki, O., Matsumoto, R., 2014. Last glacial emplacement of methane-derived authigenic carbonates in the Sea of Japan constrained by diatom assemblage, carbon-14, and carbonate content. Marine and Petroleum Geology 56, 51–62.

Hoyanagi, K., Miyasaka, S., Watanabe, Y., Kimura, G., Matsui, M., 1986. Depositions of turbidites in the Miocene collision zone, central Hokkaido. Monograph of the Association for the Geological Collaboration in Japan 31, 265–284.

Ibaraki, M., 1994. Ages and paleoenvironments of Tertiary in northwestern Kyushu from the viewpoint of planktonic foraminifer assemblages. The Earth Monthly (Gekkan Chikyu) 16, 150–153. (in Japanese, original title translated)

Irwin, H., Curtis, C., Coleman, M., 1977. Isotopic evidence for source of diagenetic carbonates formed during burial of organic-rich sediments. Nature 269, 209–213.

Ishida, M., Soya, T., Suda, Y., 1980. Geological Map of Japan 1:200,000, Sapporo. Geological Survey of Japan, Tsukuba.

Jolivet, L., Tamaki, K., 1992. Neogene kinematics in the Japan Sea region and volcanic activity of the northeast Japan arc. In: Tamaki, K., Suyehiro, K., Allan, J., et al.

(Eds.), Proceedings of the Ocean Drilling Program, Scientific Results, Vol. 127/128 (Part 2). Ocean Drilling Program, College Station, TX, pp. 1311–1331.

Kanno, S., Ogawa, H., 1964. Molluscan fauna from the Momijiyama and Takinoue districts, Hokkaido, Japan. Science Reports of the Tokyo Kyoiku Daigaku, Section C 8, 269–294.

Kano, K., Ohguchi, T., Hayashi, S., Uto, K., Danhara, T., 2002. Toga volcano: an alkali-rhyolite tuff-ring in the western end of Oga Peninsula, NE Japan. Kazan (Volcano) 47, 373–396. (in Japanese with English abstract)

Kano, K., Ohguchi, T., Yanagisawa, Y., Awata, Y., Kobayashi, N., Sato, Y., Hayashi, S., Kitazato, H., Ogasawara, K., Komazawa, M., 2011. Geology of the Toga and Funakawa District. Quadrangle Series, 1:50,000, Geological Survey of Japan, AIST, 127 pp. (in Japanese with English abstract)

Kato, S., Hiramatsu, C., Miwa, M., Nobuhara, T., 2011. Geological age and sedimentary environment of the Anazawa Limestone in the Middle Miocene Bessho Formation, Nagano Prefecture, central Japan. Bulletin of Mizunami Fossil Museum 37, 135–147. (in Japanese with English abstract)

Kawakami, G., Shiono, M., Kawamura, A., Urabe, A., Koizumi, I., 2002. Stratigraphy and depositional age of the Miocene Kawabata Formation, Yubari Mountains,

central Hokkaido, Japan. Journal of the Geological Society of Japan 108, 186–200. (in Japanese with English abstract)

Kiel, S., Glodny, J., Birgel, D., Bulot, L.G., Campbell, K.A., Gaillard, C., Graziano, R., Kaim, A., Lazăr, L., Sandy, M.R., Peckmann, J., 2014. The paleoecology, habitats, and stratigraphic range of the enigmatic Cretaceous brachiopod *Peregrinella*. PLoS ONE 9, e109260.

Kitazato, H., 1975. Geology and geochronology of the younger Cenozoic of the Oga Peninsula. Contributions from the Institute of Geology and Paleontology, Tohoku University 75, 17–49. (in Japanese with English abstract)

Kubota, S., Motoyama, I., Kawamura, K., Kamikuri, S., Ogasawara, K., 2010. Radiolarian biostratigraphy of the Miocene rocks in the vicinity of the Horomui River, Iwamizawa City, Hokkaido. Journal of the Japanese Association for Petroleum Technology 75, 371–381. (in Japanese with English abstract)

Kvenvolden, K.A., 1988. Methane hydrate—a major reservoir of carbon in the shallow geosphere? Chemical Geology 71, 41–51.

Lallemand, S., Jolivet, L., 1985. Japan Sea: a pull-apart basin? Earth and Planetary Science Letters 76, 375–389.

Lécuyer, C., Hutzler, A., Amiot, R., Daux, V., Grosheny, D., Otero, O., Martineau, F.,

Fourel, F., Balter, V., Reynard, B., 2012. Carbon and oxygen isotope fractionations between aragonite and calcite of shells from modern molluscs. Chemical Geology 332–333, 92–101.

Machiyama, H., Matsumoto, R., Hiromatsu, M., 2009. Pictorial 2: ROV observation of sea-floor methane hydrate and methane-seep-induced, characteristic collapse structures. Journal of Geography 118, ii.

Martire, L., Natalicchio, M., Petrea, C.C., Cavagna, S., Clari, P., Pierre, F.D., 2010. Petrographic evidence of the past occurrence of gas hydrates in the Tertiary Piedmont Basin (NW Italy). Geo-Marine Letters 30, 461–476.

Matsumoto, R., Okuda, Y., Hiruta, A., Tomaru, H., Takeuchi, E., Sanno, R., Suzuki, M., Tsuchinaga, K., Ishida, Y., Ishizaki, O., Takeuchi, R., Komatsubara, J., Freire, A.F., Machiyama, H., Aoyama, C., Joshima, M., Hiromatsu, M., Snyder, G., Numanami, H., Satoh, M., Matoba, Y., Nakagawa, H., Kakuwa, Y., Ogihara, S., Yanagawa, K., Sunamura, M., Goto, T., Lu, H., Kobayashi, T., 2009. Formation and collapse of gas hydrate deposits in high methane flux area of the Joetsu basin, eastern margin of Japan Sea. Journal of Geography 118, 43–71. (in Japanese with English abstract)

Matsuno, K., Hata, M., 1960. Geological Map of Japan 1:50,000, Oiwake. Hokkaido Development Agency, Sapporo.

Matsuno, K., Tanaka, K., Mizuno, A., Ishida, M., 1964. Geological Map of Japan 1:50,000, Iwamizawa. Hokkaido Development Agency, Sapporo.

Miyajima, Y., Nobuhara, T., Koike, H., 2017. Taxonomic reexamination of three vesicomyid species (Bivalvia) from the middle Miocene Bessho Formation in Nagano Prefecture, central Japan, with notes on vesicomyid diversity. Nautilus 131, 51–66.

Miyajima, Y., Watanabe, Y., Yanagisawa, Y., Amano, K., Hasegawa, T., Shimobayashi, N., 2016. A late Miocene methane-seep deposit bearing methane-trapping silica minerals at Joetsu, central Japan. Palaeogeography, Palaeoclimatology, Palaeoecology 455, 1–15.

Monzawa, N., Kaneko, M., Osawa, M., 2006. A review of petroleum system in the deep water area of the Toyama Trough to the Sado Island in the Japan Sea, based on the results of the METI Sado Nansei Oki drilling. Journal of the Japanese Association for Petroleum Technology 71, 618–627. (in Japanese with English abstract)

Muramatsu, T., 1988. Age of tuff beds around Mt. Yoneyama by fission track dating method. Research Bulletin, Geoscience Education of Niigata Prefecture 22, 70–75. (in Japanese, original title translated)

Muramatsu, T., 1989. Fission track ages of the Neogene to Quaternary strata in Joetsu

district. Research Bulletin, Geoscience Education of Niigata Prefecture 23, 52–55. (in Japanese, original title translated)

Nakagawa, M., Watanabe, Y., Kito, N., Sakai, A., Komazawa, M., Hiroshima, T., 1996. Geological Map of Japan 1:200,000, Yubaridake. Geological Survey of Japan, Tsukuba.

Nakajo, T., Funakawa, T., 1996. Eocene radiolarians from the Lower Formation of the Taishu Group, Tsushima Islands, Nagasaki Prefecture, Japan. Journal of the Geological Society of Japan 102, 751–754. (in Japanese with English tile and figure captions)

Nesbitt, E.A., Martin, R.A., Campbell, K.A., 2013. New records of Oligocene diffuse hydrocarbon seeps, northern Cascadia margin. Palaeogeography, Palaeoclimatology, Palaeoecology 390, 116–129.

Ninomiya, T., 2011. Chemosynthetic fossil molluscan faunas from the Neogene Taishu Group, distributed in Tsushima Islands, Nagasaki Prefecture, the southwest Japan. Memoirs of the Faculty of Science, Kyushu University, Series D, Earth and Planetary Sciences 32, 11–26.

Ninomiya, T., 2012. Seep limestone and chemosynthetic fossil assemblages dependent on the seep from the Neogene Taishu Group, Tsushima Island, Nagasaki Prefecture,

the southwest Japan. Science Reports of the Department of Earth and Planetary Sciences, Kyushu University, 23, 13–21. (in Japanese with English abstract)

Ninomiya, T., Shimoyama, S., Watanabe, K., Horie, K., Dunkley, D.J., Shiraishi, K., 2014. Age of the Taishu Group, southwestern Japan, and implications for the origin and evolution of the Japan Sea. Island Arc 23, 206–220.

Nobuhara, T., 2010. Exploring the mystery of success of vesicomyid bivalves through underground cross sections of methane-seep sites. Seibutsu-no-kagaku Iden (Biological Science, Inheritance) 64, 27–32. (in Japanese, original title translated)

Okada, H., Bukry, D., 1980. Supplementary modification and introduction of code numbers to the low-latitude coccolith biostratigraphic zonation (Bukry, 1973; 1975). Marine Micropaleontology 5, 321–325.

Peckmann, J., Birgel, D., Kiel, S., 2009. Molecular fossils reveal fluid composition and flow intensity at a Cretaceous seep. Geology 37, 847–850.

Peckmann, J., Thiel, V., 2004. Carbon cycling at ancient methane-seeps. Chemical Geology 205, 443–467.

Peckmann, J., Thiel, V., Michaelis, W., Clari, P., Gaillard, C., Martire, L., Reitner, J., 1999. Cold seep deposits of Beauvoisin (Oxfordian; southeastern France) and Marmorito (Miocene; northern Italy): microbially induced authigenic carbonates.

International Journal of Earth Sciences 88, 60–75.

Reitner, J., Peckmann, J., Reimer, A., Schumann, G., Thiel, V., 2005. Methane-derived carbonate build-ups and associated microbial communities at cold seeps on the lower Crimean shelf (Black Sea). Facies 51, 66–79.

Saito, T., 1999. Revision of Cenozoic magnetostratigraphy and the calibration of planktonic microfossil biostratigraphy of Japan against this new time scale. Journal of Japanese Association for Petroleum Technology 64, 2–15.

Sakai, H., Yuasa, T., 1998. K-Ar ages of the Mogi and Ugetsuiwa subaqueous pyroclastic flow deposits in the Taishu Group, Tsushima Islands. Memoirs of National Science Museum, Tokyo 31, 23–28.

Sasa, Y., Tanaka, K., Hata, M., 1964. Geological Map of Japan 1:50,000, Yubari. Hokkaido Development Agency, Sapporo.

Seki, J., 1983. Molluscan fossils. In: Editorial Committee on History of Akashina-machi (Ed.), History of Akashina-machi. Volume 1 Nature. With Geological Map of Akashina district at 1:25,000. Board of Education of Akashina-machi, Subcommittee on Publication of History of Akashina-machi, Nagano, pp. 182–238. (in Japanese, original title translated)

Shirai, M., Tada, R., 2000. Sedimentary successions formed by fifth-order glacio-

eustatic cycles in the middle to upper Quaternary formations of the Oga Peninsula, northeast Japan. Journal of Sedimentary Research 70, 839–849.

Takahashi, K., Taniguchi, H., Watanabe, J., Ishimaru, S., 2002. Geological Map of Japan 1:50,000, Momijiyama. Geological Survey of Hokkaido, Sapporo.

Takeuchi, K., Yoshimura, T., Kato, H., 1996. Geology of the Kakizaki District. Geological Sheet Map at 1:50,000, Geological Survey of Japan, 48 pp. (in Japanese with English abstract)

Tanaka, K., 1959. Molluscan fossils from central Shinano, Nagano Prefecture, Japan (Part 1)—Fossils from Akanuda Limestone—. Journal of the Shinshu University, Faculty of Education 8, 115–133.

Tarutani, T., Clayton, R.N., Mayeda, T., 1969. The effect of polymorphism and magnesium substitution on oxygen isotope fractionation between calcium carbonate and water. Geochimica et Cosmochimica Acta 33, 987–996.

Taylor, J.D., Glover, E.A., 2010. Chemosymbiotic bivalves. In: Kiel, S. (Ed.), The Vent and Seep Biota. Topics in Geobiology. Springer, Heidelberg, pp. 107–135.

The Ministry of International Trade and Industry, 1972. Annual Report on the Regional Geological Survey 1971, Tsushima-Kamigata District (1), 29 pp. (in Japanese, original title translated)

The Ministry of International Trade and Industry, 1973. Annual Report on the Regional Geological Survey 1972, Tsushima-Kamigata District (2), 34 pp. (in Japanese, original title translated)

The Ministry of International Trade and Industry, 1974. Annual Report on the Regional Geological Survey 1973, Tsushima-Kamigata District (3), 52 pp. (in Japanese, original title translated)

Tong, H., Wang, Q., Peckmann, J., Cao, Y., Chen, L., Zhou, W., Chen, D., 2016. Diagenetic alteration affecting $\delta^{18}O$, $\delta^{13}C$ and $^{87}Sr/^{86}Sr$ signatures of carbonates: A case study on Cretaceous seep deposits from Yarlung-Zhangbo Suture Zone, Tibet, China. Chemical Geology 444, 71–82.

Watanabe, Y., Nakai, S., Hiruta, A., Matsumoto, R., Yoshida, K., 2008. U-Th dating of carbonate nodules from methane seeps off Joetsu, eastern margin of Japan Sea. Earth and Planetary Science Letters 272, 89–96.

Yamada, N., Sato, Y., Hiroshima, T., Suda, Y., 1990. Geological Map of Japan 1:200,000, Izuhara. Geological Survey of Japan, Tsukuba.

Yanagisawa, Y., Akiba, F., 1998. Refined Neogene diatom biostratigraphy for the northwest Pacific around Japan, with an introduction of code numbers for selected diatom biohorizons. Journal of the Geological Society of Japan 104, 395–414.

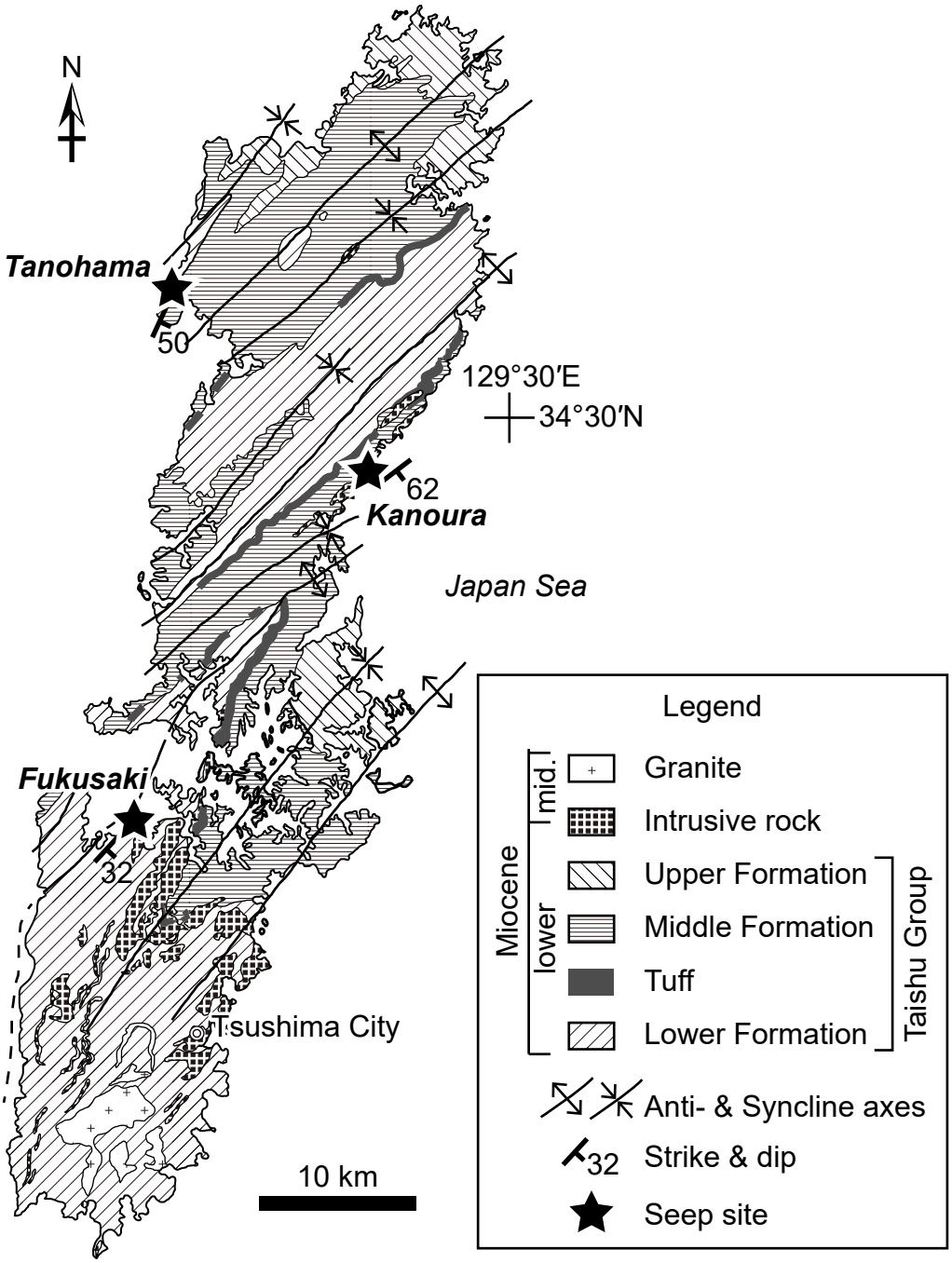

Fig. A.1. Geological map of Tsushima Island (modified from The Ministry of International Trade and Industry, 1972, 1973, 1974 and Ninomiya et al., 2014).

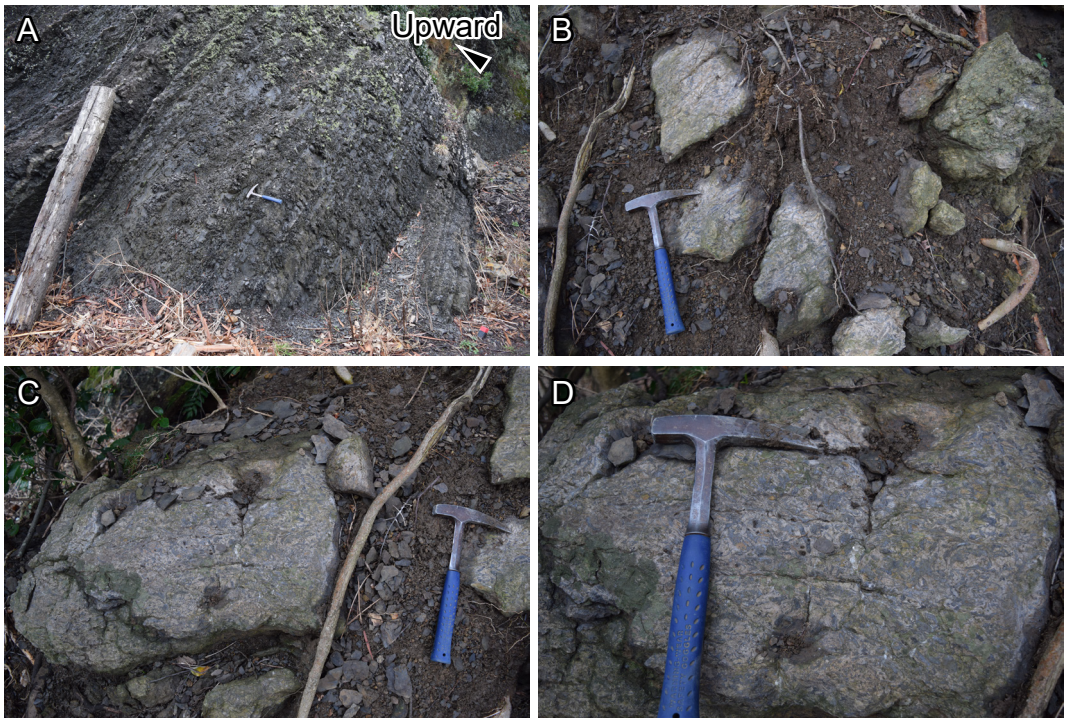

Fig. A.2. Field photographs at the Kanoura seep site. (A) Siltstone-rich alternation of sandstone and siltstone of the Middle Formation of the Taishu Group. Hammer is 33 cm long. (B–D) Carbonate boulders packed densely with bivalve fossils, derived from the seep carbonate body in the siltstone.

Fig. A.3. Field photographs at the Fukusaki seep site. (A) Slumping structure of the sandstone-rich alternation of sandstone and siltstone of the Lower Formation of the Taishu Group. (B) Carbonate boulder containing a bivalve fossil (*Bathymodiolus*, white arrow) and whitish veins. (C) Carbonate lens (white arrow) exposed in the siltstone. (D) Small carbonate concretions scattered throughout the siltstone below the carbonate lens shown in (C).

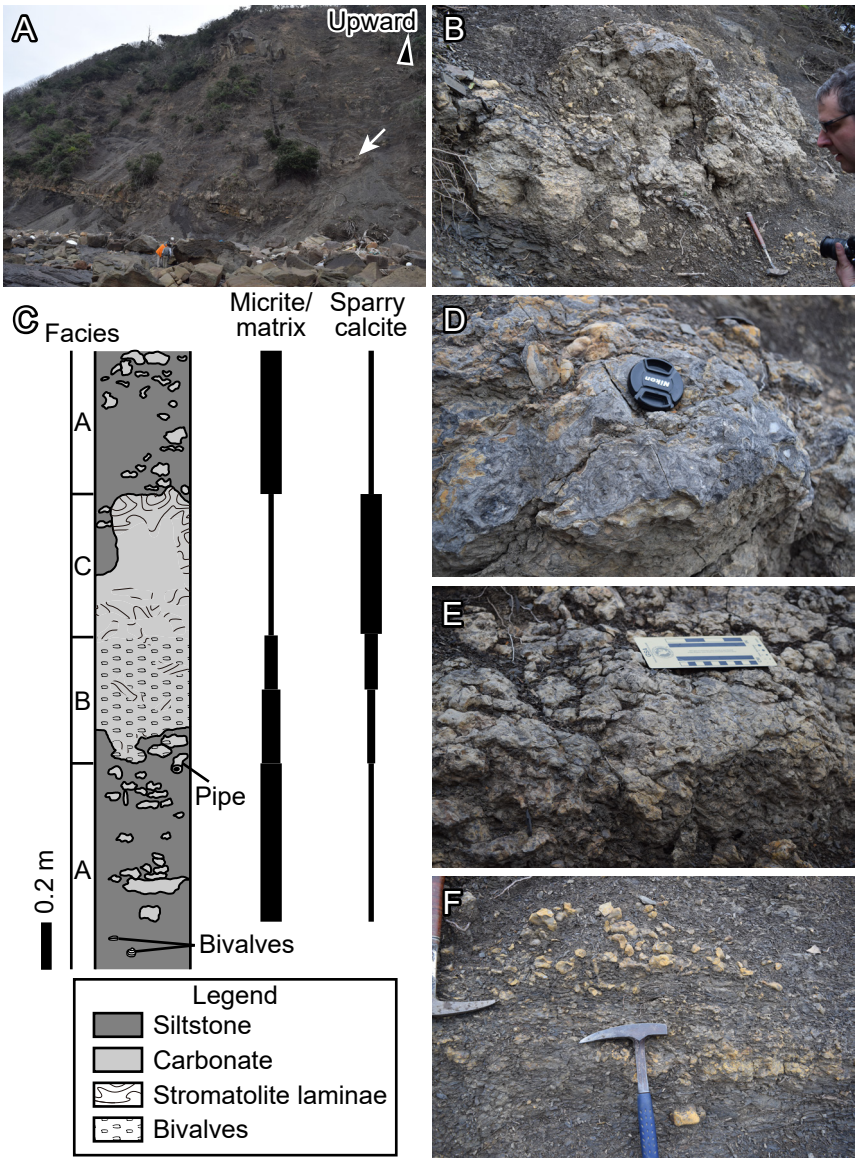

Fig. A.4. Field photographs and columnar section at the Tanohama seep site. (A) Siltstone-rich alternating beds of sandstone and siltstone of the Lower Formation of the Taishu Group. White arrow indicates the seep carbonate body. (B) Seep carbonate body. (C) Columnar section of the seep carbonate body and surrounding siltstone. Facies division of the carbonate body (see text for detail) is indicated on the left side of the columnar section. Bars on the right side indicate distribution of the micrite/recrystallized matrix and the sparry calcite cement. Width of the bars indicates relative abundance of the carbonate phases. (D) Stromatolite-like laminae of Facies C. Camera cap is 5 cm diameter. (E) Bivalve-rich carbonate of Facies B. (F) Siltstone of Facies A with small carbonate concretions scattered.

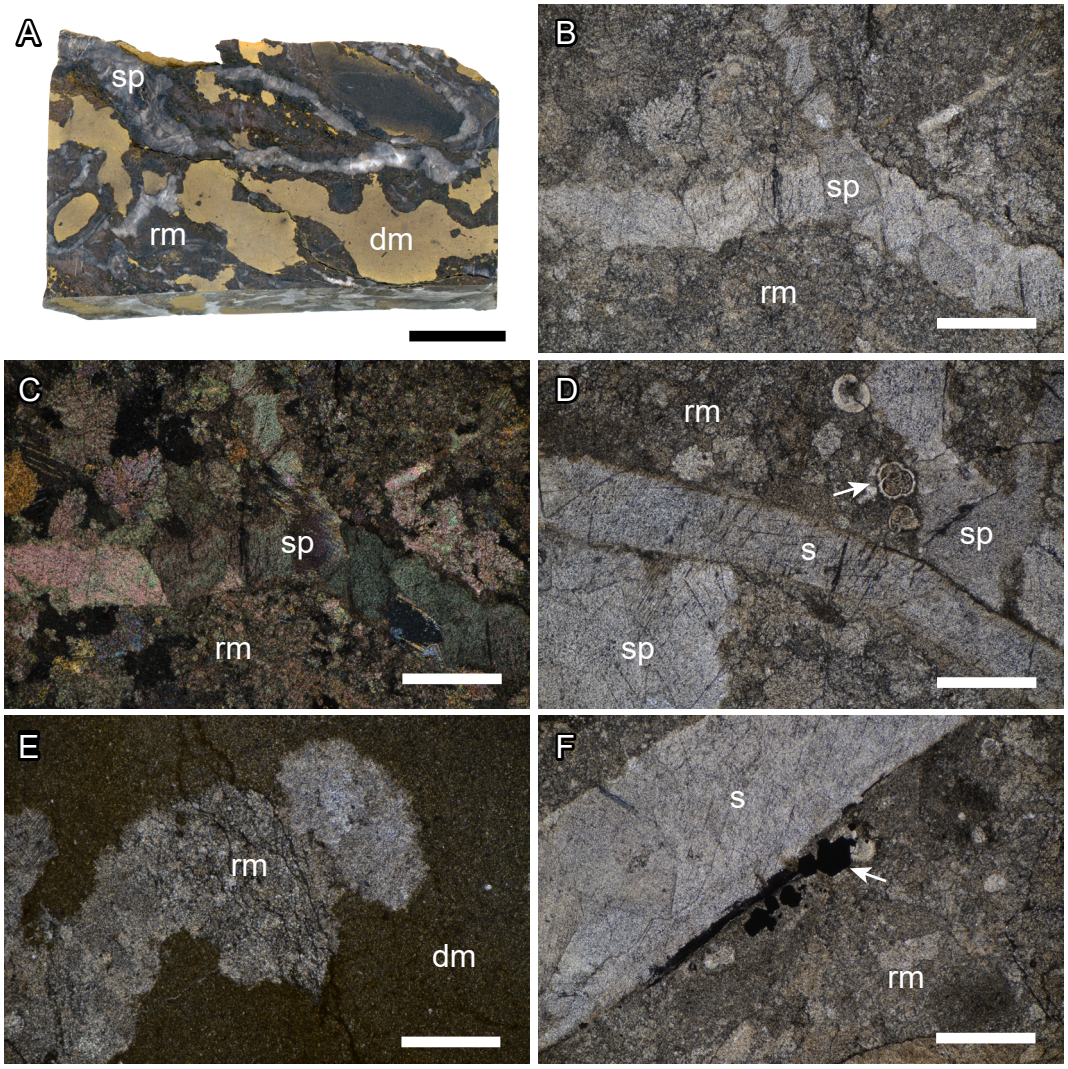

Fig. A.5. Petrography of the Kanoura seep carbonate. (A) Polished slab of a carbonate boulder showing dark-gray recrystallized matrix (rm), gold patches of dolomicrite (dm), and veins of sparry calcite (sp). (B) Recrystallized matrix (rm) crosscut by sparry calcite (sp). Plane-polarized light. (C) Same view as (B) under cross-polarized light. (D) Bivalve shell (s) and a foraminifer test (white arrow). Plane-polarized light. (E) Dolomicrite patch (dm) having irregular contact with the recrystallized matrix (rm). Plane-polarized light. (F) Pyrite crystals (white arrow) at the rim of a bivalve shell (s). Plane-polarized light. Scale bar for (A) = 10 mm, for (B)–(F) = 500 μm.

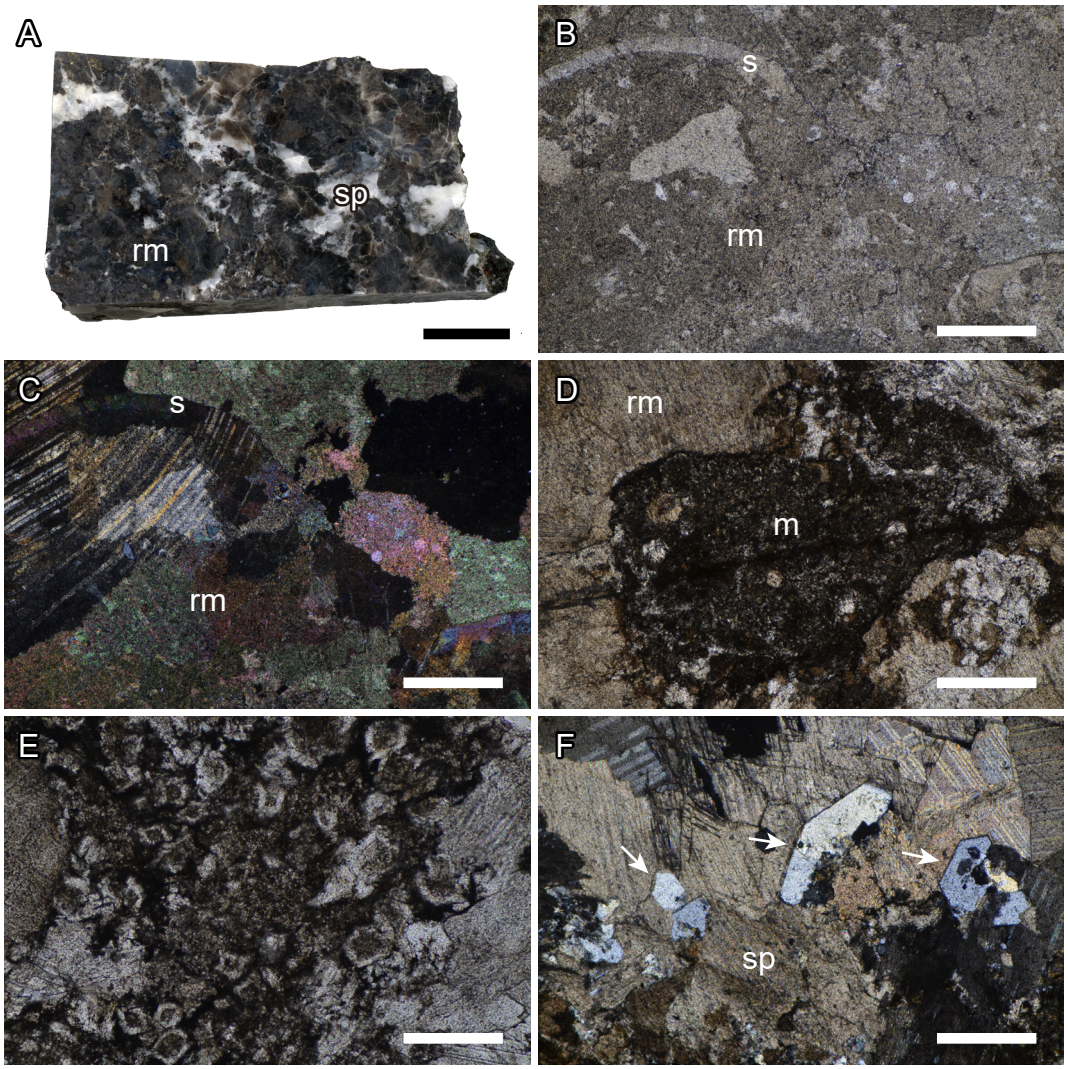

Fig. A.6. Petrography of the Fukusaki seep carbonate. (A) Polished slab of the carbonate lens showing dark-gray recrystallized matrix (rm) and veins of sparry calcite (sp). (B) Recrystallized matrix (rm) containing a bivalve shell (s). Plane-polarized light. (C) Same view as (B) under cross-polarized light. (D) Micrite patch (m) surrounded by the recrystallized matrix (rm). Plane-polarized light. (E) Aggregate of dolomite crystals. Plane-polarized light. (F) Euhedral quartz crystals (white arrows) in sparry calcite (sp). Cross-polarized light. Scale bar for (A) = 10 mm, for (B)–(F) = 500 μm.

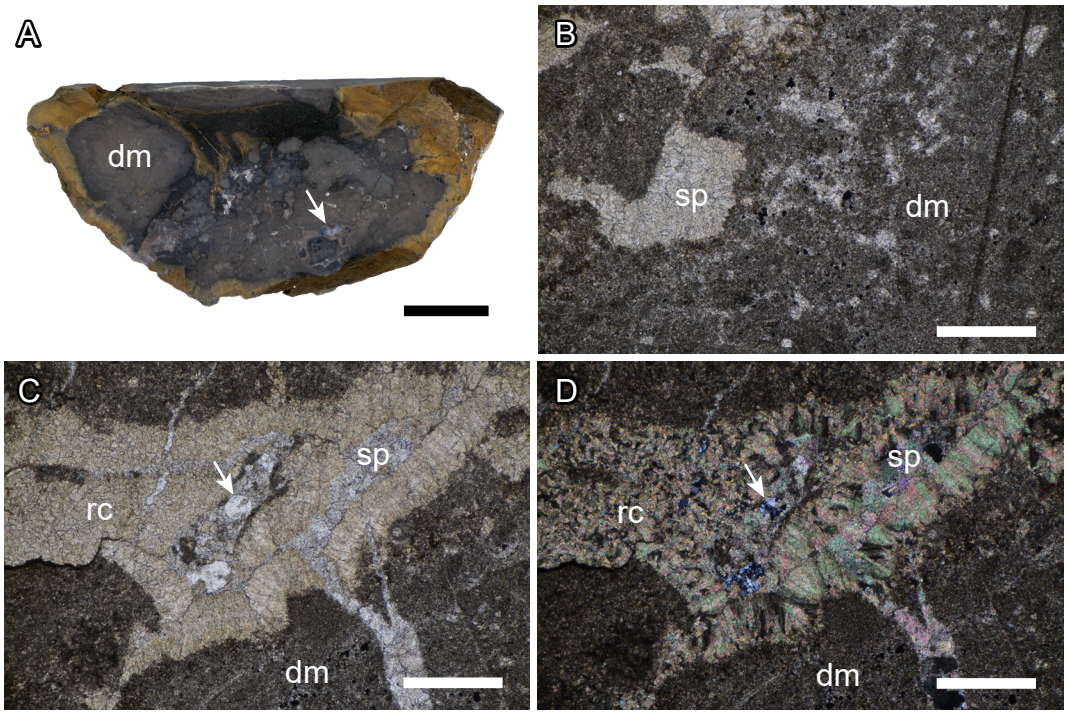

Fig. A.7. Petrography of the carbonate of Facies A of the Tanohama seep. (A) Polished slab of a carbonate concretion showing dark-gray dolomicrite (dm) containing sparry calcite cement (white arrow). (B) Dolomicrite (dm) showing clotted fabric and sparry calcite cement (sp). Plane-polarized light. (C) Void space rimmed with radial calcite (rc) and filled with sparry calcite (sp) and globular chalcedony (white arrow). Plane-polarized light. (D) Same view as (C) under cross-polarized light. Scale bar for (A) = 10 mm, for (B)–(D) = 500 μm.

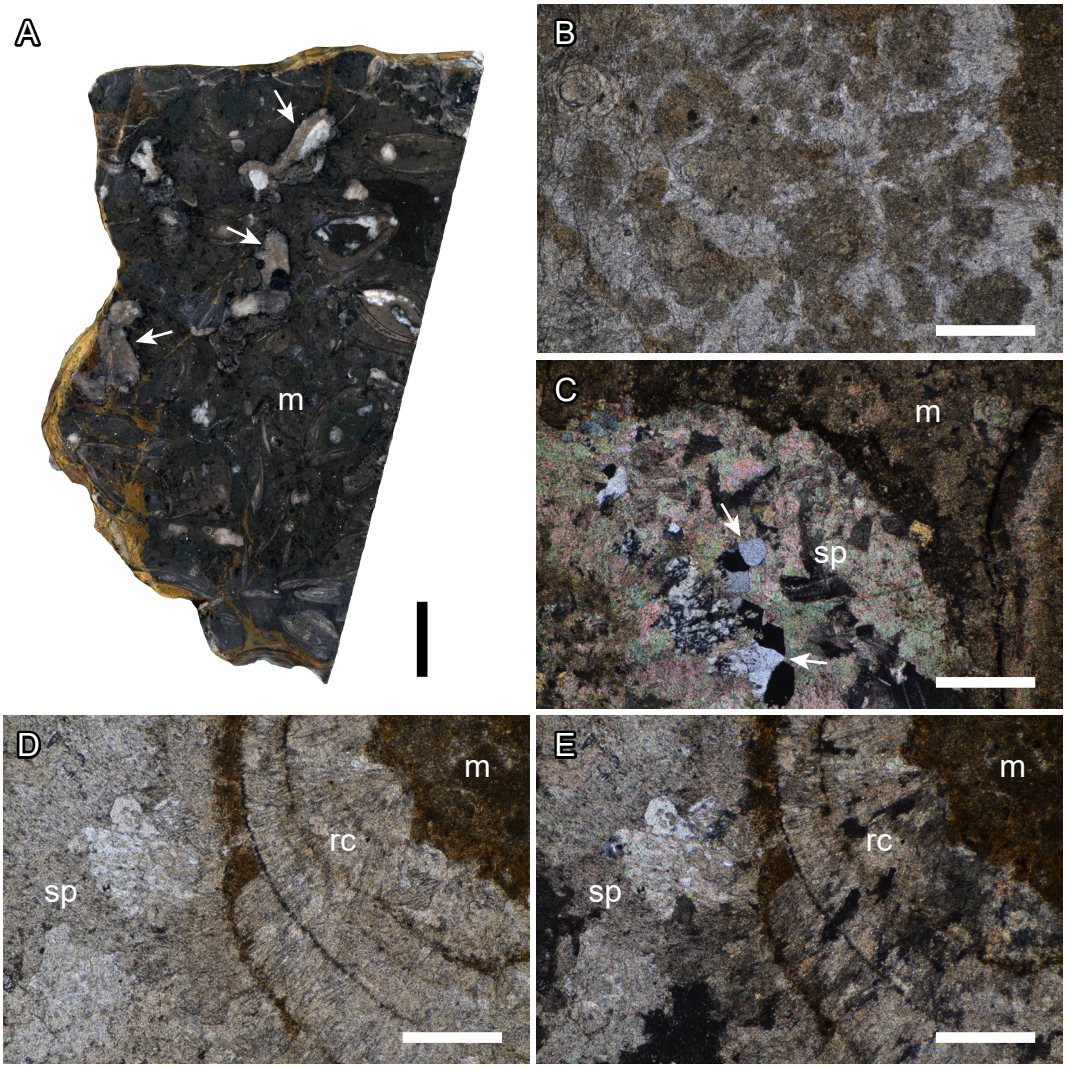

Fig. A.8. Petrography of the carbonate of Facies B of the Tanohama seep. (A) Polished slab of the carbonate body showing dark-gray micrite (m) containing sparry calcite cements (white arrows). (B) Micrite showing clotted fabric. Plane-polarized light. (C) Void space filled with sparry calcite (sp) and quartz crystals (white arrows). Cross-polarized light. (D) Void space rimmed with radial calcite (rc) and filled with sparry calcite (sp). Plane-polarized light. (E) Same view as (D) under cross-polarized light. Scale bar for (A) = 10 mm, for (B)–(E) = 500 μm.

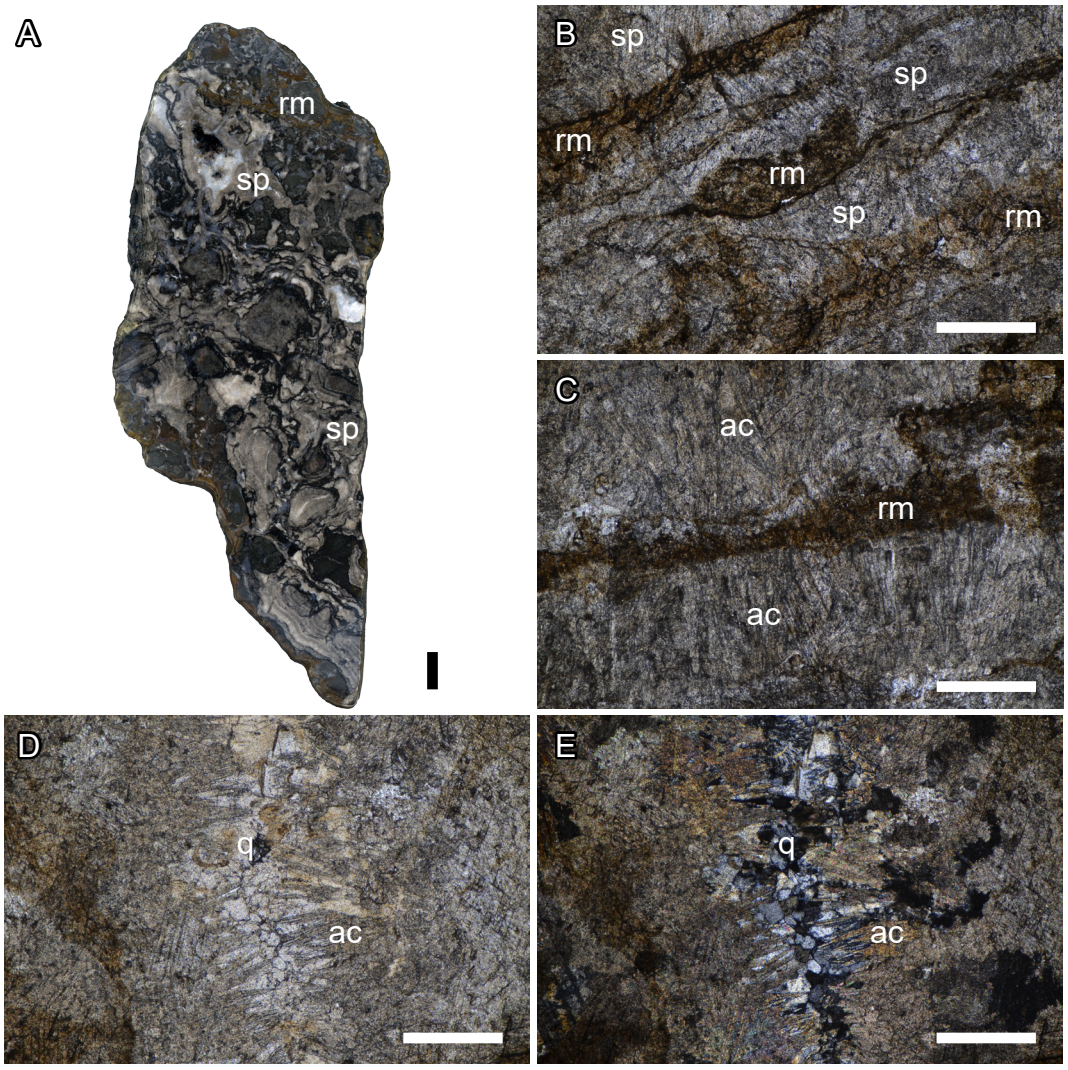

Fig. A.9. Petrography of the carbonate of Facies C of the Tanohama seep. (A) Polished slab of the carbonate body showing the stromatolite-like fabric composed of dark-gray recrystallized matrix (rm) and grayish sparry calcite cements (sp). (B) Alternation of the recrystallized matrix (rm) and the sparry calcite cement (sp). Plane-polarized light. (C) Acicular ghosts (ac) of the sparry cements lining the recrystallized matrix (rm). Plane-polarized light. (D) Void space rimmed with acicular crystals (ac) and filled with quartz (q). Plane-polarized light. (E) Same view as (D) under cross-polarized light. Scale bar for (A) = 10 mm, for (B)–(E) = 500 μm.

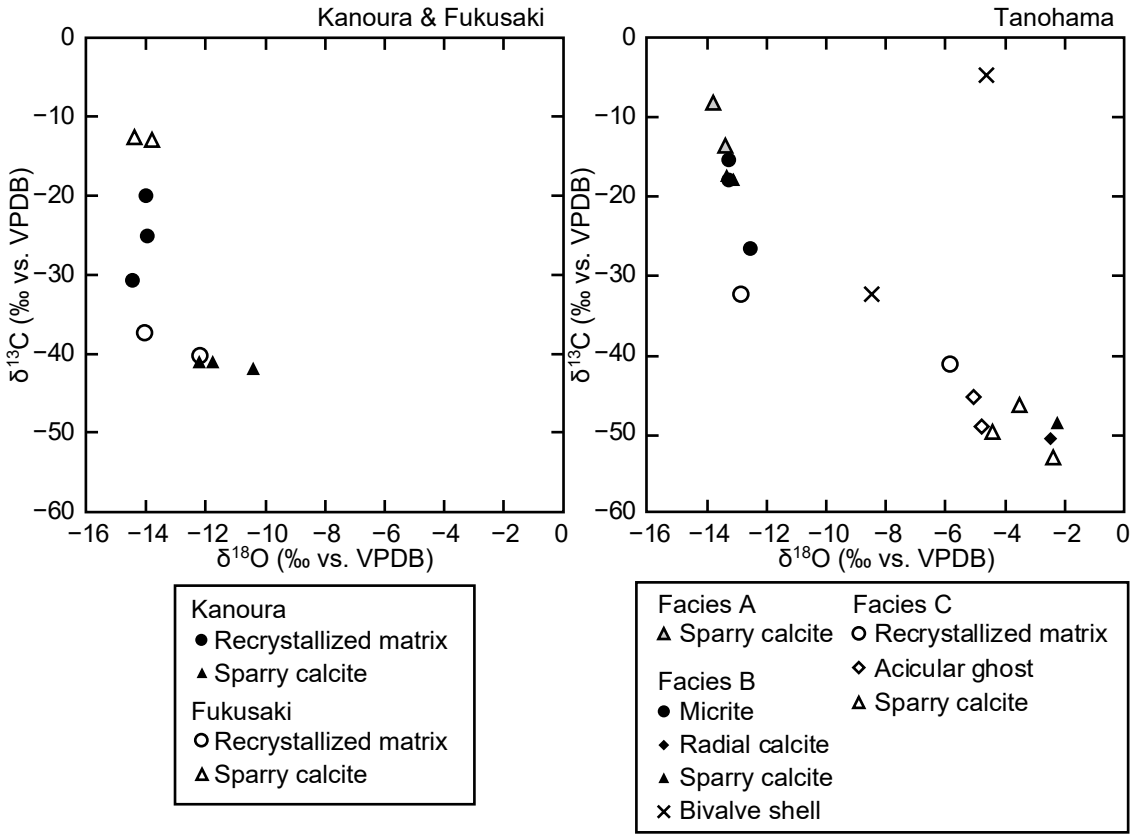

Fig. A.10. Stable carbon and oxygen isotopic compositions of selected carbonate phases from the Kanoura and Fukusaki seeps (left) and the Tanohama seep (right).

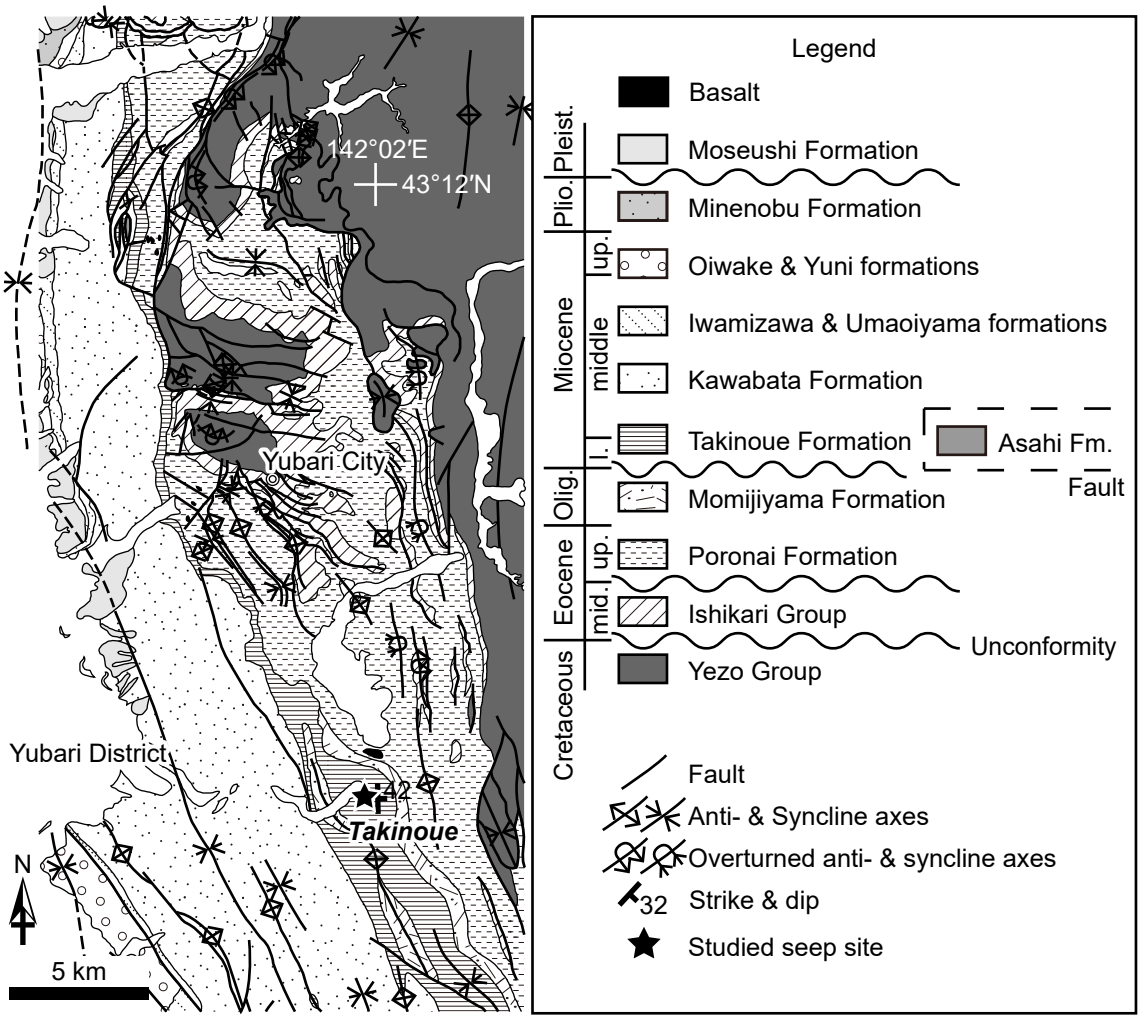

Fig. A.11. Geological map of the Yubari area (modified from Matsuno and Hata, 1960; Matsuno et al., 1964; Sasa et al., 1964; Ishida et al., 1980; Nakagawa et al., 1996; Takahashi et al., 2002). l., lower; Olig., Oligocene; Pleist., Pleistocene; Plio., Pliocene.

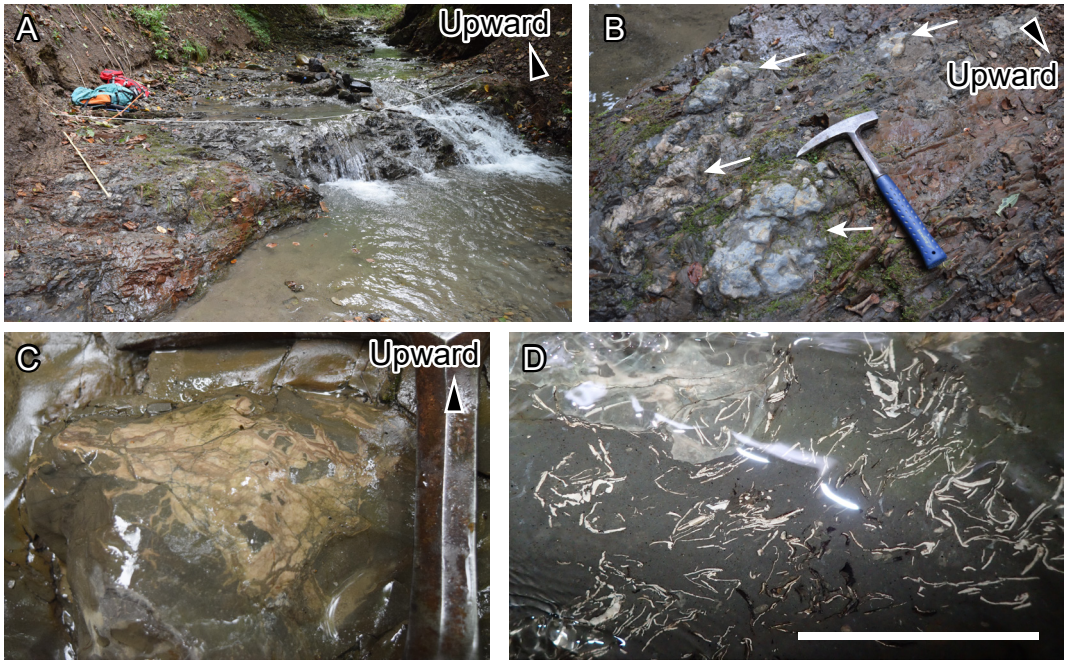

Fig. A.12. Field photographs at the Takinoue seep. (A) Photograph of the whole outcrop (~7.5 m across) that contains carbonate concretions. (B) Carbonate concretions (white arrows) within the siltstone. (C) Pinkish cement filling cracks of a concretion. (D) Densely-packed vesicomyid shells in the siltstone (Photo by R.G. Jenkins, Kanazawa University, Japan). Scale bar = 5 cm.

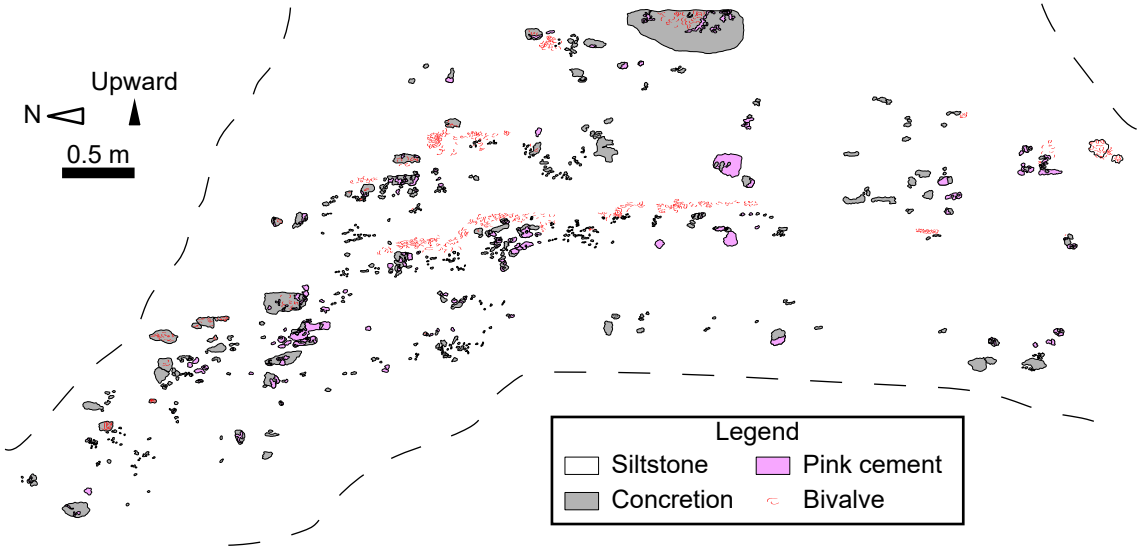

Fig. A.13. Sketch of the Takinoue outcrop shown in Fig. A.12A.

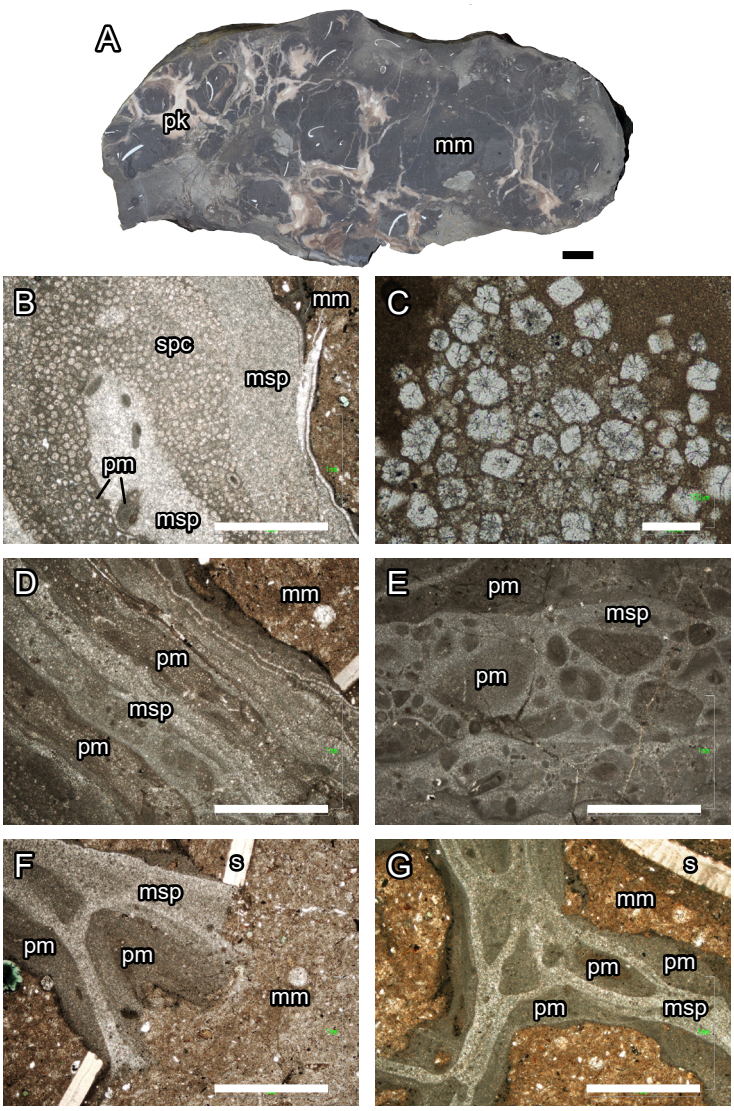

Fig. A.14. Petrography of the Takinoue seep carbonate. (A) Polished slab of a concretion, showing abundant cracks filled with pinkish cement (pk) in the dark-gray matrix micrite (mm). (B) Pinkish cement consisting of pure micrite (pm), microsparite (msp), and spherical crystal aggregates (spc). Plane-polarized light. (C) Enlarged view of spherical crystal aggregates. Plane-polarized light. (D) Laminated fabric consisting of alternating pure micrite (pm) and microsparite (msp). Plane-polarized light. (E) Peloids and clasts of pure micrite (pm), surrounded by microsparite (msp). Plane-polarized light. (F, G) Non-gravitational fabric, characterized by incongruent geopetal infillings by pure micrite (pm) within single cavities. Also note the clasts of pure micrite floating within microsparite (msp). s, bivalve shell. Plane-polarized light. Scale bars for (A) = 10 mm, for (B) and (D)–(G) = 1 mm, for (C) = 100 μm.

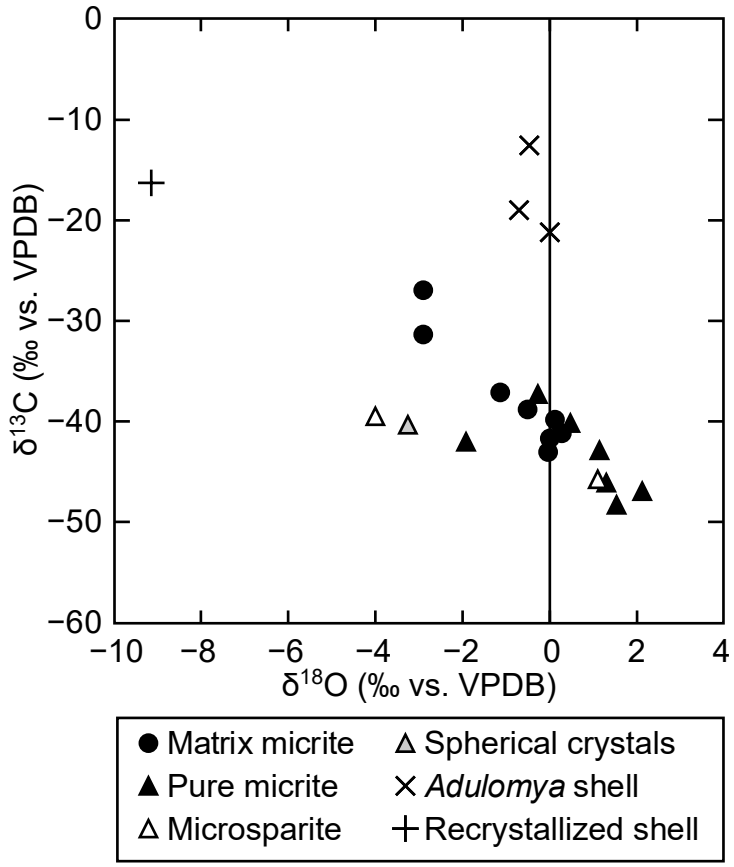

Fig. A.15. Stable carbon and oxygen isotopic compositions of selected carbonate phases from the Takinoue seep.

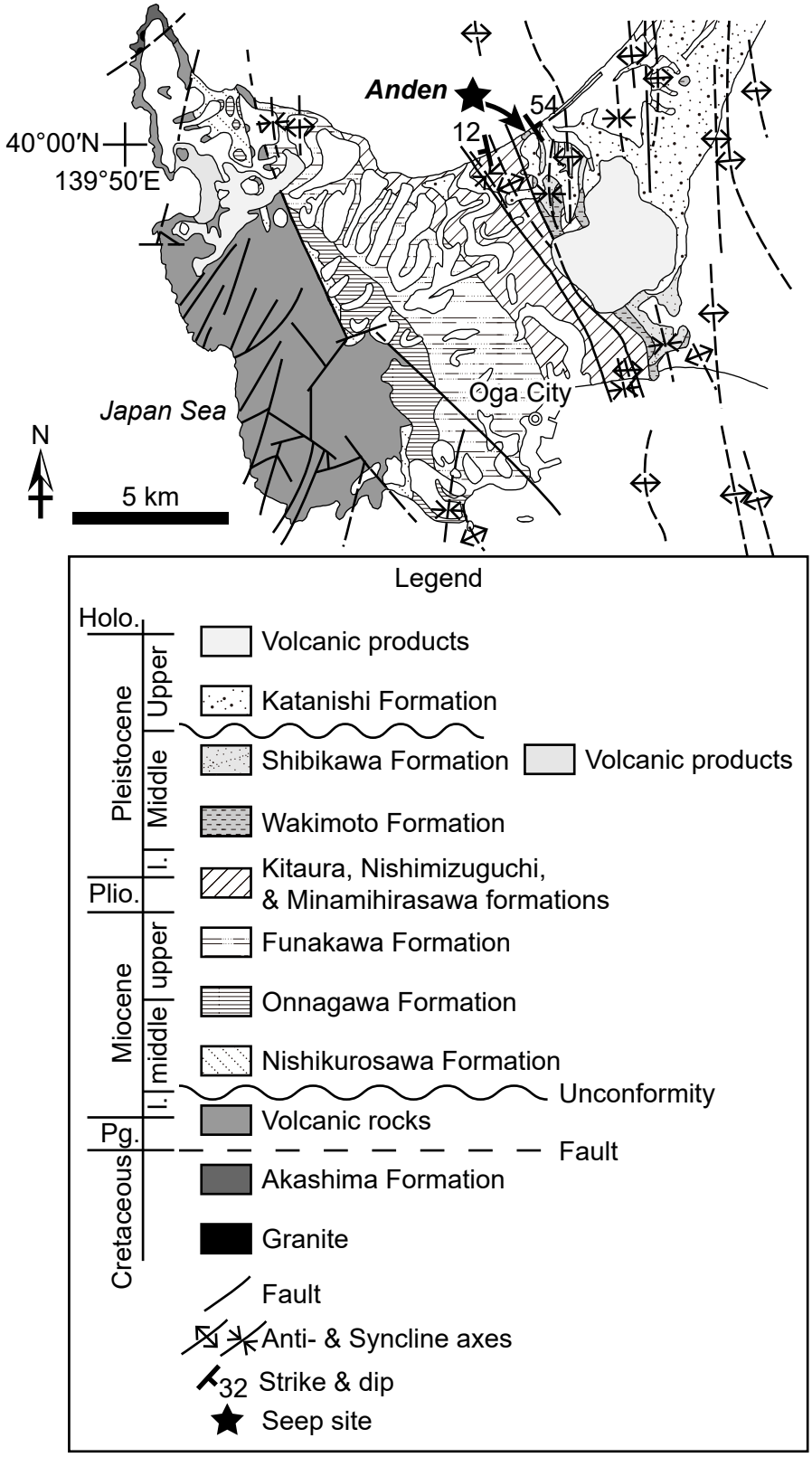

Fig. A.16. Geological map of the Oga Peninsula (modified from Kano et al., 2011). Holo., Holocene; l., lower; Pg., Paleogene; Plio., Pliocene.

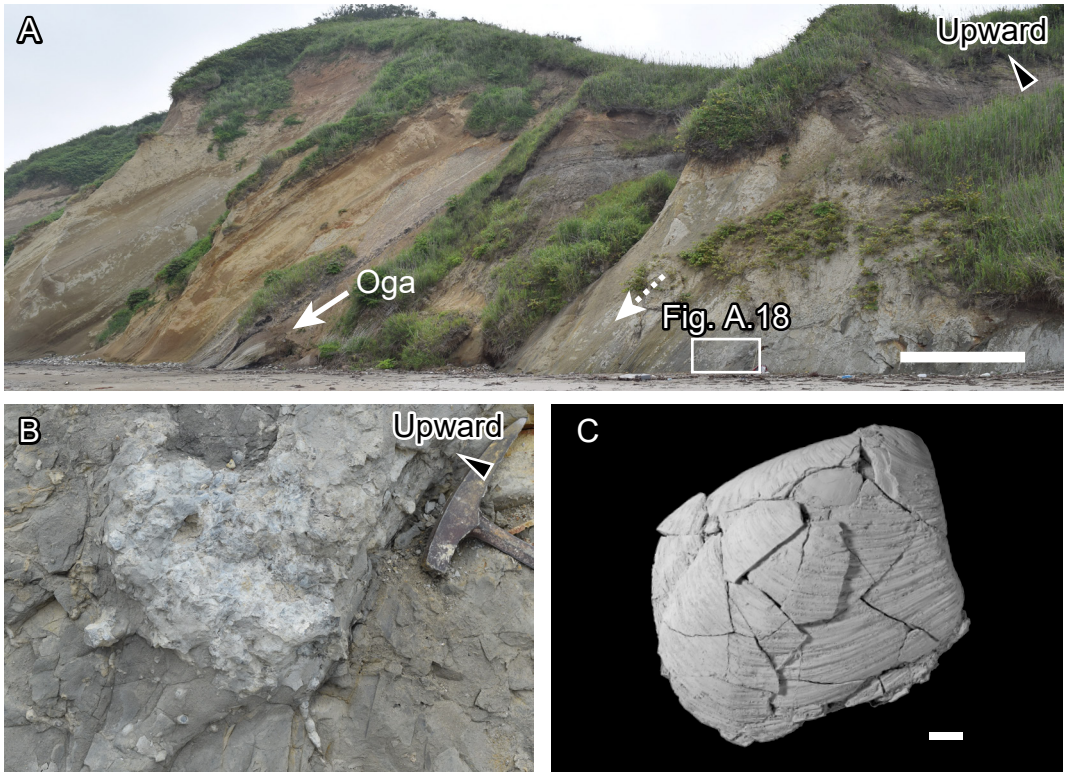

Fig. A.17. Field photographs and molluscan fossil at the Anden seep. (A) Whole outcrop including carbonate-concretion-bearing zone of the Wakimoto Formation (marked by square), the boundary between the Wakimoto and Shibikawa formations (dashed arrow), and the "Oga" tuff bed (solid arrow). Scale bar = 5 m. (B) Carbonate concretion of ~240 mm in diameter within the sandy siltstone of the Wakimoto Formation. (C) *Conchocele bisecta* collected from the sandy siltstone surrounding the concretions. Scale bar = 10 mm.

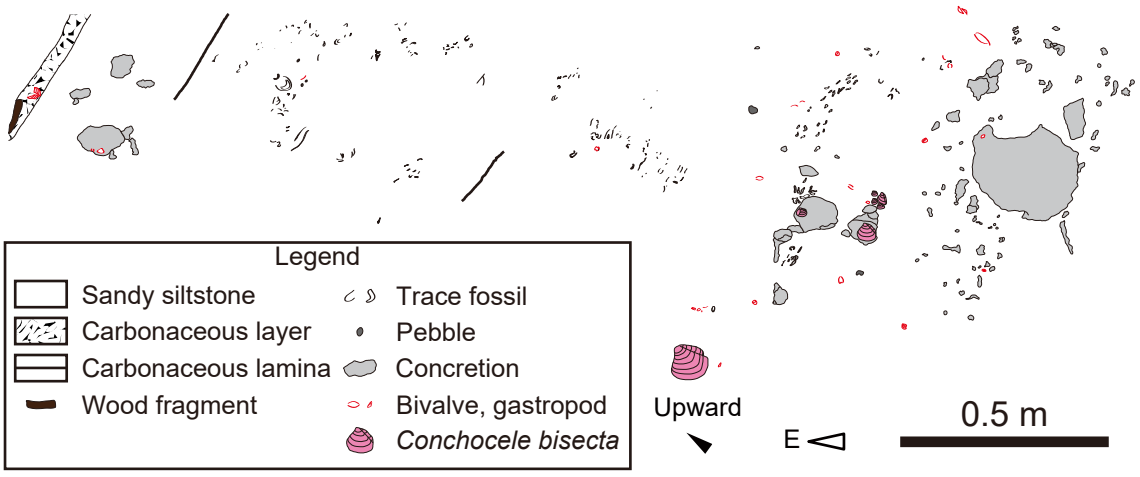

Fig. A.18. Sketch of concretion-bearing zone at the Anden seep, marked by square in Fig. A.17A.

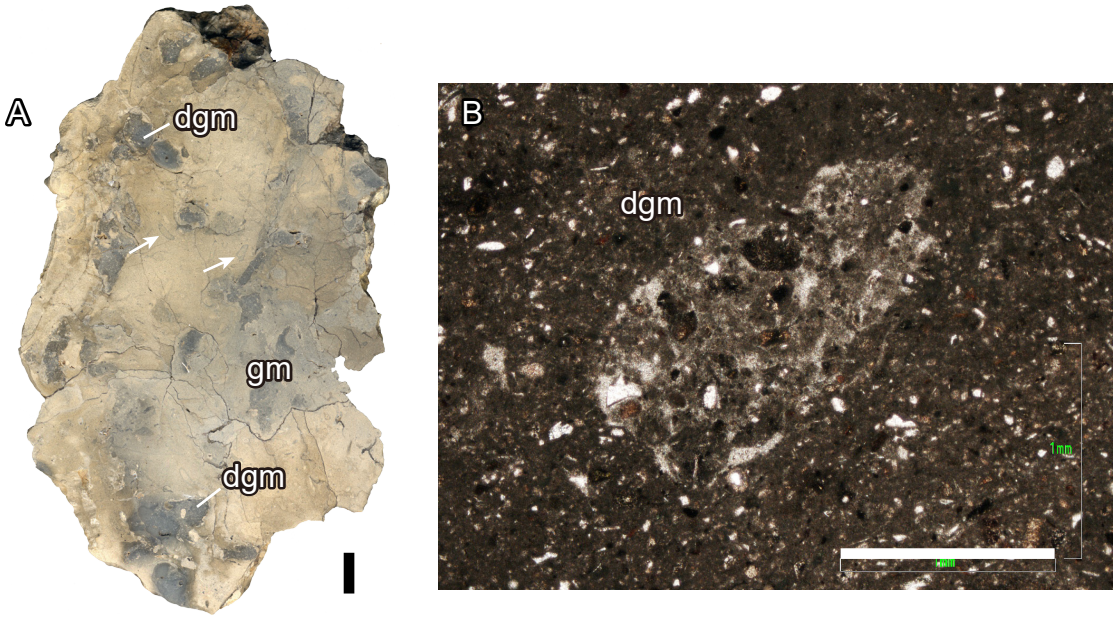

Fig. A.19. Petrography of the Anden seep carbonate. (A) Polished slab of a concretion (Fig. A.17B) that consists of gray micrite (gm) and patches of dark-gray micrite (dgm), surrounded by cream-colored and loosely cemented matrix. White arrows indicate trace fossils. Scale bar = 10 mm. (B) Dark-gray micrite (dgm) showing clotted fabric. Plane-polarized light. Scale bar = 1 mm.

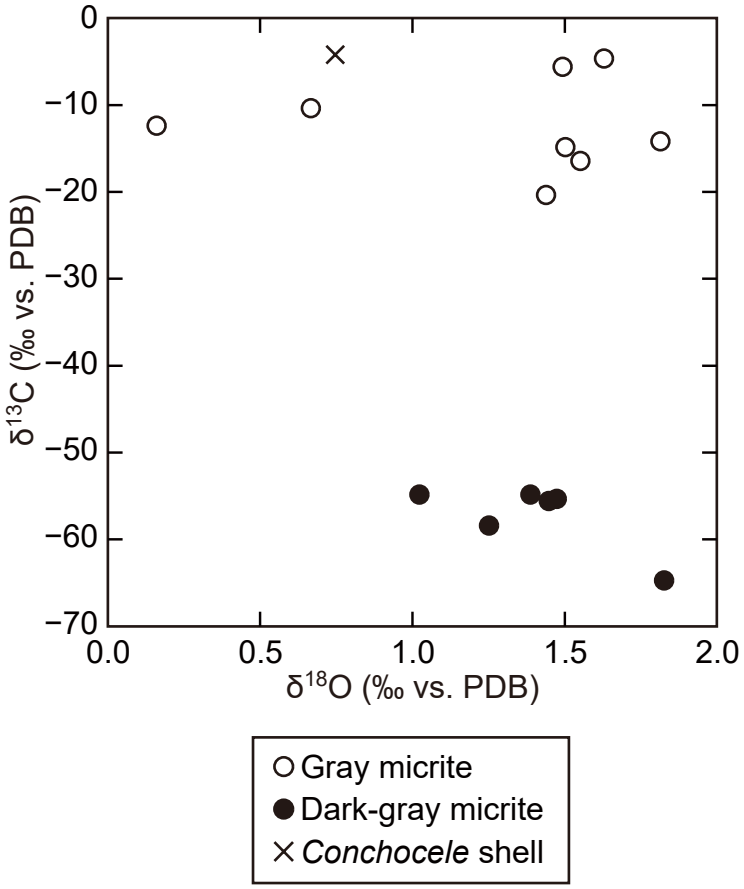

Fig. A.20. Stable carbon and oxygen isotopic compositions of selected carbonate phases from the Anden seep.

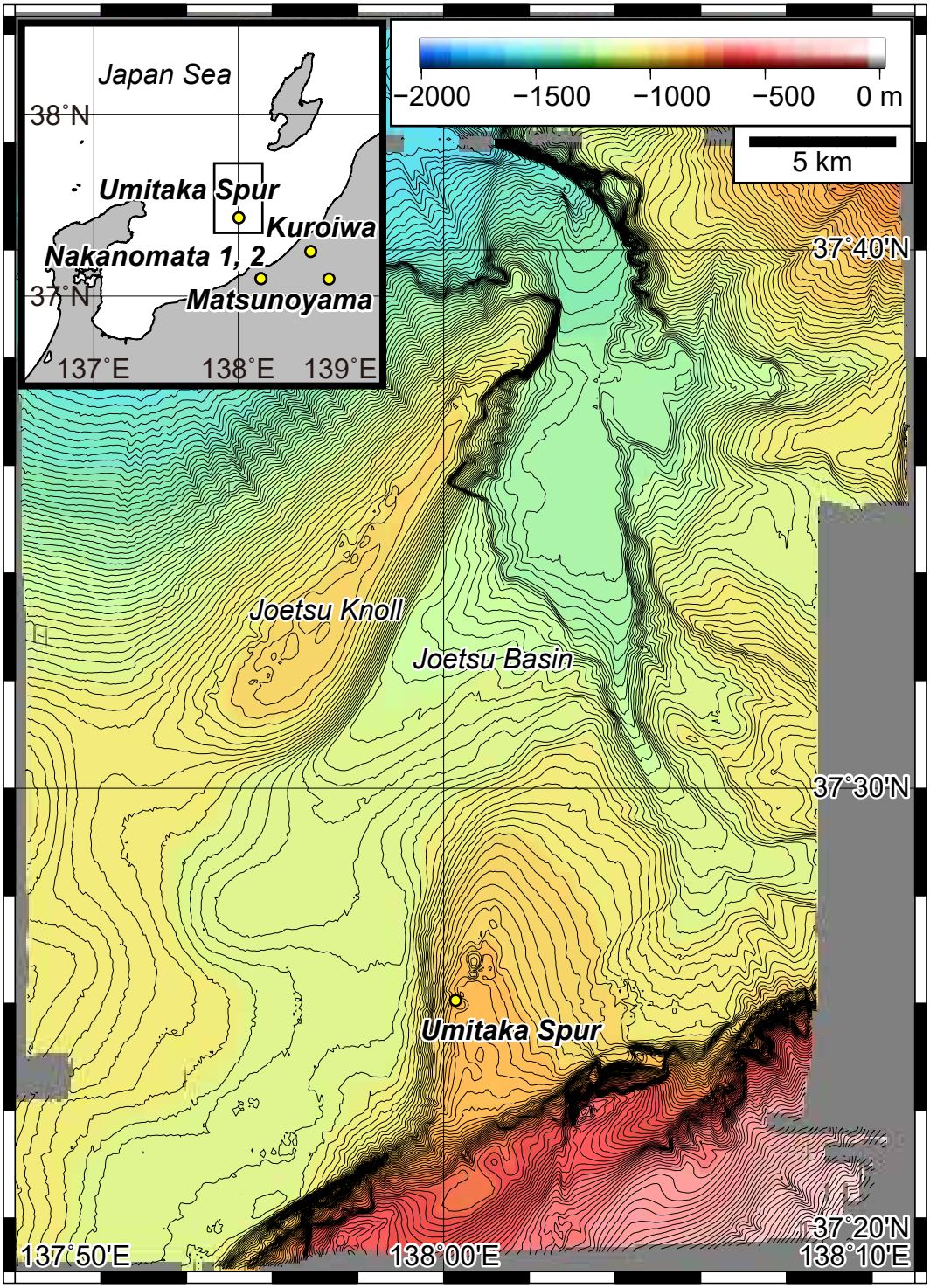

Fig. A.21. Bathymetric map showing the location of the Umitaka Spur central seep site (map provided by R.G. Jenkins, Kanazawa University, Japan). Inset shows locations of the bathymetric map (marked by square) and another study sites on land (circles).

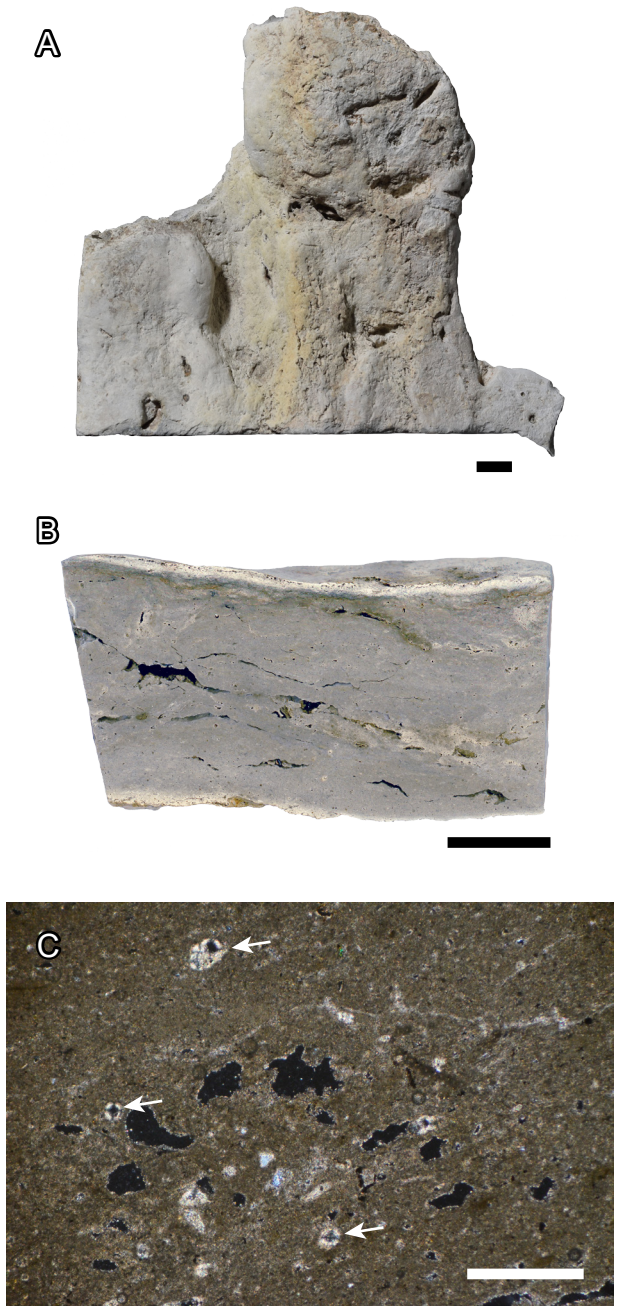

Fig. A.22. Petrography of carbonate nodule from the Umitaka Spur central seep. (A) Plane view of a platy nodule, collected at Site 5 of the HPD_00759 dive survey during NT07-20 cruise. Scale bar = 10 mm. (B) Polished slab of the same sample shown in (A), showing porous texture. Scale bar = 10 mm. (C) Micrite containing foraminifer tests (arrows). Black parts are pore spaces. Cross-polarized light. Scale bar = 500 μm.